Universität Potsdam
Institut für Erd- und Umweltwissenschaften
und
Helmholtz-Zentrum Potsdam –
Deutsches GeoForschungsZentrum GFZ
Sektion 5.2 – Klimadynamik und Landschaftsentwicklung

Reconstructing climate from the Dead Sea sediment record using high-resolution micro-facies analyses

Kumulative Dissertation

zur Erlangung des akademischen Grades
"doctor rerum naturalium"
(Dr. rer. nat.)
in der Wissenschaftsdisziplin Geologie/Paläoklimatologie

eingereicht an der
Mathematisch-Naturwissenschaftlichen Fakultät
der Universität Potsdam

von
Ina Neugebauer

Potsdam, 01. April 2015

Published online at the
Institutional Repository of the University of Potsdam:
URN urn:nbn:de:kobv:517-opus4-85266
http://nbn-resolving.de/urn:nbn:de:kobv:517-opus4-85266

Supervisor

Prof. Dr. Achim Brauer

Universität Potsdam
Helmholtz-Zentrum Potsdam, Deutsches GeoForschungsZentrum GFZ

Erklärung

Hiermit erkläre ich gemäß §12 Abs. 1 Nr. 7 der Promotionsordnung der Mathematisch-Naturwissenschaftlichen Fakultät der Universität Potsdam, dass ich die von mir vorgelegte Dissertation mit dem Titel

Reconstructing climate from the Dead Sea sediment record using high-resolution micro-facies analyses

selbstständig angefertigt, die benutzten Quellen und Hilfsmittel vollständig angegeben und wörtliche und sinngemäße Zitate als solche gekennzeichnet habe sowie Tabellen, Karten und Abbildungen, die anderen Werken in Wortlaut oder dem Sinn nach entnommen sind, in jedem Einzelfall als Entlehnung kenntlich gemacht habe. Ich erkläre außerdem, dass diese Dissertation noch keiner anderen Fakultät oder Hochschule zur Prüfung vorgelegen hat; dass sie, abgesehen von unten angegebenen Teilpublikationen, noch nicht veröffentlicht worden ist sowie, dass ich eine solche Veröffentlichung vor Abschluss des Promotionsverfahrens nicht vornehmen werde. Die Bestimmungen der Promotionsordnung sind mir bekannt.

Teilveröffentlichungen

- Neugebauer, I., Brauer, A., Schwab, M.J., Waldmann, N.D., Enzel, Y., Kitagawa, H., Torfstein, A., Frank, U., Dulski, P., Agnon, A., Ariztegui, D., Ben-Avraham, Z., Goldstein, S.L., Stein, M. and DSDDP Scientific Party, 2014: **Lithology of the long sediment record recovered by the ICDP Dead Sea Deep Drilling Project (DSDDP).** *Quaternary Science Reviews 102*, 149-165.
- Neugebauer, I., Schwab, M.J., Waldmann, N.D., Tjallingii, R., Frank, U., Hadzhiivanova, E., Naumann, R., Taha, N., Agnon, A, Enzel, Y., A. Brauer, and DSDDP Scientific Party, submitted: **Hydroclimatic variability during the early last glacial (~117-75 ka) derived from micro-facies analyses of the Dead Sea ICDP sediment record.** *Climate of the Past, submitted for review*.
- Neugebauer, I., Brauer, A., Schwab, M.J., Dulski, P., Frank, U., Hadzhiivanova, E., Kitagawa, H., Litt, T., Schiebel, V., Taha, N., Waldmann, N.D., and DSDDP Scientific Party, accepted: **Evidences for centennial dry periods at ~3300 and ~2800 cal yr BP from micro-facies analyses of the Dead Sea sediments.** *The Holocene*.

Potsdam, 1. April 2015

Ort, Datum, Unterschrift (Ina Neugebauer)

Abstract

The sedimentary record of the Dead Sea is a key archive for reconstructing climate in the eastern Mediterranean region, as it stores the environmental and tectonic history of the Levant for the entire Quaternary. Moreover, the lake is located at the boundary between Mediterranean sub-humid to semi-arid and Saharo-Arabian hyper-arid climates, so that even small shifts in atmospheric circulation are sensitively recorded in the sediments. This DFG-funded doctoral project was carried out within the ICDP Dead Sea Deep Drilling Project (DSDDP) that intended to gain the first long, continuous and high-resolution sediment core from the deep Dead Sea basin. The drilling campaign was performed in winter 2010-11 and more than 700 m of sediments were recovered. The main aim of this thesis was (1) to establish the lithostratigraphic framework for the ~455 m long sediment core from the deep Dead Sea basin and (2) to apply high-resolution micro-facies analyses for reconstructing and better understanding climate variability from the Dead Sea sediments.

Addressing the first aim, the sedimentary facies of the ~455 m long deep-basin core 5017-1 were described in great detail and characterised through continuous overview-XRF element scanning and magnetic susceptibility measurements. Three facies groups were classified: (1) the marl facies group, (2) the halite facies group and (3) a group involving different expressions of massive, graded and slumped deposits including coarse clastic detritus. Core 5017-1 encompasses a succession of four main lithological units. Based on first radiocarbon and U-Th ages and correlation of these units to on-shore stratigraphic sections, the record comprises the last ca 220 ka, i.e. the upper part of the Amora Formation (parts of or entire penultimate interglacial and glacial), the last interglacial Samra Fm. (~135-75 ka), the last glacial Lisan Fm. (~75-14 ka) and the Holocene Ze'elim Formation. A major advancement of this record is that, for the first time, also transitional intervals were recovered that are missing in the exposed formations and that can now be studied in great detail.

Micro-facies analyses involve a combination of high-resolution microscopic thin section analysis and μXRF element scanning supported by magnetic susceptibility measurements. This approach allows identifying and characterising micro-facies types, detecting event layers and reconstructing past climate variability with up to seasonal resolution, given that the analysed sediments are annually laminated. Within this thesis, micro-facies analyses, supported by further sedimentological and geochemical analyses (grain size, X-ray diffraction, total organic carbon and calcium carbonate contents) and palynology, were applied for two time intervals:

(1) The early last glacial period ~117-75 ka was investigated focusing on millennial-scale hydroclimatic variations and lake level changes recorded in the sediments. Thereby, distinguishing six different micro-facies types with distinct geochemical and sedimentological characteristics allowed estimating relative lake level and water balance changes of the lake.

Comparison of the results to other records in the Mediterranean region suggests a close link of the hydroclimate in the Levant to North Atlantic and Mediterranean climates during the time of the build-up of Northern hemisphere ice sheets during the early last glacial period.

(2) A mostly annually laminated late Holocene section (~3700-1700 cal yr BP) was analysed in unprecedented detail through a multi-proxy, inter-site correlation approach of a shallow-water core (DSEn) and its deep-basin counterpart (5017-1). Within this study, a ca 1500 years comprising time series of erosion and dust deposition events was established and anchored to the absolute time-scale through ^{14}C dating and age modelling. A particular focus of this study was the characterisation of two dry periods, from ~3500 to 3300 and from ~3000 to 2400 cal yr BP, respectively. Thereby, a major outcome was the coincidence of the latter dry period with a period of moist and cold climate in Europe related to a Grand Solar Minimum around 2800 cal yr BP and an increase in flood events despite overall dry conditions in the Dead Sea region during that time. These contrasting climate signatures in Europe and at the Dead Sea were likely linked through complex teleconnections of atmospheric circulation, causing a change in synoptic weather patterns in the eastern Mediterranean.

In summary, within this doctorate the lithostratigraphic framework of a unique long sediment core from the deep Dead Sea basin is established, which serves as a base for any further high-resolution investigations on this core. It is demonstrated in two case studies that micro-facies analyses are an invaluable tool to understand the depositional processes in the Dead Sea and to decipher past climate variability in the Levant on millennial to seasonal time-scales. Hence, this work adds important knowledge helping to establish the deep Dead Sea record as a key climate archive of supra-regional significance.

Kurzfassung

Die Sedimente des Toten Meeres stellen ein wichtiges Archiv für Klimarekonstruktionen im ostmediterranen Raum dar, da die gesamte quartäre Umwelt- und Tektonikgeschichte der Levante darin gespeichert ist. Außerdem führt die Lage des Sees im Grenzbereich zwischen mediterranem subhumidem bis semiaridem Klima und saharo-arabischem hyperaridem Klima dazu, dass selbst kleine Veränderungen der atmosphärischen Zirkulation sensibel in den Sedimenten verzeichnet werden. Diese Doktorarbeit wurde von der DFG finanziert und im Rahmen des ICDP Dead Sea Deep Drilling Project (DSDDP) durchgeführt, welches sich zur Aufgabe gestellt hat, den ersten langen, kontinuierlichen und hoch aufgelösten Sedimentkern vom tiefen Becken des Toten Meeres zu erlangen. Die Bohrkampagne fand im Winter 2010-11 statt, bei der mehr als 700 m Sedimente geteuft wurden. Die Zielsetzung dieser Doktorarbeit beinhaltete (1) den lithostratigraphischen Rahmen für den ~455 m langen Sedimentkern vom tiefen Becken des Toten Meeres zu erarbeiten und (2) hoch aufgelöste Mikrofazies-Analysen an den Sedimenten des Toten Meeres anzuwenden, um Klimavariabilität rekonstruieren und besser verstehen zu können.

Bezüglich erst genannter Zielsetzung wurden die Sedimentfazies des ~455 m langen Kerns 5017-1 vom tiefen Becken detailliert beschrieben und an Hand kontinuierlicher XRF Elementscanner-Daten und Messungen der magnetischen Suszeptibilität charakterisiert. Drei Faziesgruppen wurden unterschieden: (1) die Mergel-Faziesgruppe, (2) die Halit-Faziesgruppe und (3) eine verschiedene Ausprägungen massiver, gradierter oder umgelagerter Ablagerungen sowie grob-klastischen Detritus umfassende Gruppe. Der Kern 5017-1 ist durch die Abfolge von vier lithologischen Haupt-Einheiten charakterisiert. Basierend auf ersten Radiokarbon- und U-Th- Altern und Korrelation dieser Einheiten mit den am Ufer aufgeschlossenen stratigraphischen Abschnitten, umfasst der Datensatz die letzten ca 220 Tausend Jahre (ka), einschließlich des oberen Abschnitts der Amora-Formation (Teile von oder gesamtes vorletztes Interglazial und Glazial), die Samra-Fm. des letzten Interglazials (~135-75 ka), die Lisan-Fm. des letzten Glazials (~75-14 ka) und die holozäne Ze'elim-Formation. Ein entscheidender Fortschritt dieses Records ist, dass erstmals Übergangsbereiche erfasst wurden, die in den aufgeschlossenen Formationen fehlen und nun detailliert studiert werden können.

Mikrofazies-Analysen umfassen eine Kombination hoch aufgelöster mikroskopischer Dünnschliff-Analysen und μXRF Elementscanning, die durch die Messung der magnetischen Suszeptibilität unterstützt werden. Dieser Ansatz erlaubt es, Mikrofazies-Typen zu identifizieren und zu charakterisieren, Eventlagen aufzuzeichnen und die Klimavariabilität der Vergangenheit mit bis zu saisonaler Auflösung zu rekonstruieren, vorausgesetzt, dass die zu analysierenden Sedimente jährlich laminiert sind. Im Rahmen dieser Doktorarbeit wurden Mikrofazies-Analysen für zwei Zeitabschnitte angewendet, unterstützt durch weitere sedimentologische und

geochemische Analysen (Korngrößen, Röntgen-Diffraktometrie, gesamter organischer Kohlenstoff- und Kalziumkarbonat-Gehalte) sowie Palynologie.

(1) Das frühe letzte Glazial ~117-75 ka wurde hinsichtlich hydroklimatischer Variationen und in den Sedimenten verzeichneter Seespiegeländerungen auf tausendjähriger Zeitskala untersucht. Dabei wurden sechs verschiedene Mikrofazies-Typen mit unterschiedlichen geochemischen und sedimentologischen Charakteristika bestimmt, wodurch relative Änderungen des Seespiegels und der Wasserbilanz des Sees abgeschätzt werden konnten. Ein Vergleich der Ergebnisse mit anderen Records aus dem Mittelmeerraum lässt vermuten, dass das Hydroklima der Levante eng mit dem nordatlantischen und mediterranen Klima während der Zeit des Aufbaus nordhemisphärischer Eisschilde im frühen letzten Glazial verknüpft war.

(2) Ein weitestgehend jährlich laminierter spätholozäner Abschnitt (~3700-1700 kal. J. BP – kalibrierte Jahre vor heute) wurde in größtem Detail an Hand eines Multiproxie-Ansatzes und durch Korrelation eines Flachwasser-Bohrkerns (DSEn) mit seinem Gegenstück aus dem tiefen Becken (5017-1) untersucht. In dieser Studie wurde eine ca. 1500 Jahre umfassende Zeitreihe von Erosions- und Staubablagerungs-Ereignissen erstellt und an Hand von ^{14}C-Datierung und Altersmodellierung mit der absoluten Zeitskala verankert. Ein besonderer Fokus dieser Studie lag in der Charakterisierung zweier Trockenphasen, von ~3500 bis 3300 beziehungsweise von ~3000 bis 2400 kal. J. BP. Dabei war ein wichtiges Resultat, dass letztgenannte Trockenphase mit einer Phase feuchten und kühlen Klimas in Europa, in Zusammenhang mit einem solaren Minimum um 2800 kal. J. BP, zusammen fällt und dass trotz der generell trockeneren Bedingungen in der Toten Meer Region zu dieser Zeit verstärkt Flutereignisse verzeichnet wurden. Diese unterschiedlichen Klimasignaturen in Europa und am Toten Meer waren wahrscheinlich durch komplexe Telekonnektionen der atmosphärischen Zirkulation verknüpft, was eine Veränderung synoptischer Wettermuster im ostmediterranen Raum zur Folge hatte.

Zusammenfassend lässt sich sagen, dass innerhalb dieser Doktorarbeit der lithostratigraphische Rahmen eines einzigartigen, langen Sedimentkerns vom tiefen Becken des Toten Meeres erstellt wurde, welcher als Basis für jegliche weitere hoch aufgelöste Untersuchungen an diesem Kern dient. In zwei Fallstudien wird demonstriert, dass Mikrofazies-Analysen ein unschätzbares Werkzeug darstellen, Ablagerungsprozesse im Toten Meer zu verstehen und die Klimavariabilität der Vergangenheit in der Levante auf tausendjährigen bis saisonalen Zeitskalen zu entschlüsseln. Diese Arbeit enthält daher wichtige Erkenntnisse, die dabei helfen die Schlüsselstellung des Records vom tiefen Toten Meer als Klimaarchiv überregionaler Bedeutung zu etablieren.

Acknowledgements

I would like to thank a number of people, who helped me to challenge and finish this thesis. First of all, I like to express my gratitude to my supervisor Achim Brauer for his continuous support in every scientific situation and for letting me benefit from his profound knowledge. No less important was the constant encouragement and help of Markus J. Schwab. Thank you, Markus (also for driving and supplying me with unhealthy things, when urgently needed…)! I also wish to thank the DFG for funding and two external reviewers for evaluating this thesis.

Many thanks go to all the excellent scientists involved in the Dead Sea project, with whom I had the pleasure to work and to learn from their experience and who shared their ideas with me; among them Moti Stein, Zvi Ben-Avraham, Amotz Agnon, Yehouda Enzel, Daniel Ariztegui, Hiroyuki Kitagawa, Steve Goldstein, Elisa Kagan and many more! I very much appreciated the company of the other PhD students of this project Lisa Coianiz, Camille Thomas, Daniel Palchan and Elan Levy and our great exchange. Special thanks goes out to Nicolas Waldmann for a great cooperation, fantastic field trips and kind hospitality and as well to Revital Bookman for nice discussions and Elitsa Hadzhiivanova for running so many grain size analyses. I also wish to thank Ronald Conze for DIS-support and the downhole-logging crew for exploring Israel with me.

Furthermore, I would like to thank everybody from GFZ Section 5.2 (and beyond) for support, inspiration, standing the 'Dead Sea smell' and creating such a warm atmosphere. Christine Gerschke is kindly thanked for solving every bureaucratic problem, Andreas Hendrich patiently helped with figures and Marcus Günzel and Matthias Köppl kept the computer running. Gabi Arnold, Dieter Berger and Micha Köhler prepared countless thin sections, Brian Brademann opened hundreds of sediment cores and Birgit Plessen, Sylvia Pinkerneil and Petra Meier measured the geochemistry with great creativity. Peter Dulski, Florian Ott, Sabine Wulf and Rik Tjallingii supported the XRF measurements, Rudolf Naumann ran the XRD, Ute Frank and Norbert Nowaczyk took care about everything magnetic and Jens Mingram about the microscopes. Thank You! Another thanks goes to my PhD fellows Markus Czymzik, Lucas Kämpf and Florian Ott for coffee breaks and nice evenings and special thanks go to my office mates Stefan Lauterbach and Gordon Schlolaut for simply everything, especially for making me laugh a lot!

Last but not least, I want to express my deep gratitude to my family and all my friends outside of the science world for their tremendous support and patience and for helping me to keep the balance between work and life!

Dankeschön! **תודה רבה!**

Table of Contents

List of Figures

List of Tables

1 Introduction

1.1 The Dead Sea as palaeoclimate archive

To improve climate projections and adaptation strategies to global warming, a better understanding of past natural climate variability is crucial (IPCC, 2012). In this respect, palaeoclimate archives, such as ice sheets in Greenland (e.g. Johnsen et al., 1992; NGRIP Members, 2004; Rasmussen et al., 2014) and Antarctica (e.g. EPICA Community Members, 2004; 2006), speleothems (e.g. Bar-Matthews et al., 1999; Wang et al., 2001; Fleitmann et al., 2003), tree rings (e.g. Cook et al., 1998; Esper et al., 2002; Briffa et al., 2004), corals (e.g. Fairbanks, 1989; Bard et al., 1990; 1996), marine (e.g. Shackleton and Opdyke, 1973; Shackleton, 1987; Chapman et al., 2000) and lacustrine sediments (e.g. Brauer et al., 1999a; 1999b; 2008; Nakagawa et al., 2012), store the climatic and environmental history with up to annual resolution and provide important information about past abrupt climate changes and changing frequencies of hydrometeorological extremes, like droughts or floods, when human influence was minor or absent.

The Mediterranean region is especially vulnerable to climate change, as water scarcity raises and hydrometeorological hazards become more frequent with increasing global temperature and atmospheric concentration of greenhouse gases (e.g. Hoerling et al., 2011; Seager et al., 2014; Sippel and Otto, 2014). In the Mediterranean region, climate reconstructions are obtained mainly from marine sediment cores (e.g. Cheddadi and Rossignol-Strick, 1995; Sánchez Goñi et al., 1999; Ariztegui et al., 2000; Sánchez Goñi et al., 2002; Almogi-Labin et al., 2009; Desprat et al., 2013) and from terrestrial archives in the northern Mediterranean realm (see Tzedakis, 2007). For example, long sequences of past climate variability are available from Lake Banyoles, Spain (e.g. Pèrez-Obiol and Julià, 1994; Höbig et al., 2012), Lago Grande di Monticchio, Italy (e.g. Allen et al., 2000; Brauer et al., 2007; Martin-Puertas et al., 2014), Lake Ohrid, Albania/Macedonia (e.g. Wagner et al., 2009; 2014), Tenaghi Philippon, Greece (e.g. Tzedakis et al., 2006; Pross et al., 2009) and Lake Van, Turkey (e.g. Litt and Anselmetti, 2014; Stockhecke et al., 2014). The southern Mediterranean/North African region is, however, relatively underrepresented, as only few terrestrial records are available, for instance from Lake Tigalmamine, Morocco (Lamb and van der Kaars, 1995; Cheddadi et al., 1998) and Dar Fatma, Tunisia (Ben Tiba and Reille, 1982).

In the eastern Mediterranean region, most important palaeoclimate archives are marine records from the Levantine Sea (e.g. Rossignol-Strick, 1985; Cheddadi and Rossignol-Strick, 1995; Almogi-Labin et al., 2009) and from the Red Sea (e.g. Arz et al., 2003; Lamy et al., 2006), and terrestrial records from Lake Van, eastern Anatolia (see references above), Lake Yammoûneh, Lebanon (Develle et al., 2011; Gasse et al., 2015), Soreq Cave, Israel (e.g. Bar-Matthews et al., 1997; 1999; 2000; 2003) and the Dead Sea (e.g. Stein, 2001; 2014), all of which covering large parts of the Quaternary climate history.

Among these archives, the Dead Sea is an exceptional climate recorder because it is situated at the boundary between Mediterranean climate in its northern and western drainage area and the hyperarid Saharo-Arabian desert belt in its south and southeast, leading to a large rainfall gradient from >800 mm/year in the Golan Heights and at Mt. Hermon to <100 mm/year in the Negev, the Arava valley and at the Dead Sea itself (Fig. 1-1). Furthermore, the Dead Sea is located at one of the deepest continental depressions on Earth that is bounded by steep escarpments to the east and west of the basin (Fig. 1-1). Due to this combination of extreme climatic and morphologic gradients, the Dead Sea acts as a rain gauge with small changes in precipitation over its drainage area being sensitively recorded through changing lake levels and in the sediments (e.g. Enzel et al., 2003; Bookman (Ken-Tor) et al., 2004).

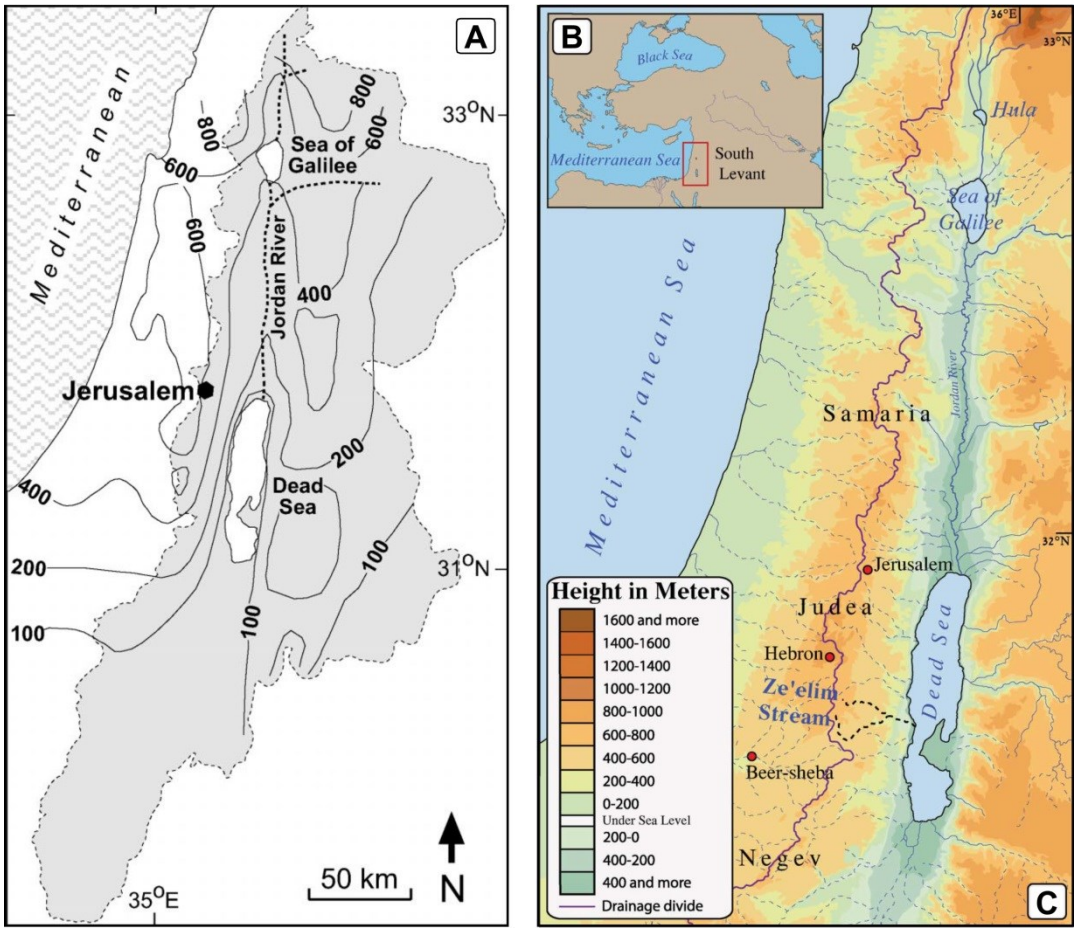

Figure 1-1: (A) Mean annual precipitation (in mm) over the drainage area of the Dead Sea (grey) (Bookman (Ken-Tor) et al., 2004); (B) setting of the southern Levant and (C) topographic map of Israel and adjacent areas with indicated watershed line (Langgut et al., 2014).

Lake levels of the Holocene Dead Sea and its Pleistocene precursor lakes, i.e. lakes Lisan, Samra and Amora, strongly fluctuated in the past. For example, during the last glacial maximum the lake level of Lake Lisan was about 270 m higher (~160 m below mean sea level) than today (~428 m bmsl) (Bartov et al., 2002). The climatic-hydrological information over time that led to

these extreme fluctuations is stored in the sedimentary record of the water bodies. Therefore, the characteristic sediment formations are subject of a multitude of palaeoclimatic and palaeoenvironmental studies in and at the margins of the Dead Sea (Fig. 1-2).

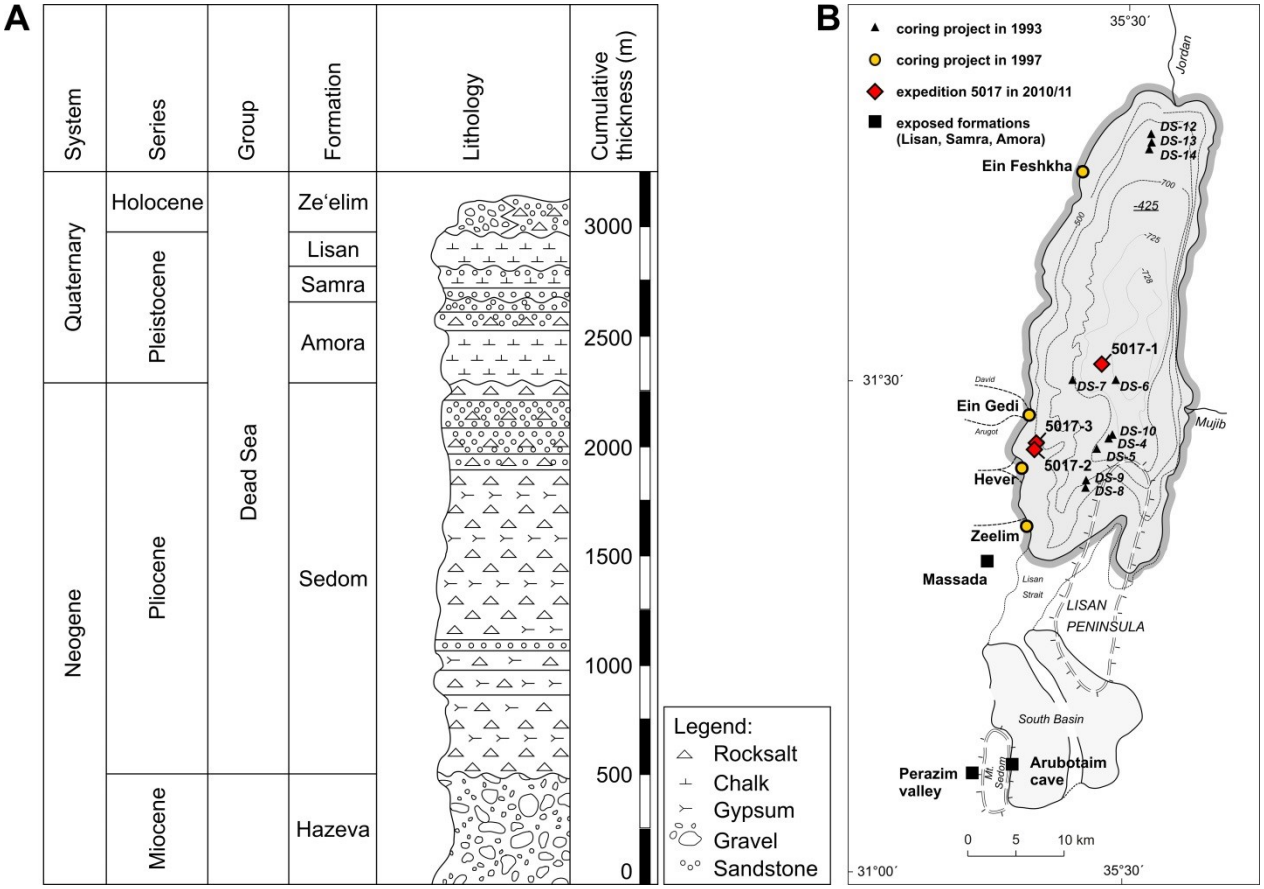

Figure 1-2: (A) General stratigraphic section of the Dead Sea Group (adapted from Zak, 1967; Waldmann et al., 2009); (B) map of the Dead Sea and site locations of the drilling campaigns in 1993 (Heim et al., 1997; Ben-Avraham et al., 1999), in 1997 (Migowski et al., 2004; Migowski et al., 2006) and in 2010/11 (Stein et al., 2011; Neugebauer et al., 2014), as well as selected sites, where exposed sediment formations were intensively studied, i.e. the Lisan Formation at Massada (e.g. Bartov et al., 2002; Prasad et al., 2009), the Lisan and Samra Formations at Perazim valley (Haase-Schramm et al., 2004; Waldmann et al., 2009) and the Amora Formation at Arubotaim (Torfstein et al., 2009).

1.2 Projects related to this thesis

The ICDP Dead Sea Deep Drilling Project

The Dead Sea Deep Drilling Project (DSDDP) – *"The Dead Sea as a Global Paleo-environmental, Tectonic, and Seismological Archive"* – commenced after several decades of extensive study in the Dead Sea basin, starting with the early works of Y. K. Bentor (1961; 1969), D. Neev (e.g. Neev and Emery, 1967; Neev and Hall, 1979), Z. Garfunkel (e.g. Garfunkel

et al., 1981; Garfunkel and Ben-Avraham, 1996), I. Zak (1967) and many more. Based on these pioneering works, numerous studies expanded our knowledge about the structure and tectonics of the basin, the physical, chemical and biological characteristics of this exceptional lake and about the evolution of the Quaternary water bodies in the basin with respect to environmental changes (summarized in Niemi et al., 1997; Enzel et al., 2006; Garfunkel et al., 2014).

Previous studies of the Dead Sea sediments were mainly restricted to sediment formations that are exposed at the margins of the lake (Fig. 1-2). Due to the strong lake level fluctuations in the past, these outcrops are, however, mostly incomplete and lack information especially about drier periods and low lake stands. Earlier attempts to drill in the deep basin were hampered by thick salt sequences that could not be penetrated (Heim et al., 1997; Ben-Avraham et al., 1999). Therefore, a promising way to gain a continuous, long sediment record from the deep DSB was through an ICDP drilling using the sophisticated drilling technique of the DLDS (Deep Lake Drilling System) operated by DOSECC (Drilling, Observation and Sampling of the Earth's Continental Crust) Exploration Services. This drilling system is designed to recover up to 1400 m long sediment sequences from water depths of max. 400 m and has been successfully applied in several deep lakes, for example Lake Van, Turkey (Litt and Anselmetti, 2014), and Lake Ohrid, Albania/Macedonia (Wagner et al., 2014).

The main objective of drilling in the deep Dead Sea basin was to obtain the longest, most continuous and best preserved, high-resolution sediment record in the Levant that covers several past glacial-interglacial cycles. The main research goals of the project included:

- Reconstructing the environmental conditions during extreme lake level drops;
- Estimating the extent and duration of lake level fluctuations and their implications;
- Estimating how regional climate was modulated by global climate during the Pleistocene;
- Reconstructing a long-term palaeoseismic record that accompanied the regional tectonic movements;
- Answering questions about the evolution of physical properties of the Dead Sea sediments including salt diagenesis;
- Understanding the relation between tectonics, i.e. uplift and subsidence, sediment accumulation and the limnological-hydrological history through the Pleistocene;
- Establishing a high-resolution U-Th chronology by U-series dating of primary aragonite, supported by oxygen isotope stratigraphy, ^{14}C dating and varve chronologies;
- Establishing the palaeomagnetic history of the Dead Sea basin;
- Investigating the relation between human culture development and climatic changes in the region;
- Comparing the sedimentary records of the deep basin with those of the basin margins;
- And studying the history of wind-blown desert dust to the lakes and monitoring palaeo-storm tracks.

DFG-Projects

This dissertation was performed at the Helmholtz Centre Potsdam – GFZ German Research Centre for Geosciences, Section 5.2 Climate Dynamics and Landscape Evolution, within two projects funded by the DFG German Research Foundation in the Priority Program (Schwerpunktprogramm) SPP 1006 International Continental Scientific Drilling Program (ICDP). Both of these projects specifically relate to the ICDP Dead Sea Deep Drilling Project.

Project FR 1672/2-1, entitled *"Holocene dust storms and flood events in the Dead Sea region"*, ran from 2010 to 2012. The main subject of this project was the development of scientific standards for high-resolution analyses of sediments from the Dead Sea and the application of these standards within the ICDP Dead Sea Deep Drilling Project (DSDDP). A combination of petrographic thin section analysis, X-ray fluorescence element scanning and high-resolution magnetic susceptibility measurements was aimed to be applied to identify flood and dust storm layers and to establish Holocene time series of these event deposits. The study was supposed to be carried out mainly on existing core material from the western margin of the Dead Sea (Fig. 1-2). The objectives of this study furthermore included the synchronization of these on-shore sediment sections with their deep-basin counterpart as recovered by the DSDDP.

Project BR 2208/10-1, entitled *"Interglacial climate variability recorded in the Dead Sea sediments"*, was realized from 2012 to 2014. The aim of this project was to reconstruct palaeoclimatological changes in the Dead Sea basin and adjacent areas during the last two interglacials as archived in the ICDP DSDDP sediment cores. Thereby, the scientific standards for high-resolution sediment analyses developed within project FR 1672/2-1 were supposed to be applied to the deep-basin sediment cores in order to enhance our understanding of interglacial climate variability in the eastern Mediterranean region.

The doctoral candidate was responsible for sedimentological and geochemical investigations, as well as for the compilation of composite profiles and inter-site correlation, as requested by the above-described projects. The doctoral candidate participated at the ICDP DSDDP coring campaign for five weeks in winter 2010-11, co-organized and co-supervised the arrival, core opening and sampling campaigns at the GFZ in 2011 and 2012 and arranged the transport of the cores to the storing facility at Marum, Bremen, together with Dr. Markus Schwab and under the leadership of Prof. Achim Brauer.

1.3 Main objectives of the doctoral project

This thesis aims on a detailed reconstruction of past climate changes in the Levant from multi-millennial to centennial, annual and even seasonal time-scales, using high-resolution micro-facies analyses for the Dead Sea sediment record. The main objectives of this thesis are outlined in the following:

i) Providing the lithostratigraphic framework for the long ICDP deep-basin core including correlation to on-shore sediment formations.

ii) Establishing micro-facies analyses of annually laminated sediments by combined thin section microscopy and μXRF measurements as a tool for high-resolution climate reconstruction from the Dead Sea sediments.

iii) Obtaining high-resolution, multi-proxy time-series of extreme events, like floods and dust storms, and deciphering their relation to changing climate conditions in the Dead Sea region for the Holocene.

iv) Reconstructing palaeoclimatic changes in the Dead Sea and adjacent areas during the last two interglacials as archived in the ICDP Dead Sea record.

1.4 Material and methods

Sediment cores

In the frame of the ICDP Dead Sea Deep Drilling Project more than 700 m of sediment cores were recovered from three sites during the drilling campaign in winter 2010-2011 (Chapter 2; Stein et al., 2011). The longest, ca 455 m and ~220,000 years comprising core 5017-1 was retrieved from the deep basin at ~300 m water depth and was lithologically described and correlated to on-shore sediment sections within this study (Chapter 2). A ca 13 m long section of the Holocene Ze'elim Formation of the core was investigated in more detail in comparison to a sediment core from the western margin (Chapter 4). As a second section of interest for higher resolution analyses, a ca 60 m long section as part of the last interglacial/early last glacial Samra Formation was investigated (Chapter 3). Furthermore, a ca 12 m long section of the upper last glacial Lisan Formation was sampled and measured for μXRF (Appendix A3); investigations are ongoing.

The sediment cores DSEn (Ein Gedi), DSF (Ein Feshkha) and DSZ (Ze'elim) from the western margin of the Dead Sea (Fig. 1-2) were obtained during a drilling campaign in 1997 and were available for this study. These sediment cores have been investigated within the scope of a doctoral work by C. Migowski (2001), who analysed the laminated sediments and established the palaeoseismic and palaeoclimatic history of the Holocene Dead Sea (Migowski et al., 2004; 2006). Cores DSF and DSZ feature both fluvial and lacustrine sediments and exhibit major hiatuses. Hence, these cores were not further considered within this doctoral project. For the purpose of high-resolution micro-facies analyses, the DSEn core is most suitable as it continuously presents mainly lacustrine sediments that were proposed to be varved, i.e. annually laminated, in some parts (Migowski, 2001). An updated radiocarbon-based age model for the ca 21 m long DSEn core, using the IntCal13 calibration curve (Reimer et al., 2013) and a

P-sequence deposition model (Bronk Ramsey, 2008), is provided in the Appendix (A2). A ca 3 m long, mostly varved section of this core was analysed in greater detail and correlated to the deep-basin core 5017-1 (Chapter 4).

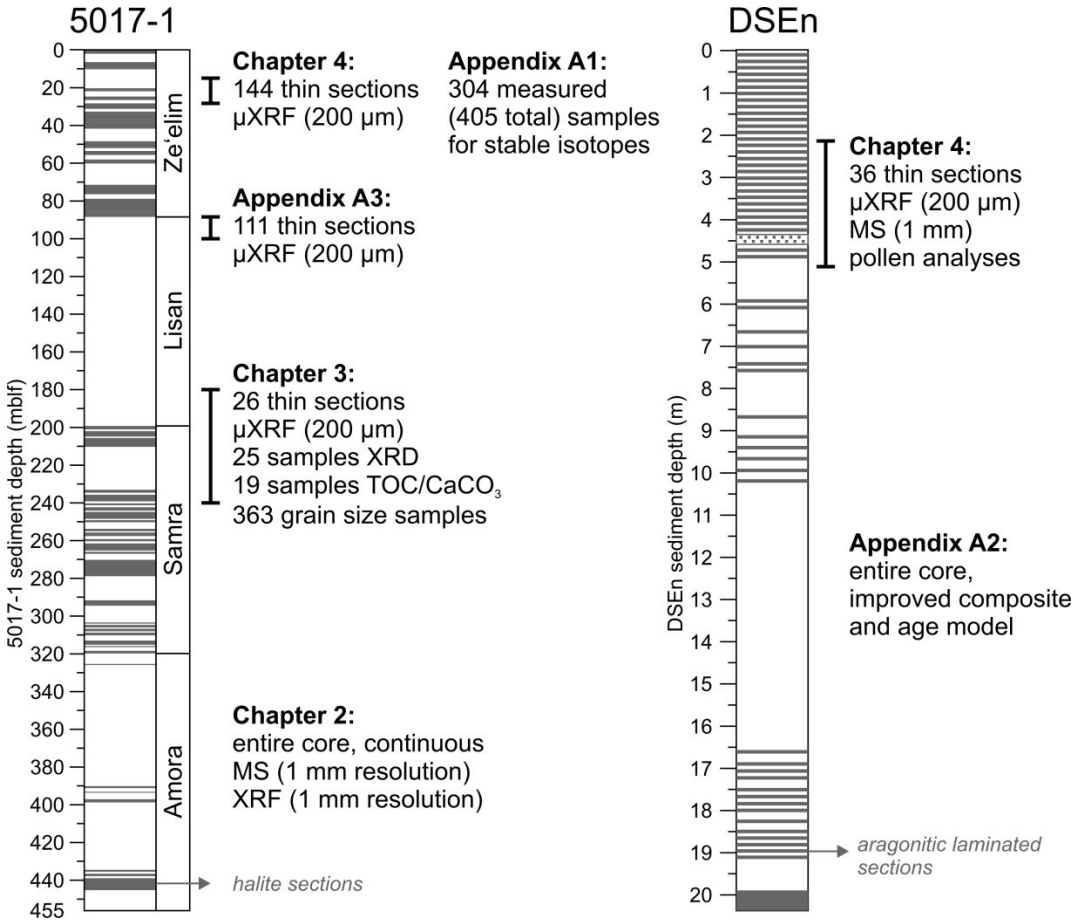

Figure 1-3: Overview about the sampling strategy for the deep-basin core 5017-1 and core DSEn from the western margin, which comprises the Holocene Ze'elim Formation; marked are the related chapters in this thesis; MS – magnetic susceptibility.

Micro-facies analyses

For analysing the Dead Sea sediments at high resolution, a combination of petrographic thin section microscopy and µXRF element scanning was applied, supported by magnetic susceptibility measurements. This combined methodological approach is referred to as 'micro-facies analyses'. Given a varved nature of the investigated sediments, this approach allows interpreting seasonal palaeoclimate signals including extreme events and the dynamics of abrupt climate changes (Brauer et al., 2009).

Within the project, a total of 281 thin sections from the 5017-1 composite core and 36 thin sections from the DSEn composite core were prepared (Fig. 1-3). The preparation of the 10 cm long thin sections followed the standard procedure for soft sediments (e.g. Brauer et al., 1999b)

including freeze-drying of the sediment blocks and impregnation with epoxy resin. However, to avoid salt crystallisation during the preparation process, all further steps, i.e. sawing and polishing, had to be carried out without using any liquids. Final polishing was done manually to adjust the thickness of the thin section, when the sediment grain size was heterogeneous.

For a geochemical characterisation of the Dead Sea sediments, the split-core sediment surface was measured using an ITRAX μXRF spectrometer available at the GFZ. Details of this method are provided in Chapters 2 to 4. Continuous XRF element scanning data with 1 mm resolution were obtained for all 5017 core sections, whereas high-resolution μXRF scanning was only performed for specific intervals of cores 5017-1 and DSEn (Fig. 1-3). Magnetic susceptibility was measured for all cores investigated in this project.

Further methods

Beneath micro-facies analyses, further methods were applied within this project, which are described in detail in the respective manuscripts or in the Appendix. These methods include:

- Stable oxygen and carbon isotope measurements of single aragonite and detrital laminae; see Appendix A1;
- Grain size measurements; see Chapter 3;
- X-ray diffraction (XRD), TOC and $CaCO_3$ measurements; see Chapter 3
- Age modelling with OxCal 4.2; see Chapter 4 and Appendix A2.

1.5 Thesis structure

This cumulative thesis is based on three manuscripts that are or are to be published in peer-reviewed international journals (Chapters 2 to 4). The doctoral candidate is the leading author of all three manuscripts. One manuscript (Chapter 2) has been published, the second manuscript is under review (Chapter 3) and the third is accepted (Chapter 4). The thesis is structured according to these manuscripts. The main conclusions of the thesis and future perspectives are drawn in Chapter 5. A summary of the three manuscripts and the contribution of the doctoral candidate to these publications is provided in the following:

Manuscript #1 (Chapter 2)

Title: Lithology of the long sediment record recovered by the ICDP Dead Sea Deep Drilling Project (DSDDP)

Authors: Ina Neugebauer, Achim Brauer, Markus J. Schwab, Nicolas D. Waldmann, Yehouda Enzel, Hiroyuki Kitagawa, Adi Torfstein, Ute Frank, Peter Dulski, Amotz Agnon, Daniel Ariztegui, Zvi Ben-Avraham, Steven L. Goldstein, Mordechai Stein, DSDDP Scientific Party

Published in Quaternary Science Reviews 102, 2014 (http://dx.doi.org/10.1016/j.quascirev.2014.08.013).

This paper provides an overview about the ICDP DSDDP project and aims on introducing the lithology and basic geochemical characteristics of the ~455 m long sediment record 5017-1 from the deep Dead Sea basin. Based on preliminary dating and correlation of the main sediment formations to on-shore deposits, core 5017-1 comprises the last ~220,000 years and, hence, two glacial-interglacial cycles. This paper serves as a base for any further higher resolution studies of the deep core.

The doctoral candidate was the leading author and contributed ca 75% to this paper. She compiled the composite profile, described the lithology, evaluated all data and wrote the manuscript. H. Kitagawa and A. Torfstein provided radiocarbon and U-Th ages, respectively, and U. Frank and P. Dulski were in charge of continuous magnetic susceptibility and XRF measurements, respectively. All other co-authors act as principal investigators of the ICDP DSDD Project and/or have profound knowledge about the sedimentology of the Dead Sea basin and as such contributed through proof-reading and discussions to the manuscript, especially A. Brauer and M. Stein.

Manuscript #2 (Chapter 3)

Title: Hydroclimatic variability during the early last glacial (~117-75 ka) derived from micro-facies analyses of the Dead Sea ICDP sediment record

Authors: Ina Neugebauer, Markus J. Schwab, Nicolas D. Waldmann, Rik Tjallingii, Ute Frank, Elitsa Hadzhiivanova, Rudolf Naumann, Nimer Taha, Amotz Agnon, Yehouda Enzel, Achim Brauer, DSDDP Scientific Party

Submitted to Climate of the Past (under review).

This paper deals with the climate history of the Dead Sea during the early last glaciation from ~117 to 75 thousand years before present; a period that was so far poorly understood due to the lack of continuous sediment records in this region. Detailed micro-facies analyses of the respective sediment section from the 5017-1 core allowed reconstructing the hydroclimatic conditions at the lake in terms of relative lake level and water balance changes. The main conclusion drawn from this study proposes a persistent moisture supply from the Atlantic-Mediterranean system to the eastern Mediterranean-Levant during this interval.

The doctoral candidate was the leading author of this paper with a contribution of ca 70%. Thin section and μXRF analyses, the evaluation of all other data and writing of the manuscript was carried out by the doctoral candidate. N.D. Waldmann, E. Hadzhiivanova and N.Taha performed grain size measurements, R. Tjallingii contributed to the interpretation of μXRF data, U. Frank was responsible for magnetic susceptibility measurements and R. Naumann was in charge of XRD measurements. M.J. Schwab, N.D. Waldmann, A. Agnon, Y. Enzel and A. Brauer contributed through proof-reading and discussions.

Manuscript 3 (Chapter 4)

Title: Evidences for centennial dry periods at ~3300 and ~2800 years BP from micro-facies analyses of the Dead Sea sediments

Authors: Ina Neugebauer, Achim Brauer, Markus J. Schwab, Peter Dulski, Ute Frank, Elitsa Hadzhiivanova, Hiroyuki Kitagawa, Thomas Litt, Vera Schiebel, Nimer Taha, Nicolas D. Waldmann, DSDDP Scientific Party

Accepted for publication in The Holocene.

This paper focusses on two centennial-scale dry periods in the Dead Sea region during the late Holocene, from ca 3700 to 1700 cal BP. For the purpose of detailed reconstruction of climatic fluctuations and related changes in the frequency of extreme flood and dust deposition events, an annually laminated sequence from the western-shore DSEn record was compared with its deep-basin counterpart from the ICDP core 5017-1. A combination of high-resolution thin section microscopy and μXRF element scanning, supported by palynology, allowed constructing a varve chronology for this interval and detecting single event layers. The main outcome of this study is that dry conditions around 2800 years BP, which coincide with the Homeric Grand Solar Minimum, were superimposed by an increased occurrence of flash-floods most likely caused by a change in synoptic weather patterns.

The doctoral candidate was the leading author and contributed ca 80% to this paper. She compiled the age models and the varve chronology, performed micro-facies analyses, evaluated all other data and wrote the manuscript. P. Dulski supervised the μXRF measurements, U. Frank provided magnetic susceptibility data, E. Hadzhiivanova and N. Taha provided some grain size data, H. Kitagawa measured samples for radiocarbon dating of core 5017-1, and Th. Litt and V. Schiebel analysed pollen samples. A. Brauer, M.J. Schwab and N.D. Waldmann contributed through proof-reading and discussions.

2 Lithology of the long sediment record recovered by the ICDP Dead Sea Deep Drilling Project (DSDDP)

Ina Neugebauer [a, *], Achim Brauer [a], Markus J. Schwab [a], Nicolas D. Waldmann [b, c], Yehouda Enzel [d], Hiroyuki Kitagawa [e], Adi Torfstein [d, f], Ute Frank [a], Peter Dulski [a], Amotz Agnon [d], Daniel Ariztegui [g], Zvi Ben-Avraham [h, i], Steven L. Goldstein [j], Mordechai Stein [k], and DSDDP Scientific Party [#]

a Helmholtz Centre Potsdam, GFZ German Research Centre for Geosciences, Section 5.2 – Climate Dynamics and Landscape Evolution, Telegrafenberg, D-14473 Potsdam, Germany
b Department of Marine Geosciences, Leon H. Charney School of Marine Sciences, University of Haifa, Mount Carmel 31905, Israel
c Department of Earth Science, University of Bergen, Allégaten 41, Bergen 5007, Norway
d The Fredy & Nadine Herrmann Institute of Earth Sciences, The Hebrew University of Jerusalem, Givat Ram, Jerusalem 91904, Israel
e Graduate School of Environmental Studies, Nagoya University, Chikusa-ku, Nagoya 464-8601, Japan
f The Interuniversity Institute for Marine Sciences of Eilat, Eilat 88103, Israel
g Department of Earth Sciences, University of Geneva, Rue des Maraichers 13, CH-1205 Geneva, Switzerland
h Department of Geophysical, Atmospheric and Planetary Sciences, Tel Aviv University, Tel Aviv 69978, Israel
i Leon H. Charney School of Marine Sciences, University of Haifa, Mount Carmel 31905, Israel
j Lamont-Doherty Earth Observatory and Department of Earth and Environmental Sciences, Columbia University, 61 Route 9W, Palisades, NY 10964, USA
k Geological Survey of Israel, 30 Malkhe Israel St., Jerusalem 95501, Israel
The complete list of scientists involved in the DSDDP can be found at http://www.icdp-online.org

Published in Quaternary Science Reviews (http://dx.doi.org/10.1016/j.quascirev.2014.08.013)

Abstract

The sedimentary sections that were deposited from the Holocene Dead Sea and its Pleistocene precursors are excellent archives of the climatic, environmental and seismic history of the Levant region. Yet, most of the previous work has been carried out on sequences of lacustrine sediments exposed at the margins of the present-day Dead Sea, which were deposited only when the lake surface level rose above these terraces (e.g. during the last glacial period) and typically are discontinuous due to major lake level variations in the past. Continuous sedimentation can only be expected in the deepest part of the basin and, therefore, a deep drilling has been accomplished in the northern basin of the Dead Sea during winter of 2010-2011 within the Dead Sea Deep Drilling Project (DSDDP) in the framework of the ICDP program. Approximately 720 m of sediment cores have been retrieved from two deep and several short boreholes. The longest profile (5017-1), revealed at a water depth of ~300 m, reaches 455 m below the lake floor (blf, i.e. to ~1175 m below global mean sea level) and comprises approximately the last 220-240 ka. The record covers the upper part of the Amora (penultimate glacial), the last interglacial Samra, the last glacial Lisan and the Holocene Ze'elim Formations and, therewith, two entire glacial-interglacial cycles. Thereby, for the first time, consecutive sediments deposited during the MIS 6/5, 5/4 and 2/1 transitions were recovered from the Dead Sea basin, which are not represented in sediments outcropping on the present-day lake shores. In this paper, we present essential lithological data including continuous magnetic susceptibility and geochemical scanning data and the basic stratigraphy including first chronological data of the long profile (5017-1) from the deep basin. The results presented here (a) focus on the correlation of the deep basin deposits with main on-shore stratigraphic units, thus providing a unique comprehensive stratigraphic framework for regional paleoenvironmental reconstruction, and (b) highlight the outstanding potential of the Dead Sea deep sedimentary archive to record hydrological changes during interglacial, glacial and transitional intervals.

Keywords

Sediment facies; laminated sediments; hypersaline lakes; ICDP Dead Sea Deep Drilling Project; Levant paleoclimate.

2.1 Introduction

The hypersaline and terminal Dead Sea is situated at the lowermost exposed place on Earth. It is located between the Mediterranean climate zone and the Sahara-Arabian desert belt. The location near the Sinai-Negev land bridge between Africa and Asia provides a key geographical setting along the pathway of humankind migration out of Africa. The lake occupies the Dead Sea basin (DSB), which is a pull-apart structure with steep escarpments to the east and west and flat extensions into the Arava and Jordan valleys to the south and north, respectively. During the Quaternary, the basin has been occupied by several different terminal water-bodies, which responded to hydro-climate conditions in their large watershed (e.g. Bentor, 1961; Neev and Emery, 1967; Begin et al., 1974; Stein et al., 1997). In consequence, the lake's composition, limnological structure and surface levels have strongly fluctuated through time resulting in pronounced changes in surface areas and served as proxies for past climate reconstructions. The maximum known N-S extent (>270 km) was achieved during the last glacial maximum (LGM), when Lake Lisan extended northward over the Jordan and Beisan valleys and merged with the freshwater Sea of Galilee (Fig. 2‑1b; e.g. Begin et al., 1974; Neev and Emery, 1995; Stein et al., 1997; Stein, 2001; Bartov et al., 2003).

The DSB and its infilling sediments offer the possibility to address a wide range of geoscientific challenges, spanning from seismicity and magnetism along the Dead Sea Transform fault to environmental and climatic reconstructions of the Levantine region. Already in the middle of the 19th century, the bathymetry of the lake was determined (Lynch, 1849), followed by first monitoring and drilling attempts and chemical analyses of the water body in the 1930s and 1940s (Niemi et al., 1997 and references therein). A pioneering step forward in Dead Sea research was achieved in the 1960s, when Neev and Emery (1967) conducted a comprehensive survey to sample and analyze the brine and sediments. In the last decades, Dead Sea research, summarized in Niemi et al. (1997) and Enzel et al. (2006), has been focused on sediments from the Amora, Samra, Lisan and Ze'elim Formations, which are currently exposed in the surroundings of the Dead Sea. These records mirror past hydro-climatic changes from glacial-interglacial scale down to seasonal resolution (e.g. Machlus et al., 2000; Bookman (Ken-Tor) et al., 2004; Haase-Schramm et al., 2004; Prasad et al., 2004; Migowski et al., 2006; Torfstein et al., 2009; Waldmann et al., 2009; Torfstein et al., 2013a; 2013b). Yet, these reconstructions are often interrupted by depositional gaps at times when lake levels rapidly decreased during dry periods and due to transgressive erosion during lake level rises (e.g. Bartov et al., 2007). Previous attempts to recover continuous sediment sequences from the present lake bottom were hampered by the presence of thick salt intervals and only short sequences covering the last few thousand years have been revealed (e.g. Heim et al., 1997; Ben-Avraham et al., 1999).

Through the International Continental Scientific Drilling Program (ICDP), an international team of scientists aimed at recovering the past several glacial-interglacial cycles in a continuous high-resolution sediment core from the Dead Sea deep basin. Main research goals of the Dead Sea Deep Drilling Project (DSDDP) include reconstructing the environmental, climatic and tectonic

history of the region, with high-resolution chronologies established by AMS radiocarbon and U-series dating (Stein et al., 2011), complemented by varve counting of selected sequences.

The main focus of this study is to document the lithology and stratigraphy of the 455 m long core from the northern deep DSB (site 5017-1, water depth of ~300 m) and provide first insights into the exceptionally heterogeneous sediment succession proving the sensitivity of sediment deposition in the DSB to environmental and hydrological changes in the past. Together with ongoing efforts to construct a precise chronology for this sediment record, the data presented here will serve as a robust framework for all future, more detailed and high-resolution investigations. In addition, the new cores from the deep basin are tied to the stratigraphies reported from onshore environments as a first step for detailed comparison of shallow and deep water sedimentary environments.

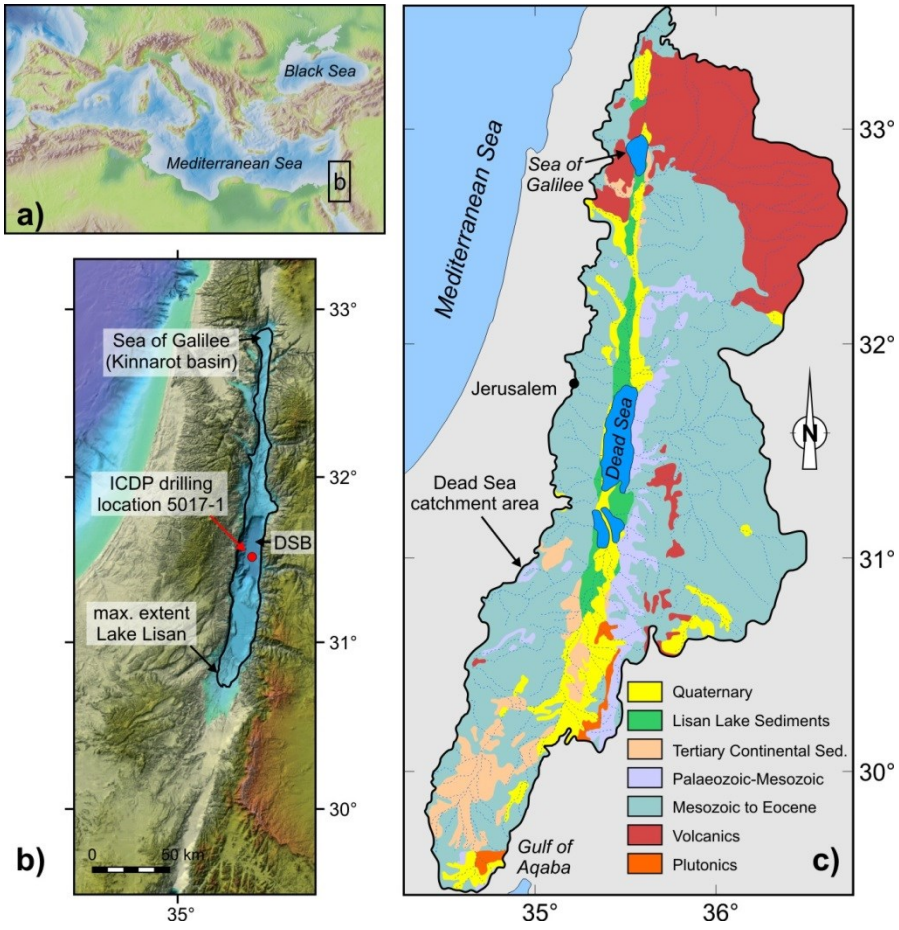

Figure 2-1: a) Location of the Dead Sea in the Levant and Eastern Mediterranean; b) shaded relief image of the central Levant (modified after Hall, 1997), black line: maximum extent of the last glacial Lake Lisan (from Bartov et al., 2002), red point: deep drilling location 5017-1, ~300 m water depth, light green to blue colors indicate areas below mean sea level, DSB: Dead Sea basin; c) main geological units exposed in the Dead Sea catchment area (modified after Bentor, 1961).

2.2 The late Neogene Dead Sea basin infill

During late Neogene times Mediterranean Sea water entered the Jordan-Dead Sea tectonic depression possibly via the Jezreel Valley and formed the Sedom Lagoon (Zak, 1967; Belmaker et al., 2013). Long sequences of salt, intercalated by gypsum, anhydrite, dolomite and some detrital marl were deposited in the lagoon (Sedom Formation, e.g. Neev and Emery, 1967; Zak, 1967). The ingressing evaporated seawater interacted with the Cretaceous limestone that comprises the basin wall producing the Ca-chloride brine that played a major role in the geochemical history of the Dead Sea water bodies and for the deposited sediments (Stein, 2001). After the disconnection of the Sedom Lagoon from the Mediterranean Sea, a series of lacustrine water-bodies evolved in the basin (for a comprehensive overview see Stein, 2001; 2014): the early to middle Pleistocene Lake Amora (Amora Fm.; Torfstein et al., 2009), the last interglacial Lake Samra (Samra Fm. ~135-70 ka; Kaufman et al., 1992; Bartov et al., 2007; Waldmann et al., 2009), the last glacial Lake Lisan (Lisan Fm. ~70-14 ka; e.g. Stein et al., 1997; Bartov et al., 2002; Haase-Schramm et al., 2004; Torfstein et al., 2013a; 2013b) and the Holocene Dead Sea (e.g. Yechieli et al., 1993; Bookman (Ken-Tor) et al., 2004; Migowski et al., 2006), accumulating the Ze'elim Formation. These sedimentary sequences in the DSB vary significantly in their composition showing a direct connection to the lake's limnological properties (Stein et al., 1997; Stein, 2001) and particular relationships with regional precipitation and atmospheric circulation (Enzel et al., 2008). During more humid climatic conditions annually laminated (varved) primary aragonite and silty detritus couplets described as ***aad*** facies (alternating aragonite and detritus; Neev and Emery, 1967; Begin et al., 1974; defined by Machlus et al., 2000) have been deposited in the basin and are indicative for positive freshwater input providing the bi-carbonate ions required for aragonite deposition from the bi-carbonate poor Ca-chloride brine (Stein et al., 1997). The ***aad*** facies characterizes the relatively high lake level stages during the glacial Amora and Lisan Formations. Aragonite precipitated in the water column during dry season evaporation, while the silty detritus (calcite, quartz and clay minerals) has been washed into the lake by flash-floods during the rainy season (Stein et al., 1997; Haliva-Cohen et al., 2012). Occasionally, primary gypsum was deposited in large amounts during discrete episodes of pronounced lake level decline (Torfstein et al., 2005; 2008). The Samra and Ze'elim Formations in the exposed sections are predominantly constituted of silty detritus layers or laminae of the ***ld*** facies (Haliva-Cohen et al., 2012), couplets of the ***aad*** facies and triplets of silty detritus, aragonite and gypsum (described by Migowski et al., 2004; 2006) with occasional intercalations of coarse clastic fan-deltas and shore deposits (Bartov et al., 2002). These deposits reflect shallow water environments during periods of low-stands of the lake during arid interglacial climates, when the supply of bi-carbonate to the lake was limited (Stein, 2001; Waldmann et al., 2007). The aragonite-silty detritus couplets and the aragonite-gypsum-silty detritus triplets were counted in specific sequences of the drilled littoral cores of the Ze'elim Formation and combined with radiocarbon ages were interpreted as annual sequences (Migowski et al., 2004). This interpretation confirmed earlier investigations from the only, up to 4.4 m long sediment cores that were recovered from the Dead Sea lake bottom before the DSDDP ICDP drilling (Heim et al.,

1997). Heim et al. (1997) described in these cores alternations of halite and short intervals of finely laminated sediments consisting of similar aragonite, gypsum and detrital marl sub-layers, which they interpreted as evaporitic varves.

2.3 Regional setting

The Dead Sea occupies the deepest continental pull-apart basin of a series of structures along the Dead Sea Transform fault, which is an active left lateral tectonic system separating the Sinai and Arabian plates (Quennel, 1958; Garfunkel and Ben-Avraham, 1996 and references therein). The lake is located at the lowest exposed site on earth, with a current (2013) level of 427 m below mean sea level (bmsl). However, due to the intense utilization of water for irrigation and consumption purposes from both the Jordan and Yarmouk rivers, levels have greatly descended since 1978 at an average rate of 0.7 m/yr (Abu Ghazleh et al., 2009) and since 1996 have even accelerated to ~1 m/yr (Lensky et al., 2005). The hypersaline Dead Sea is an endorheic lake, mainly fed from the north by the perennial Jordan River, the Mujib River coming from the east and several ephemeral fluvial systems from the Jordan Plateau and Judean Mountains, on the east and west, respectively (e.g. Enzel et al., 2003; Greenbaum et al., 2006). This hydrological situation creates one of the largest catchment areas in the Levantine region (~40,000 km²; Bentor, 1961; Fig. 2‑1c).

The lake's catchment area encompasses several climate zones spanning from subhumid-semiarid Mediterranean climate in its northern part to the Sahara-Arabian arid-hyperarid belt in its south. In this geographical configuration there is significant precipitation during northern hemisphere winters (October-May) through eastern Mediterranean mid-latitude cyclones (Cyprus Lows; Enzel et al., 2003; Ziv et al., 2006) and occasional incursions of the Active Red Sea Trough. The latter, a surface trough extending from East Africa through the Red Sea towards the eastern Mediterranean, brings moisture also from the tropics and promotes flash-floods mainly during fall and winter seasons (Kahana et al., 2002; Dayan and Morin, 2006).

The exposed geological formations within the drainage area include: a) Late Proterozoic granites and metamorphic rocks of the Arabian-Nubian Shield (ANS), b) Phanerozoic limestones, sands and marls that were deposited in platformic environment overlying the ANS crystalline basement, c) Tertiary marine and continental sediments in the southwest, d) Quaternary sand, gravel, conglomerates, marl, sandstone and evaporites in the Jordan and Arava valleys, and e) alkali basalt of mainly Neogene to Quaternary age erupted in the north and northeast (Shaliv, 1991; Heimann et al., 1996; Sneh, 1998; Fig. 2‑1c). The dominant rock types exposed in the catchment are Mesozoic to Cenozoic marine sediments (mainly limestone and dolomite). Yet, while the freshwater entering the lake discharges from aquifers located within these lithologies and reflect them in their chemical and isotope properties (Stein et al., 1997), most of the fine detrital sediments in the lakes formations were derived from desert dust that has settled on the mountain relief washed into the lake by runoff and floods (Belmaker et al., 2011; Haliva-Cohen et al., 2012; Belmaker et al., 2013). Thus, the lake sediments provide information on both the regional aquifers and far distant sources of the desert dust (Palchan et al., 2013).

2.4 Methods

2.4.1 Drilling campaign

Drilling in the deep northern Dead Sea basin was carried out with the Deep Lake Drilling System (DLDS) between November 2010 and March 2011 operated by the non-profit corporation DOSECC (Drilling, Observation and Sampling of the Earth's Continental Crust). The drill platform (Atlas Copco T3WDH) is a top-head-drive rotary rig. Two different drilling operations have been applied according to the expected lithology; (i) the rotating extended core bit (termed 'Alien') has been used for hard salt sequences, while (ii) the hydraulic piston core tool (HPC) was deployed to core soft sediment intervals. Guar gum powder (an organic polymer acting as viscosifier) served as the drilling fluid when mixed with surface lake water that is generally characterized by ~300-340 g/l salinity and winter temperatures of ~16-23 ˚C for the period from 1992 - 1999 (Gertman and Hecht, 2002; Katz and Starinsky, 2009).

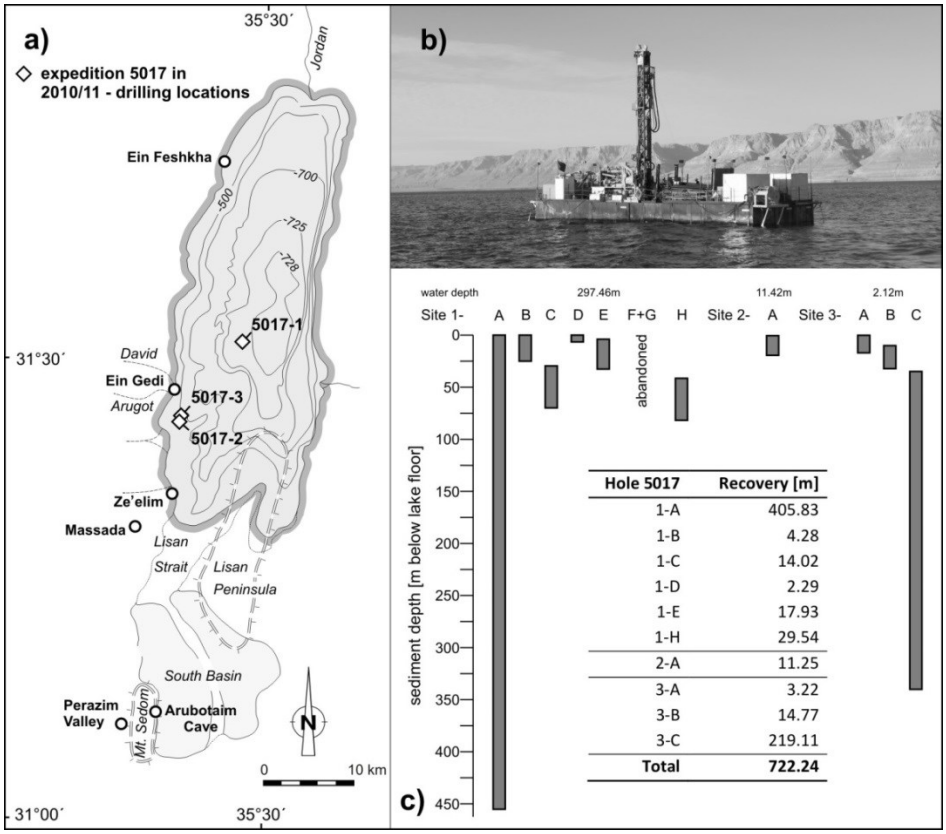

Hole 5017	Recovery [m]
1-A	405.83
1-B	4.28
1-C	14.02
1-D	2.29
1-E	17.93
1-H	29.54
2-A	11.25
3-A	3.22
3-B	14.77
3-C	219.11
Total	**722.24**

Figure 2-2: a) Bathymetric map of the Dead Sea (modified after Neev and Hall, 1979) and drilling locations of the ICDP Dead Sea Deep Drilling Project (DSDDP; expedition 5017), further marked are selected shallow-water drilling and exposure locations of the Dead Sea sediments: Ein Feshkha, Ein Gedi and Ze'elim covering the Holocene Ze'elim Fm. (e.g. Bookman (Ken-Tor) et al., 2004; Migowski et al., 2006), last glacial Lisan Fm. exposed sections at Massada and Perazim Valley (e.g. Stein et al., 1997; Bartov et al., 2002), the latter also covering the last interglacial Samra Fm. (Waldmann et al., 2009), and the early to late Pleistocene Amora Fm. at Arubotaim Cave (Torfstein et al., 2009); b) the DSDDP drilling was performed by DOSECC (Drilling, Observation and Sampling of the Earth's Continental Crust) with the Deep Lake Drilling System (DLDS; photo: © OSG-GFZ, ICDP); c) overview about the recovered sediment cores from all holes of sites 5017-1, -2 and -3.

2.4.2 Coring locations

Details about the three drilling locations and core recoveries are shown in Table 2-1 and Figure 2-2. This study concentrates on the sediment record of the deepest borehole at site 5017-1 close to the deepest point of the basin. Based on geophysical investigations (Coianiz et al., 2013) this site was expected to represent the most complete sediment sequence. In addition, it is located most distal with respect to turbidity currents and slope instability features. The second coring site 5017-2 was selected at a near-shore location in a shallow bay (11.4 m water depth). The third drilling location 5017-3 was located near the second site but even closer to the shore at 2.1 m water depth. Both shallow sites are situated off the Ein Gedi spa shore, where several cores recovering the Holocene, Lateglacial and top glacial time intervals were retrieved earlier (Migowski et al., 2004; 2006; Stein et al., 2010).

In total ~720 m of sediment cores have been retrieved from all three drilling sites. The longest core sequence reaching 455 m sediment depth (~750 m below the 2010 Dead Sea lake level; 1175 m below mean sea level) was drilled at borehole 5017-1-A. Parallel to this long sequence, five additional but shorter cores were retrieved: holes 5017-1-B, 5017-1-C, 5017-1-D, 5017-1-E and 5017-1-H. At coring site 5017-2 a ~19 m long core was drilled, while the longest core taken at site 5017-3 reached a length of ~271 m (borehole 5017-3-C).

Table 2-1: Depths and core recoveries of the Dead Sea Deep Drilling Project; m bll = meter below lake level, m blf = meter below lake floor.

	water depth [m]	top depth [mbll]	top depth [mblf]	bottom depth [mblf]	total drilled length [m]	core recovery [m]	core recovery [%]
Site 5017-1 (N 31°30'28.98", E 35°28'15.60")							
A	297.46	297.46	0	455.34	455.34	405.83	89.13
B	297.46	297.46	0	24.39	24.39	4.28	17.53
C	297.46	328.03	30.57	68.65	38.08	14.37	37.74
D	297.46	297.46	0	5.15	5.15	2.32	45.05
E	297.46	300.55	3.09	32.00	28.91	17.93	62.02
H	297.46	337.13	39.67	81.36	41.69	29.57	70.93
Site 5017-2 (N 31°25'13.998", E 35°23'38.4")							
A	11.42	11.42	0	19.28	19.28	11.25	58.35
Site 5017-3 (N 31°25'22.74", E 35°23'39.58")							
A	2.12	2.35	0.23	16.63	16.40	3.22	19.63
B	2.12	11.32	9.20	31.47	22.27	14.77	66.32
C	2.12	36.69	34.57	339.45	270.93	219.11	80.87
				Total	**922.44**	**722.65**	**78.34**

2.4.3 Downhole logging and on-site core handling

Downhole logging was conducted by the ICDP Operational Support Group with special slimhole logging probes (max. outer diameter = 52 mm) for geophysical measurements in small-scale drill holes with 10 cm sampling rate. Magnetic susceptibility data of borehole 5017-1-A are presented here (Fig. 2-5). The data processing of other measured parameters, e.g. natural gamma ray and resistivity, is in progress and the results will be discussed elsewhere.

Information about each core, section lengths, core-catchers and respective depths have been supplied to the on-site Drilling Information System (DIS) Internet database interface platform facilitated by ICDP Germany. The cores were kept at 4˚C in the GFZ Potsdam cold storage during the core opening and sampling party and afterward transported to the final storage at the MARUM – IODP Bremen Core Repository (Germany).

2.4.4 Core opening and non-destructive analyses

After splitting of the cores several non-destructive analyses were carried out in the GFZ Potsdam laboratories on all cores, including visual description, optical line scanning, magnetic susceptibility analyses and µXRF element scanning. Magnetic susceptibility measurements at 1 mm resolution were carried out on one core half using a Bartington MS2E sensor, while the other half was scanned with the ITRAX core scanner (COX Analytical Systems) to determine element compositions. We applied a Chromium tube at 30 kV voltage and 30 mA current, which is particular sensitive for the lighter elements. The standard reference sample SCo-1 USGS cody shale and an internal reference glass provided by COX Analytical Systems were measured on a daily basis for quality control approx. every 10 measured meters. The aim of µXRF element scanning was to provide a quick overview about element compositions at 1 mm resolution so that a very short exposure time of 1 s has been chosen instead of common exposure times between 10 and 30 s. Obviously, the reduced exposure time can only be used for preliminary interpretation and does not replace detailed analyses and calibration. Here, we selected elements with sufficient count rates including Si, S, Cl, K, Ca, Ti, Fe and Sr as main indicator elements for major mineralogical variations of the Dead Sea sediments. Elements with lower count rates like Mg, Al, or Zr were not further considered. Also not considered was Mn due to the overlap of the major Mn peak with that of Cr from the X-ray tube. µXRF scanner data are given as count rates (cps = counts per second).

2.4.5 Chronology of the core

The establishment of a robust chronology for sediment records is a major task for every paleoclimate and paleoenvironmental study. The efforts to establish such a chronology for the exposed sequences of the Dead Sea lacustrine formations continues now for more than two decades applying radiocarbon (e.g. Yechieli et al., 1993; Neev and Emery, 1995; Ken-Tor et al., 2001), U-Th dating (e.g. Kaufman, 1971; 1993; Schramm et al., 2000; Haase-Schramm et al., 2004; Torfstein et al., 2009; 2013a; 2013b) and floating $\delta^{18}O$ stratigraphy methods (Torfstein et

al., 2009; 2013a), reviewed by Stein and Goldstein (2006) and Stein (2014). Here, we briefly report on the ongoing efforts to establish an age-depth model for the long sediment record from the deep basin and provide a few data points in support of our stratigraphic framework.

2.4.5.1 Radiocarbon dating

For radiocarbon age determination 109 samples have been selected from the 5017-1 profile (101 macro-plant fossils, eight bulk sediment samples). In this study, the first set of eleven ^{14}C dates obtained from terrestrial plant remains is presented (Table 2-2). The samples were processed by a standard acid-alkali-acid (AAA) treatment (Mook and Streurman, 1983). The pretreated sample was combusted in a vacuum-sealed quartz tube with copper oxide, and then the CO_2 produced was reduced to graphite by a standard hydrogen reduction method using iron catalytic powder at Nagoya University (Japan). The ^{14}C measurements have been performed at the Center for Chronological Research at Nagoya University (laboratory code NUTA2) and the W.M. Keck Carbon Cycle Accelerator Mass Spectrometry Laboratory (laboratory code UCIAMS) at the University of California-Irvine. A piece of wood collected from 348.3 m blf (5017-1-A core) was adopted as ^{14}C-free materials for the blank correction. The ^{14}C dates were calibrated using OxCal 4.2 (Bronk Ramsey, 2009) and the northern hemisphere atmospheric ^{14}C calibration dataset IntCal13 (Reimer et al., 2013). The ^{14}C data are summarized in Table 2-2.

2.4.5.2 Time scale beyond radiocarbon dating

The age-depth model of the core beyond the radiocarbon range is based on a combination of U-Th dating of the primary aragonite deposited from the lake water and oxygen isotope stratigraphy (Torfstein et al., 2015). Since earlier U-Th chronologies of the Lisan Fm. aragonites required correction for the presence of detrital U and Th and hydrogenic Th (Stein and Goldstein, 2006 and references therein), the same corrections have been applied for the U-Th chronology of core 5017-1 (Torfstein et al., 2015). In this study we include only three ages from this age-depth model (Table 2-2) placed at important lithological changes in order to provide further support for our stratigraphic interpretation and correlation to the exposed terraces of the Amora (Torfstein et al., 2009), Samra (Waldmann et al., 2009) and Lisan (Haase-Schramm et al., 2004) Formations. Therefore, a detailed discussion of the entire age-depth model is beyond the scope of this paper and presented elsewhere (see Torfstein et al., 2015 for details).

Table 2-2: Dating: a) AMS ^{14}C dating of the deep 5017-1 core; all data were calibrated with OxCal 4.2 (Bronk Ramsey, 2009) and the IntCal13 atmospheric calibration curve (Reimer et al., 2013); note that sample AMS-6 is out of the IntCal13 calibration range and needs to be considered with caution; b) preliminary U-Th ages of core 5017-1.

a) radiocarbon dating

core	sample-ID	lab-code	depth		^{14}C age	range of calibrated ^{14}C age		median
5017-1-	(DSDDP)	NUTA2-*UCIAMS*-[a]	section cm[b]	m blf[c]	BP ± 1σ	68.2%	95.4%	cal BP
E-5-H-1	AMS-72	19875	61	10.92	1290 ± 40	1184-1280	1090-1298	1232 ± 44
A-7-H-2	AMS-16	*110316*	96	16.54	1985 ± 15	1898-1949	1892-1988	1931 ± 25
E-19-A-1	AMS-14	*110343*	18.3	26.86	3500 ± 15	3724-3829	3710-3835	3770 ± 36
A-25-A-1	AMS-62	19871	93	43.75	5870 ± 45	6645-6741	6561-6792	6692 ± 56
A-31-A-1	AMS-67	19855	108.5	60.11	7525 ± 50	8314-8402	8203-8413	8348 ± 57
A-43-A-1	AMS-21	19874	77	89.25	9980 ± 50	11,307-11,601	11,253-11,701	11,440 ± 119
A-44-A-1	AMS-20	19858	54	92.06	12,240 ± 57	14,046-14,227	13,963-14,436	14,145 ± 115
A-49-A-2	AMS-28	19870	24.5	108.51	17,360 ± 75	20,810-21,065	20,690-21,216	20,942 ± 131
A-51-A-3	AMS-30	19861	1	115.37	26,046 ± 165	30,114-30,646	29,780-30,769	30,340 ± 261
A-59-A-3	AMS-86	19854	28	139.60	40,250 ± 835	43,165-44,586	42,673-45,431	43,946 ± 717
A-66-A-2	AMS-6	*102378*	28	157.94	53,700 ± 3400	50,310-59,681	48,663-70,224	55,864 ± 5627

b) U-Th dating

sediment depth (m blf)	age ka[d]	remarks
195	75 ± 2	ca 4 m above the SU-II to SU-III boundary
347	150 ± 3	ca 27 m below the SU-I to SU-II boundary
395	199 ± 9	ca 60 m above the base of 5017-1
455	220 ± 10	estimated base of 5017-1, extrapolated

[a] UCIAMS lab codes are given in italics.
[b] Depth from the top of each core section.
[c] Depths from top to 60.11 m blf (sample AMS-67) are given as composite depths, below are depths from core 5017-1-A.
[d] From age-height regression model based on combined U-Th dating and oxygen isotope stratigraphy (Torfstein et al., 2015).

2.5 Results

2.5.1 Sedimentary facies and associated deposits from site 5017-1

2.5.1.1 The marl facies (aad, gd and ld)

Most of the sediments typifying the 5017-1 profile are mainly composed of packages of alternating aragonite and silty detritus of mm to cm scale (***aad***) and sequences of relatively homogeneous marl layers of thicknesses ranging mm to dm scale (***ld*** facies: laminated detritus; Figs. 2-3a and 2-3b; see Table 2-3 and Fig. 2-3 for an overview of all described facies). The ***aad*** facies is made of ~1 mm thick couplets of white aragonite laminae and dark marl laminae composed of calcite, quartz and clay minerals (Stein et al., 1997; Haliva-Cohen et al., 2012). The clay to silt-sized detrital material is commonly of grayish to black color, but greenish gray to dark green sections are found throughout the ***aad*** dominated sediment intervals. Associated with the ***aad*** facies, mm to few cm sized native sulfur concretions (Fig. 2-3d) are scattered at various

specific depths of the core. Interrupting the ***aad*** intervals, well laminated to massive gypsum deposits are found within marl units (***gd*** facies: gypsum and detritus) that can reach up to several cm in thickness (Fig. 2-3c). The ***ld*** facies is characterized by laminated marl of mm to dm thickness, occasionally intercalated by 1-5 mm thick aragonite and gypsum laminae (Fig. 2-3b). The marl predominantly consists of calcite, quartz and different clay minerals and is characterized by a gray, olive, brown or black color.

Table 2-3: Sedimentary facies description of the 5017-1 core (~300 m water depth).

group	facies	description	fig. 2-3
marl facies	***aad***	***a****lternating* ***a****ragonite and silty* ***d****etritus*; ~1 mm thick annual couplets of white aragonite laminae and gray, black or green, clay to silt-sized marl laminae, composed of calcite, quartz and clay minerals; associated are native sulfur concretions (mm-cm)	a, d
	ld	***l****aminated* ***d****etritus*; homogeneous marl layers (mm-dm) of gray, olive, brown or black color, intercalated by aragonite and gypsum laminae (~1-5 mm thick)	b
	gd	***g****ypsum and* ***d****etritus*; massive gypsum layers (1- several cm thick) within clayey-silty marl units	c
halite facies	***lh***	***l****ayered* ***h****alite*; alternations of white-gray fine-grained halite layers (0.2-4 cm), layers of transparent irregular-shaped halite crystals (1-10 mm) and/or thin gray marl laminae (<1 mm)	e, f
	hh	***h****omogeneous* ***h****alite*; transparent irregular-shaped halite crystals within marl matrix	g
	hd	***h****alite and* ***d****etrital* ***m****arl*; cubic halite crystals (mm-cm) scattered within homogeneous marl units	h
massive, graded and slumped deposits	***mtd***	***m****ass* ***t****ransported* ***d****eposits*; homogenites of clay-silt sized marl, can contain coarse base, when graded; deposits with coarse base or intraclast breccia, followed by a light gray middle part and a dark gray clay top; various slumped, folded, brecciated and displaced sediment structures; mm-m thick	k, l, m, n
	htd	***h****alite* ***t****ransported* ***d****eposits*; consolidated fine-grained halite and clayey-silty marl matrix with graded (upwards fining) irregular single halite crystals (mm-cm), some aragonite and gypsum layer fragments and clastic grains (mm)	i
	ccd	***c****oarse* ***c****lastic* ***d****etritus*; gravel beds of 2-10 mm sub-rounded sub-angular limestone, dolomite, halite and minor quartz and feldspar clasts; fining upwards and embedded in clay-silt sized marl; one occurrence of pure homogeneous gravel without finer detritus; rarely coarse gravels up to 35 mm	j

2.5.1.2 The halite facies (lh, hh and hd)

About 20% of the sedimentary record recovered in core sequence 5017-1 consists of consolidated halite that is either layered (***lh*** facies) or homogeneous (***hh*** facies). The layered halite units consist of three types: (1) white to grayish fine-grained halite (0.2-4 cm thick layers) characterized by perfectly µm-sized cubic-shaped crystals, (2) transparent layers made of 1-10 mm sized and irregular-shaped halite crystals, and (3) thin gray marl laminae (typically <1 mm thick), often including different amounts of gypsum. Typically, these layers show an alternating pattern of types 1 + 2 or 1 + 3 couplets, or 1 + 2 + 3 triplets (Figs. 2-3e and 2-3f). The ***hh*** facies is composed of transparent irregular-shaped halite crystals (as in type 2 of the ***lh*** facies) within a detrital matrix (Fig. 2-3g). Furthermore, cubic halite crystals (mm-cm) appear scattered within predominant homogeneous marl units (***hd*** facies: halite and detritus; Fig. 2-3h).

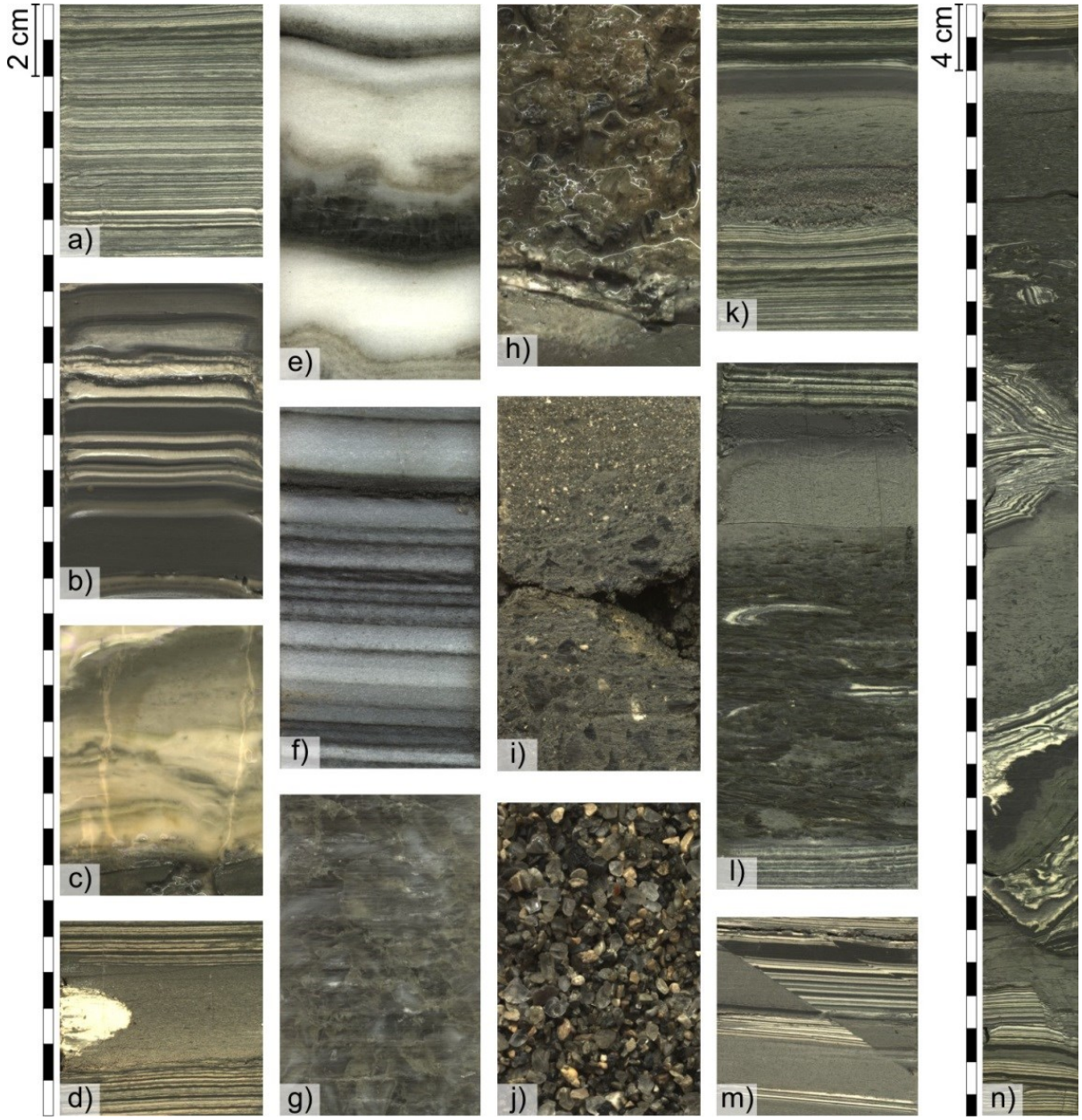

Figure 2-3: Exemplary core images of the sedimentary facies and structures of the 5017-1 profile: a) alternating aragonite and detritus (*aad* facies, core 5017-1-A-48-A-2, ~105.8 m blf); b) laminated marl containing aragonite and gypsum layers (*ld* facies, core 5017-1-A-12-A-1, ~21.2 m blf); c) massive gypsum deposit within marl (*gd* facies, core 5017-1-A-44-A-1, ~91.7 m blf); d) native S concretion, associated with greenish colored *aad* (core 5017-1-A-135-A-1, ~347.2 m blf); e) layered halite with thin dark detrital layers, transparent irregular-shaped halite crystal layers and whitish fine-grained halite layers (*lh* facies, core 5017-1-A-101-A-1, ~257.8 m blf); f) layered halite with thin dark detrital layer and thicker white to grayish salt layer couplets (*lh* facies, core 5017-1-A-91-A-2, ~234.2 m blf); g) consolidated homogeneous halite with irregular-shaped crystals and some fine detrital material (*hh* facies, core 5017-1-A-100-A-3, ~256 m blf); h) halite crystals and marl (*hd* facies, core 5017-1-E-1-H-1, ~3.7 m blf); i) brecciated halite within a fine-grained halite-detrital matrix (*htd*, core 5017-1-A-175-A-1, ~441 m blf); j) gravel of halite, limestone, dolomite, minor quartz and feldspar (*ccd*, core 5017-1-A-92-A-1, ~234.9 m blf); k) graded layer with coarse basal layer, upwards fining and dark clay top (*mtd*, core 5017-1-A-48-A-2, ~105.7 m blf); l) as in k but the coarse base is replaced by intraclast breccia (*mtd*, core 5017-1-A-49-A-1, ~107.7 m blf); m) displaced sediments of *aad* (associated with *mtd*, core 5017-1-A-151-A-1, ~389.1 m blf); n) slumped and folded sediments of *aad* (followed by *mtd* as in l), core 5017-1-A-49-A-2, ~108.5 m blf).

2.5.1.3 Massive, graded and slumped deposits (mtd and htd)

The laminated sediments are frequently intercalated by commonly up to several cm-thick graded layers with dark gray, coarse silt to sand-sized basal layers, fining upwards to light gray silt to clay-sized marl and commonly succeeded by a dark clay top (Fig. 2-3k). In many cases the coarse base of these deposits is replaced by intraclast breccia (Fig. 2-3l). Furthermore, clay to silt-sized homogenites, often containing a coarser base, are ubiquitous in the 5017-1 core. Associated with the graded or homogeneous deposits (***mtd*** – mass transported deposits) are slumped, folded (Fig. 2-3n), brecciated and displaced (Fig. 2-3m) sedimentary structures of various compositions, grain-size and thicknesses ranging from mm to meter scale (Hadzhiivanova et al., 2013). Brecciated halite layers occasionally exist within the massive salt sequences (***htd*** - halite transported deposits; Fig. 2-3i). These units are characterized by consolidated fine-grained halite and clay to silt-sized marl matrix, with some occasional fragmented and distorted single aragonite or gypsum layers, interceded by fining upward graded irregular single halite crystals of mm to cm scale and some mm scale clastic grains.

2.5.1.4 Coarse clastic detritus (ccd)

Gravel deposits have been only very rarely found in the 5017-1 core sequence. Two coarse clastic units (***ccd***) have been identified in association with a massive halite sequence at ~235 m and ~229 m blf (35 cm and ~60 cm thick, respectively; Fig. 2-3j). These gravel beds are mainly composed of ~2-8 mm big sub-rounded and sub-angular limestone, dolomite, halite, minor quartz and feldspar grains. The upper gravel deposit shows distinct grading and fining upwards and is embedded in clay to silt-sized marl, whereas the lower one only consists of well-sorted gravel. Additional gravel deposits have been identified solely in the basal parts of exceptionally thick graded layers in fine-grained matrix sediments. The grain sizes of these gravels range from 2 to 10 mm but may reach up to 35 mm in diameter. Such deposits occur predominantly within ***aad***-dominated units at various depths (e.g. ~153 m, ~154 m, ~284 m, ~357 m and ~366 m blf).

2.5.2 Composite profile 5017-1

For the uppermost 80 m of the sediment sequence the long core (5017-1-A) has been combined with five shorter parallel cores (5017-1-B, C, D, E, H) to one composite profile (Fig. 2-4). The lower part of the stratigraphical log for site 5017-1 down to 455 m sediment depth is based on the single core sequence 5017-1-A with inherent gaps depending on the core recovery rates, which in turn vary depending on the sediment facies (Table 2-1; Fig. 2-2). The composite profile of the upper 80 m has been established using 24 well-defined marker layers and facies boundaries identified in at least two parallel cores (Table 2-4). Despite overlapping cores in the upper part, there are still minor gaps even in the composite profile (Fig. 2-4) due to low core recoveries especially in sediment intervals characterized by alternations of soft marl and hard halite units, which are extremely difficult to drill.

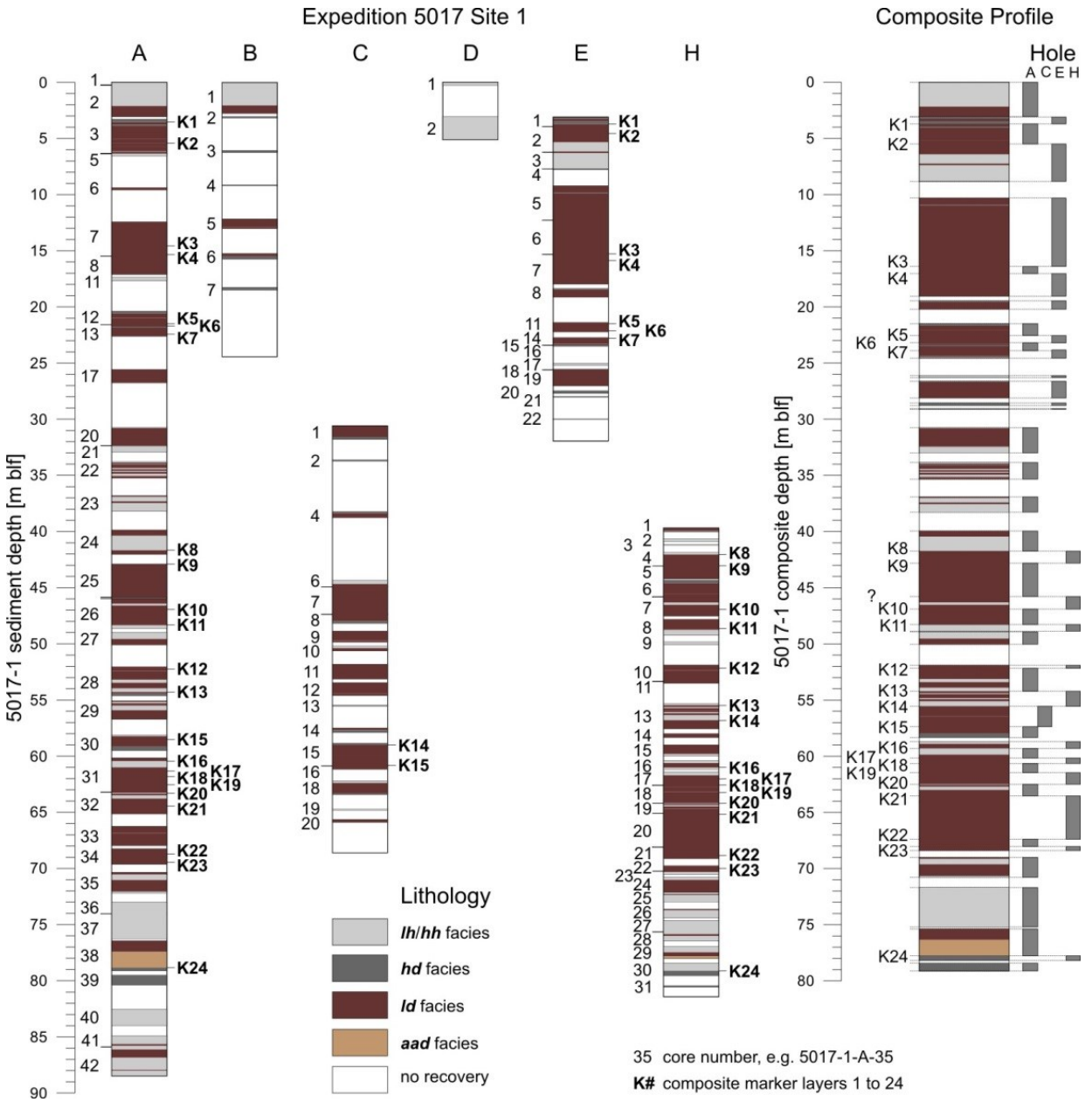

Figure 2-4: Composite profile for site 5017-1 based on correlation of distinct marker layers and facies boundaries. The profile continues with 5017-1-A below 80 m sediment depth. Gaps in the profiles are due to lacking core recovery; 15.8 m of sediment gaps remain in the composite profile of the upper 80 m composite depth.

Table 2-4: Composite marker layers and facies boundaries, respectively, K1 to K24 for site 5017-1, holes A, C, E and H, their absolute depth, position in the core sections, composite depth and description; exp = Expedition.

		master core				depth	section	composite	composite	description
exp	site	hole	core	tool	section	m blf	cm	m blf	layer	
5017	1	E	1	H	1	3.71	62	3.715	**K1**	boundary ***hd*** - ***ld***
5017	1	A	3	H	1	3.56	27			
5017	1	A	3	H	2	5.34	53	5.495	**K2**	top of ~2 cm thick black layer
5017	1	E	2	H	1	4.51	57			
5017	1	E	6	H	2	15.21	145	16.405	**K3**	upper gypsum-aragonite lamina of a ~6 cm ***ld*** section
5017	1	A	7	H	2	14.665	82.5			
5017	1	A	7	H	2	15.29	145	17.03	**K4**	gypsum lamina below aragonite lamina
5017	1	E	7	H	1	15.94	62			
5017	1	A	12	A	1	21.455	105.5	22.545	**K5**	~5 mm thick aragonite lamina within ***ld*** facies
5017	1	E	11	H	1	21.455	7.5			
5017	1	E	11	H	1	22.095	71.5	23.185	**K6**	lower aragonite lamina of a ***ld*** section
5017	1	A	13	A	1	21.67	8			
5017	1	A	13	A	1	22.35	76	23.865	**K7**	aragonite lamina within a ***ld*** section
5017	1	E	14	H	1	22.775	3.5			
5017	1	A	24	A	2	41.66	29	41.745	**K8**	bottom of a ***lh***/***hh*** section
5017	1	H	4	A	1	42.01	16			
5017	1	H	4	A	1	43.08	123	42.815	**K9**	no distinct marker layer, calculation based on overlapping sections
5017	1	A	25	A	1	42.91	0			
5017	1	H	7	A	2	46.92	39	46.9	**K10**	bottom of a ~2.5 cm thick ***ld*** section
5017	1	A	26	A	1	46.96	100			
5017	1	A	26	A	2	48.335	110.5	48.275	**K11**	top of a ~1.5 cm thick ***ld*** section
5017	1	H	8	A	1	48.625	81.5			
5017	1	H	10	H	1	52.16	26	52.175	**K12**	top of a ~4 cm thick ***ld*** section
5017	1	A	28	A	1	52.235	18.5			
5017	1	A	28	A	2	54.27	104	54.21	**K13**	bottom of a ***lh*** section
5017	1	H	13	A	1	55.45	11			
5017	1	H	13	A	2	56.8	82	55.56	**K14**	boundary ***hh*** – ***ld*** (homogeneous)
5017	1	C	15	A	1	58.995	13.5			
5017	1	C	15	A	2	60.81	92	57.375	**K15**	~5 mm thick gypsum-aragonite lamina within a ***ld*** section
5017	1	A	30	A	1	58.525	38.5			
5017	1	H	16	A	1	61.02	60	59.3	**K16**	boundary ***ld*** (homogeneous) - ***hh***
5017	1	A	31	A	1	60.45	28			
5017	1	A	31	A	1	61.31	114	60.16	**K17**	top of a ~5 cm thick ***ld*** section
5017	1	H	17	A	1	62.035	61.5			
5017	1	H	17	A	1	62.53	111	60.655	**K18**	thin aragonite lamina
5017	1	A	31	A	2	61.815	42.5			
5017	1	A	31	A	2	62.615	122.5	61.455	**K19**	bottom of a gypsum lamina
5017	1	H	18	A	2	63.22	0.5			
5017	1	H	18	A	cc	64.255	7	62.49	**K20**	boundary ***lh***/***hh*** – ***ld*** (homogeneous)
5017	1	A	32	A	1	63.35	14			
5017	1	A	32	A	2	64.41	29	63.55	**K21**	top of a ~8 cm thick ***ld*** section
5017	1	H	20	H	1	65.14	5			
5017	1	H	21	X	1	68.86	77	67.345	**K22**	thin aragonite lamina within a ***ld*** section
5017	1	A	34	A	1	68.725	46.5			
5017	1	A	34	A	1	69.405	114.5	68.025	**K23**	light gray layer below coarse base of a ***mtd***
5017	1	H	22	H	1	69.98	21			
5017	1	A	38	A	2	78.85	101	77.73	**K24**	boundary ***aad*** - ***hd***
5017	1	H	30	A	1	79.11	66			

2.5.3 Magnetic susceptibility and µXRF element scanning

Magnetic susceptibility strongly fluctuates in the ***ld*** and ***lh/hh*** units, but remains rather constant at low values (>0 to few hundred x 10^{-6} SI) in the ***aad*** dominated intervals (Fig. 2-5). Highest values (up to ~11,000 x 10^{-6} SI) are observed in black marl layers within ***ld*** facies. Slightly negative values (down to ca -20 x 10^{-6} SI) are characteristic for massive salt layers of the ***lh/hh*** facies.

Table 2-5: µXRF element scanning data of the 5017-1 core (in 1 mm steps; n = 312,985): average intensities, standard deviation (stdev.) and maximum (max.) values (in counts per second – cps) and correlation matrix (correlation coefficients – r, values >0.6 (-0.6) in bold) of the major elements Cl, S, Sr, K, Ti, Fe, Si and Ca.

	Cl	**S**	**Sr**	**K**	**Ti**	**Fe**	**Si**	**Ca**
Average	4988	163	237	431	258	590	75	11,993
Stdev.	3376	275	152	201	175	351	45	5785
Max.	22,210	10,885	1992	1516	1768	3562	396	31,814
Cl	1	-0.14	-0.41	-0.42	-0.46	-0.42	-0.48	**-0.75**
S	-0.14	1	-0.09	-0.17	-0.16	-0.18	-0.15	0.18
Sr	-0.41	-0.09	1	0.07	-0.002	0.05	0.03	**0.63**
K	-0.42	-0.17	0.07	1	**0.91**	**0.88**	**0.86**	0.45
Ti	-0.46	-0.16	-0.002	**0.91**	1	**0.94**	**0.92**	0.39
Fe	-0.42	-0.18	0.05	**0.88**	**0.94**	1	**0.88**	0.37
Si	-0.48	-0.15	0.03	**0.86**	**0.92**	**0.88**	1	0.45
Ca	**-0.75**	0.18	**0.63**	0.45	0.39	0.37	0.45	1

µXRF core scanner data provide a general overview on the main geochemical characteristics of the sediments, which can be used as proxy for a first estimation of the mineralogical composition. The main elements detected in the sediments include Cl, S, Sr, K, Ti, Fe, Si and Ca (Table 2-5). In some cases correlation of elements allows identification of specific minerals and related sediment depositional processes. Highest positive correlations occur between K, Ti, Fe and Si (r = 0.86 - 0.95), whereas a strong negative correlation is observed between Cl and Ca (r = -0.75) and, less pronounced, between Cl and all other considered elements (r = ~-0.43, except S). Ca positively correlates with Sr (r = 0.63) and to a lesser extent with K, Ti, Fe and Si (r = ~0.4) and with S (r = 0.18). The element scanning data clearly mirror the above described facies types as follows:

- High Cl counts occur in halite layers (***lh, hh*** and ***hd*** facies), but might be also influenced by pore water contents;
- Elevated S counts concur with gypsum layers (***gd*** and partly ***ld*** facies), but highest S counts are observed for native sulfur concretions;
- High Sr counts reflect aragonite and thus are characteristic for ***aad*** (and partly ***ld***) facies;
- High Ti, K, Fe and Si counts match with the non-carbonate, siliciclastic fraction of the detrital material;

- High Ca counts mainly depict the ***aad*** facies, but since Ca occurs in three different minerals, which reflect different sedimentation processes (aragonite and gypsum formed by evaporation at different intensities; detrital carbonate reflecting surface runoff from the catchment and eolian transport), a combination of Ca with complementary elements is necessary to disentangle between those mineral phases. Elevated Ca counts paralleled by high Sr counts are indicative for aragonite, while high Ca counts in combination with high S counts are indicative for gypsum. If peaks in Ca counts are paralleled by elevated counts in detrital proxies like Ti, K, Fe and Si, this might be a rough indication of detrital carbonates. However, the latter must be further investigated and confirmed by mineralogical analyses because the ratio portions of carbonaceous and siliciclastic detrital matter not necessarily have to be always the same.

2.5.4 Lithostratigraphy

Profile 5017-1 is divided into four major sediment units (SU) based on the (i) sedimentary facies, (ii) magnetic susceptibility, and (iii) element scanner data (Fig. 2-5).

2.5.4.1 Sediment unit I (SU-I)

SU-I (Fig. 2-5) comprises the interval from the base of the core at ~455 m blf (below lake floor) to 320 m blf (hereafter all depth are given in meters blf) and is characterized by magnetic susceptibility values close to zero. SU-I is predominantly composed of ***aad*** facies intercalated by occasional ***ld*** facies at ~428-426 m, ~407-399 m and ~377-373 m, respectively, which are reflected by short-term decreases in Sr counts and slightly enhanced Ti values (Fig. 2-5). Massive gypsum layers (***gd*** facies) occur within these ***ld*** sequences, as well as in the upper ~12 m of SU-I. Furthermore, a few decimeter-thick halite sequences (***lh*** and ***hh*** facies) are present between 400 and 390 m. The lowermost ~21 m of SU-I differ from the rest of this unit and consist of basal ~11 m laminated marls (***ld*** facies) and an overlying ~10 m thick halite sequence (***lh*** and ***hh*** facies). The halite unit is clearly reflected by enhanced Cl and reduced Sr and Ca counts. Concretions of native sulfur, greenish colored ***aad*** and occasional ***mtd*** units are scattered within the ***aad***-dominated part of the unit.

2.5.4.2 Sediment unit II (SU-II)

SU-II is about 120 m thick (~320-200 m) and is distinguishable from the underlying SU-I unit by strongly fluctuating magnetic susceptibility values (Fig. 2-5). Unit SU-II is further sub-divided into five sub-units (SU-II-a to SU-II-e; from bottom to top): (1) SU-II-a consists mainly of layered halite (***lh*** facies) with some laminated marl (***ld*** facies) intercalations from ~320 to 304 m. (2) SU-II-b is characterized by laminated marl (***ld*** facies) from ~304 to 279 m including a ~3 m thick ***hd*** interval and a ~6 m thick ***aad*** sequence. (3) Sub-unit SU-II-c comprises a halite sequence (***lh*** and ***hh*** facies, intercalated by ***ld*** facies from ~279 to 233 m. This is by far the thickest halite sequence of the entire 5017-1 profile. (4) SU-II-d (~233 to 210 m) is an ***aad***-dominated unit, intercalating with some laminated marl (***ld*** facies). (5) SU-II-e from ~210 to

200 m consists of massive layered halite (***lh*** facies), occasionally interrupted by some laminated marl and alternating aragonite and detritus ***(ld*** and ***aad*** facies). These sub-units clearly differ in element counts with enhanced Cl and low Sr, Ti and Ca values in the halite dominated sections SU-II-a, SU-II-c and SU-II-e, whereas SU-II-b and especially SU-II-d exhibit an opposed pattern with low Cl counts and higher Sr, Ti and Ca values (Fig. 2-5). Sulfur peaks are relatively scarce in the lower SU-II-a and SU-II-b and become more abundant towards the top of SU-II, particularly in SU-II-d. About 2 m below and ca 4 m above the top of SU-II-c two gravel layers (***ccd*** facies) appear.

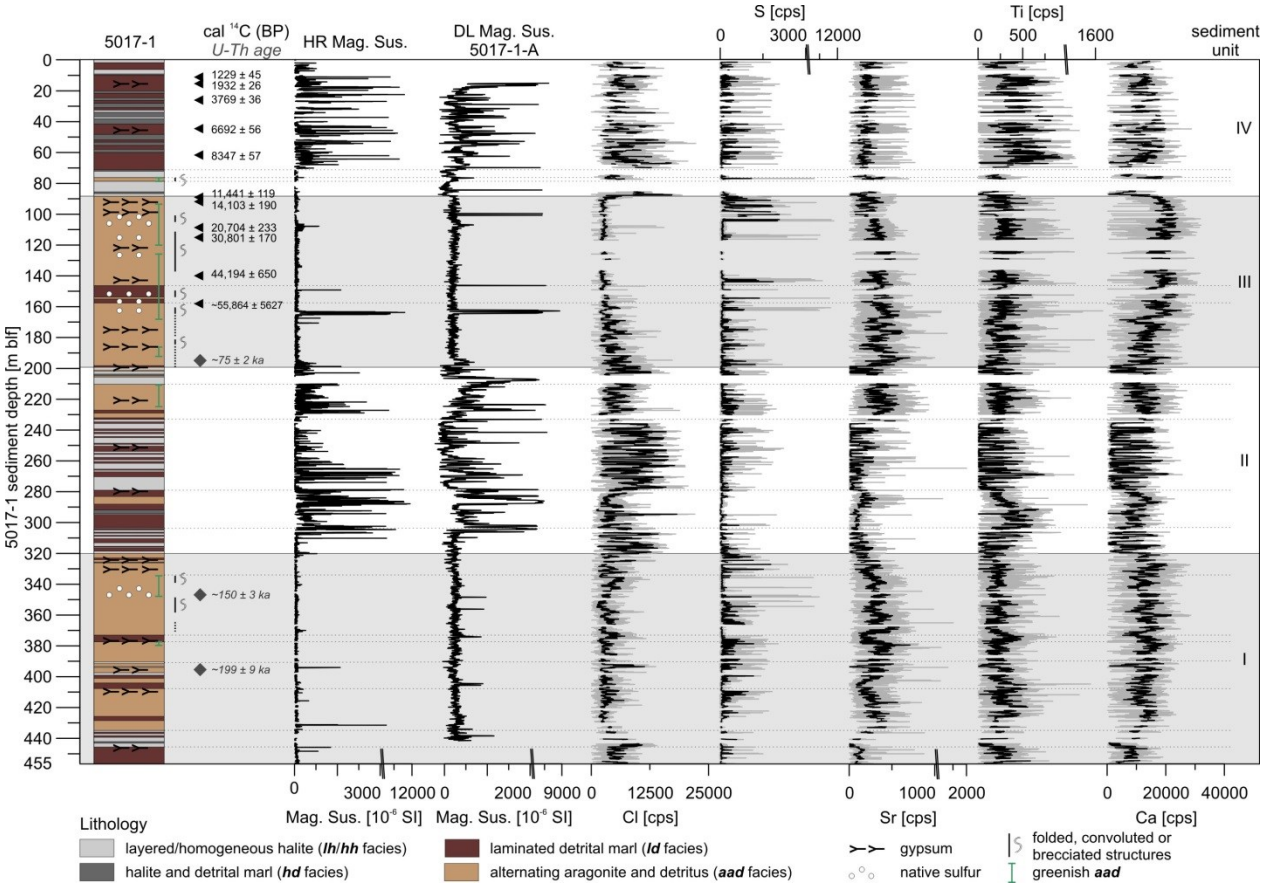

Figure 2-5: Lithological profile of 5017-1 (water depth 297 m, composite profile) with radiocarbon and U-Th ages; magnetic susceptibility data, measured with high resolution (HR; 1 mm resolution) on the splitted core surface and with low resolution (10 cm) by downhole logging (DL, hole 5017-1-A): both curves are in good agreement, excluding any depth shifts during the drilling process; µXRF profiles of Cl, S, Sr, Ti and Ca in counts per second (cps): gray curves are measured values in 1 mm steps, black overlying curves are 101-values running means (10.1 cm); gaps in the HR magnetic susceptibility curve and µXRF data are due to lacking core recovery, insufficiently smooth core surface and folded or slumped - not measured – sections, respectively.

2.5.4.3 Sediment unit III (SU-III)

Unit SU-III (~200-88 m) encompasses ~112 m and represents predominantly ***aad*** facies with the marl components of light gray, greenish gray, dark green and black colors. Only between ~157 and ~146 m a change to ***ld*** facies occurs. Furthermore, folded, convoluted and brecciated

structures associated with ***mtd*** reaching several meters in thickness frequently occur in this unit (Fig. 2-5). Magnetic susceptibility values are generally low, but from ~165 to ~163 m an interval of higher values is intercalated. Cl counts generally decrease from the base of this unit until the top. Overall elevated Sr counts slightly decrease towards the top of the unit, whereas Ca values increase. Up to 15 cm thick gypsum layers (***gd*** facies) are associated with increased S values, but highest S values appear for native S concretions.

2.5.4.4 Sediment unit IV (SU-IV)

Unit SU-IV starts with a basal ca 16 m thick (~88-72 m) layered salt sequence (***lh, hh*** and ***hd*** facies; Figs. 2-4 and 2-5) which is further sub-divided into three intervals: (1)SU-III-a consisting of a ~10 m thick halite sequence (***lh, hh*** and ***hd*** facies). (2) SU-III-b is composed of a ~2.4 m thick greenish marl and aragonite-enriched unit (***add*** facies). (3) SU-III-c is, a ~4 m thick upper halite sequence (***lh*** and ***hh*** facies). The upper ~72 m of Unit SU-IV comprise laminated marl (***ld*** facies), intercalations of halite and marl (***hd*** facies) and some massive layered halite (***lh*** and ***hh*** facies; Figs. 2-4 and 2-5) characterized by magnetic susceptibility values strongly fluctuating from slightly negative values in the halite-dominated sections to high values in marl intervals and peaking in black layers (Fig. 2-5). The halite intervals are characterized by elevated Cl counts, while Ti, K, Fe and Si counts increase in the marl intervals of unit SU-IV.

2.5.5 Radiocarbon and U-Th ages

From eleven ^{14}C dates, five were obtained from SU-III (~200-88 m) and six from SU-IV (~88-0 m; Fig. 2-5; Table 2-2). The limit for radiocarbon dating appears at a depth of about 158 m, from where one un-calibrated age of 53,700 ± 3400 yrs has been obtained. This date is already beyond the IntCal13 calibration range (Reimer et al., 2013; Table 2‑2). Radiocarbon ages obtained for the upper half of lithological unit SU-III (~140 m-~89 m depth) are in stratigraphic order and range from 43,946 ± 717 cal yrs BP to 11,440 ± 119 cal yrs BP, thus covering marine isotope stages (MIS) 3 and 2 up to the Pleistocene/Holocene boundary. Radiocarbon dates from unit SU-IV are in stratigraphic order and all of Holocene age, ranging from 8348 ± 57 cal yrs BP at ~60 m to 1232 ± 44 cal yrs BP at ~11 m.

Here, we present three U-Th preliminary ages from the core section below the dating range of radiocarbon from three different depth intervals of core 5017-1 (Table 2-2, Fig. 2-5): (1) ca 60 m above the base of the sediment profile at ~395 m (age: 199 ± 9 ka); (2) ca 27 m below the boundary of SU-I to SU-II at ~347 m (age: 150 ± 3 ka); (3) ca 4 m above the SU-II to SU-III boundary at ~195 m (age: 75 ± 2 ka). The latter age is consistent with the age of the Samra/Lisan boundary as determined by U-Th dating of the exposed terraces (Haase-Schramm et al., 2004; Waldmann et al., 2009).

2.6 Discussion

2.6.1 Lithology and sedimentary environments

Sediment sequences exposed in the marginal exposed terraces provide compelling evidence that sedimentation in the DSB is strongly influenced by the hydrological conditions in the large watershed that are reflected in the salinity of the lakes (e.g. Katz et al., 1977), their water-body configuration (e.g. layered or overturned; Stein et al., 1997; Lazar et al., 2014) and their surface level (e.g. Neev and Emery, 1995; Machlus et al., 2000; Bartov et al., 2002; Bookman (Ken-Tor) et al., 2004; Waldmann et al., 2009). As terminal lakes with water loss mainly through evaporation, the water levels of the Dead Sea and its precursors are considered as sensitive 'hydro-climatic gauge' (Neev and Emery, 1995; Enzel et al., 2003). Two major sedimentological facies describe the lacustrine sequences and reflect the limnological and hydro-climatic conditions in the lake and its watershed: (1) sequences of couplets of aragonite and silty detritus laminae (termed the ***aad*** facies; Machlus et al., 2000) characterize the sedimentation processes during periods of positive freshwater balance and supply of bi-carbonate to the lake (filled with Ca-chloride brine). The ***aad*** facies characterizes the lake level high stand intervals of the last glacial Lake Lisan (e.g. Neev and Emery, 1967; Begin et al., 1974; Stein et al., 1997; Prasad et al., 2004). Counting of the ***aad*** couplets in the Masada outcrop of the Lisan Fm. and radiocarbon dating indicated that these couplets are varves (Prasad et al., 2004). The detrital silts were deposited during winter through surface runoff processes and the primary aragonite precipitated from the interface between the upper, fresher lake water layer and the lower brine during summers (Katz et al., 1977; Haliva-Cohen et al., 2012; Lazar et al., 2014). The glacial periods are also characterized by deposition of gypsum layers, which require the supply of sulfate ions via freshwater to the lake (Stein et al., 1997; Torfstein et al., 2005; 2008). (2) Sequences of laminated silty detritus with minor appearance of aragonite, termed the ***ld*** facies (Haliva-Cohen et al., 2012), are interpreted as flood sediments that were transported to the lake during arid interglacial periods when almost no bi-carbonate was supplied to the lake (Haliva-Cohen et al., 2012). The ***ld*** facies comprises significant parts of the exposed last interglacial Samra Fm. and the Holocene Ze'elim Fm. (Waldmann et al., 2009; Haliva-Cohen et al., 2012).

In the deep 5017-1 core SU-I and SU-III are predominantly composed of ***aad*** facies and were deposited during glacials. Massive or laminated primary gypsum horizons (***gdm*** facies) in the upper part of a ***aad*** facies sequence were interpreted as indicators of falling lake level and water overturns during drier conditions (Stein et al., 1997; Torfstein et al., 2008; 2013b). Porewater extracted from the 5017-1 core suggests that the gypsum unit at the uppermost part of the Lisan Fm. was deposited at the end of a long freshening of the hypolimnic brine (Lazar et al., 2014). The occurrence of the major gypsum units in the Lisan Fm. coincides with the timing of North Atlantic Heinrich-events and was related to cooling of the east Mediterranean waters that weakened the activity of cyclonic winter rains causing regional droughts (Bartov et al., 2003; Haase-Schramm et al., 2004; Torfstein et al., 2013a; 2013b).

In the core 5017-1 the ***ld*** facies is mainly found in units SU-II and IV and in the basal part of SU-I, suggesting relatively dry conditions during the deposition of these sediments. During driest conditions and presumably lowest lakes levels massive halite sequences (***lh***, ***hh*** and ***hd*** facies) formed and are found mainly in the lower SU-I, SU-II and SU-IV units. At present, the Dead Sea is saturated with salt as a result of the man-made decline of its water level. Naturally, salt was deposited in the lake when the water level dropped below ~400 m bmsl (Neev and Emery, 1967). At around this elevation the lake level falls beneath the sill separating the northern and southern basins (e.g. Bookman (Ken-Tor) et al., 2004; Stein et al., 2010). Commonly, halite sequences are absent in the marginal terraces of the DSB which only comprise sediments that were deposited during times of lake level high stands, e.g. during the last glacial Lake Lisan. When lake levels fell below the elevation of the modern Dead Sea shores (currently at ~427 m bmsl), the elevated terraces were exposed to erosion and truncation (Bartov et al., 2007). Halite sequences exhibit distinct layering (***lh*** facies) which possibly represents even annual deposits with deposition rates ranging between 0.2 and 7 cm/year (see Fig. 2-3e and 2-3f). These values are in good agreement with rates of modern salt deposition as reflected by the uppermost ~2.20 m thick salt unit of core 5017-1 (Fig. 2-4) which has been accumulated within ca 27 years (1983-2010). The resulting average sedimentation rate of ~8.2 cm/year approximately resembles the layer thickness measured for the ***lh*** facies.

The thick homogeneous or graded deposits in the 5017-1 core sequence are interpreted as mass wasting deposits (***mtd*** and ***htd***). Such deposits frequently occur in unit SU-III corresponding to the Lisan Formation and often are associated with sediment structures interpreted as seismic events (Kagan and Marco, 2013), but triggering by hydro-meteorological extreme events might have also been possible. In some cases, characteristic broken-up layer fragments in the basal part of these deposits occur, which most likely represent ‘intraclast breccias’ or ‘mixed layers’ interpreted as seismites by Marco and Agnon (1995; see also Agnon et al., 2006). Event layers containing coarse material at the base might be of subaerial or near-shore origin, while subaquatic processes caused commonly folded slumped deposits. Mass wasting deposits are ubiquitous in the entire sediment sequence, but the thickest, up to m-thick slumped and distorted sections are mainly associated with the ***aad***-intervals in units SU-I and III. Therefore, the total sediment thickness of these lithological units is substantially increased through these additional event deposits, which add up, for example, in unit SU-III to ~60% of the total thickness (Fig. 2-5).

The interpretation of the sediment facies is consistent with magnetic susceptibility and µXRF element scanner data (Fig. 2-5). High magnetic susceptibility values are mainly observed in units SU-II and IV and explained by high concentrations of magnetic minerals (Nowaczyk, 2001). The main magnetic carrier minerals in the Dead Sea sediments are greigite and titanomagnetite (Frank et al., 2007a; 2007b; Ron et al., 2007). Greigite is a secondary mineral formation and thus reflects post-depositional reducing conditions in the sediments (Ron et al., 2007), whereas titanomagnetite is transported from the catchment into the lake and thus indicative for the amount of detrital matter from various source regions that may have changed in the past (Haliva-Cohen et

al., 2012). Due to the different origin of the magnetic susceptibility signal, it is hardly possible to apply these data as a uniform proxy for the entire sediment record. Greigite is commonly associated with black sediment intervals especially within the ***ld*** facies mainly in units SU-II and IV, which exhibit high magnetic susceptibility peaks. However, not all black sediment intervals reflect increased amount of greigite, but instead pyrite, which is paramagnetic (Frank et al., 2007b). Examples of pyrite-dominated black horizons are observed within the ***aad*** facies of units SU-I and SU-III.

Even considering the aforementioned limitation in interpretation of the rapid overview µXRF core scanning with short exposure times, the resulting element variations reflect surprisingly well the lithological changes and allow rapid assessment of mineral phases in the sediments. Sr counts are enhanced in the ***aad***-dominated units SU-I and III due to the abundance in aragonite. Enhanced S counts reflect gypsum deposits and are predominantly found in ***gd*** facies, but highest S counts indicate native sulfur concretions, which are associated with the ***aad***-dominated units SU-I and III. Sulfur concretions reflect anoxic conditions of the lower water body during time of sedimentation (Torfstein et al., 2009). Increased amounts of detrital material within ***ld*** facies in units SU-II and IV is mirrored by higher Ti counts and other indicator elements for detrital matter such as K, Fe and Si. However, these elements only reflect the siliciclastic component of the detrital material (quartz and minor feldspar and clay minerals; e.g. Neev and Emery, 1967; Heim et al., 1997; Haliva-Cohen et al., 2012). Detrital carbonates are difficult to identify in XRF scanner data because Ca counts not only reflect detrital carbonate but also primary aragonite and gypsum. Therefore, elevated Ca counts appear in all three facies (***aad***, ***gd*** and ***ld***). Nevertheless, highest Ca counts are found for ***aad*** facies in units SU-I and SU-III where Ca peaks are paralleled by peaks in Sr counts (Table 2-5), proving primary aragonite as causing these peaks. As expected, highest Cl counts indicate halite sequences (***lh***, ***hh*** and ***hd*** facies) in the lower SU-I, SU-II and SU-IV units. Other salt minerals like, for example, carnallite cannot be detected by the applied overview XRF scanning.

2.6.2 Stratigraphy

The stratigraphic interpretation of core 5017-1 is revealed through the correlation of the lithological units SU-I to IV to the exposed marginal sediments of the DSB based on sediment facies changes (Fig. 2-6): the Amora (SU-I), Samra (SU-II), Lisan (SU-III) and Ze'elim (SU-IV) Formations following previous chronological and stratigraphic studies of Haase-Schramm et al. (2004), Waldmann et al. (2007) and Torfstein et al. (2009; 2013a; 2013b). The stratigraphy for core 5017-1 in this study is corroborated by the radiocarbon ages and preliminary U-Th ages (Table 2-2).

2.6.2.1 Amora Formation

The Amora Formation comprises the sediment sequences that were deposited in the DSB from the early to late Pleistocene times (Stein, 2001). Torfstein et al. (2009) established a U-series and oxygen isotope chronology of the exposed sediments near Arubotaim Cave (AC), eastern flanks

of Mt. Sedom (Fig. 2-2a), for the middle to late Pleistocene (~740-140 ka). The AC section comprises sequences of ***aad*** facies, indicating wet conditions in the watershed, sequences of ***ld*** facies and sequences of anhydrite or gypsum. In addition, a massive, a few meter thick salt layer was dated to ~400 ka by Torfstein et al. (2009) and reflects drier conditions. Thus, the AC section represents several glacial (wet) and interglacial (dry) cycles. In core 5017-1 only the upper part of the Amora Fm. is enclosed in unit SU-I (Fig. 2-6). The bi-partition into a lower ***lh/ hh***-containing sub-unit and an upper ***aad***-dominated interval most likely coincides with the dry MIS 7 interglacial and the wet penultimate glacial (MIS 6) period, respectively. U-Th ages of 200 ka for the lower sub-unit at ~400 m depth and of 150 ka for the upper sub-unit at ~350 m (Torfstein et al., 2015) further support this interpretation. Based on interpolation of these dates, the MIS 7-6 boundary as defined at ~190 ka (Lisiecki and Raymo, 2005) appears at ~390 m depth in the Dead Sea sediment record. Directly below this depth thin salt deposits and clastic as well as gypsum layers are deposited (Fig. 2-6), probably related to drier conditions and low lake levels during the interglacial corresponding to MIS 7. Extrapolation of the U-Th ages dates the base of core 5017-1 at ~455 m at approx. 220-240 ka.

In the exposed sediment sections on the margins of the DSB an erosional unconformity was recognized between the Amora and the overlying Samra Formation between ~140 and 130 ka (Waldmann et al., 2009). Torfstein et al. (2009) report a sharp lithological transition from aragonite-gypsum facies to clastic sediments in the Perazim Valley (Fig. 2-2a) in the southern part of the DSB at ~130 ka, which has been related to a falling lake level during the early part of the last interglacial (Bartov et al., 2007; Waldmann et al., 2007). This interval is reflected in the deep basin sediments of core 5017-1 by the appearance of massive gypsum layers and a less regular ***aad*** facies at ~334-320 (Fig. 2-6) likewise indicating a period of lake level decrease (Torfstein et al., 2008).

2.6.2.2 Samra Formation

Lake Samra occupied the DSB from ~135 to 70 ka (Torfstein et al., 2009; Waldmann et al., 2009) and has been investigated so far only in the exposed sediment sections in the marginal terraces of the modern Dead Sea. Sediments of the Samra Fm. mainly consist of laminated detritus (of the ***ld*** facies; Haliva-Cohen et al., 2012), some aragonite and gypsum laminae and fluvial sand and conglomerates typical for shallow littoral environments (Waldmann et al., 2007; 2009). Lake level reconstructions suggested that the average Lake Samra level has been generally higher (~370 ± 40 m bmsl) than the average Holocene levels (~400 ± 30 m bmsl), but during most of the time lower than the Lake Lisan levels, which fluctuated between ~330 and ~160 m bmsl (Waldmann et al., 2009; Torfstein et al., 2013b). However, pronounced lake level fluctuations within the Samra stage also resulted in particular low stands below ~370 m bmsl at ~135 and at ~80-75 ka, coinciding with global sea level rises during Termination 2 and during MIS 5a, as well as higher stands of up to ~320 m bmsl at ~120 and at ~85 ka (Waldmann et al., 2009). Higher resolution speleothem records provide evidence that the high stands have been caused by

punctuated clusters of short and intense humid episodes that occurred even during the overall dry interglacial conditions caused by intrusion of moist air masses (Vaks et al., 2010).

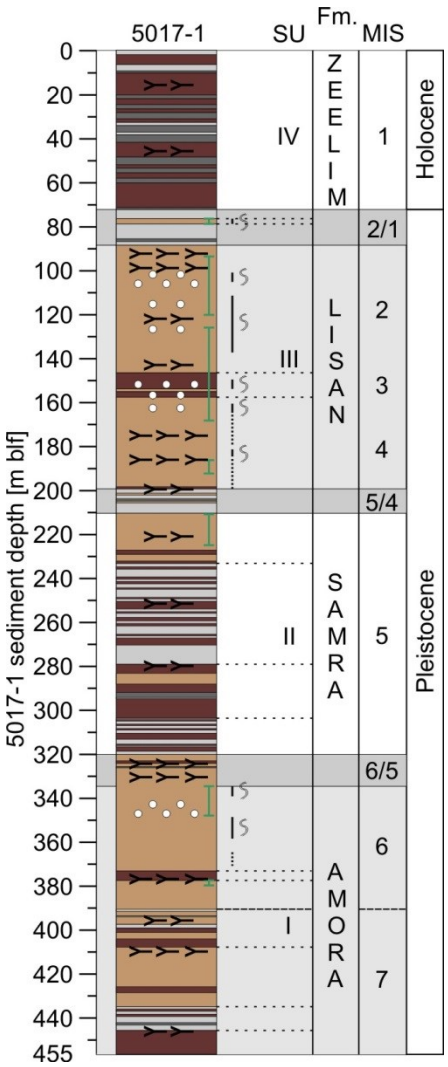

Figure 2-6: Stratigraphy of the 5017-1 profile (water depth 297 m); SU: sediment unit, Fm.: sediment formations of the Dead Sea Group, MIS: marine isotope stage. See Fig. 2-5 for a legend of the lithology.

The Samra Fm. is correlated to unit SU-II in core 5017-1 (Fig. 2-6) and further sub-divided into five sub-units (SU-II-a to SU-II-e). The alternation of halite (***lh*** and ***hh***) and detrital marl (***ld*** and ***aad***) facies indicates oscillations between lower and higher lake stands and thus pronounced oscillations between drier and wetter conditions at millennial or even longer time-scales. Most likely the most pronounced and/or longest dry period during the entire time interval covered by core 5017-1 led to the deposition of the thickest (~40 m) salt sequence in the entire core in sub-unit SU-II-c. The lake level during this time interval must have been very low so that a depositional gap in the littoral sediment sequence of the Samra Fm. must be assumed which, in turn, might explain why this was not recognized by Waldmann et al. (2009). This is a further confirmation that the sediment record from the deep DSB will aid a more comprehensive reconstruction of the lake level history of the Dead Sea and its precursor lakes.

An intriguing finding is the occurrence of a ca 35 cm thick pure gravel layer close to the top of the 40 m thick halite unit of SU-II-c at ~235 m (Fig. 2-3j). This is the only pure and well-sorted gravel layer lacking any fine detrital material that occurs in the entire sediment record. Therefore, it was suggested based on visual inspection of the gravel layer that this deposit might be a beach deposit, which led to the hypothesis of a significant draw-down of the Dead Sea in the later part of MIS 5e (Stein et al., 2011; Goldstein et al., 2012; Torfstein et al., 2015). However, a complete desiccation of the Dead Sea might be questioned, since Yechieli et al (1998) and Krumgalz et al (2000) argued that evaporation under the current water activity and relative humidity will slow

down significantly when the lake drops to ~ 550 m bmsl. On the other hand, water loss might not only be due to evaporation but also to leakage through the margins (e.g. Kiro et al., 2014). Another example for a major lake level decrease below the present day level at the end of the last glaciation (Lateglacial) has been discussed by Stein et al. (2010) in light of the depositional unconformity documented in many short cores drilled along the modern retreating shores of the Dead Sea. This unconformity spans the time interval of ~14-13 ka BP at an elevation of ~450 m bmsl requiring that the lake level fell at least below this elevation. They further argued that this inferred lake level drop is consistent with erosional channels that cut the Dead Sea floor at elevations below 500 m bmsl (mapped by Neev and Hall, 1979).

At this point of the discussion the question arises if there are alternative explanations for the occurrence of a pure gravel layer in the sediment sequence. An alternative explanation to transport such coarse material into the deepest part of the basin would be through a mass waste event as it is proven by a thick turbidite deposit (***mtd*** facies) only 6 m above the gravel layer. However, this deposit exhibits a typical fining upward structure with gravels mixed in the basal part with fine clay to silt and sandy material. Assuming a mass waste event as transport process also for the gravel layer at 235 m sediment depth would need an explanation for the lack of any fine material mixed with the gravel. In the absence of any natural process that could explain such separation of grain sizes, the only possible cause might be an artificial wining out of the material during drilling operation. Detailed analyses of the different gravel occurrences in the sediments are ongoing for an unambiguous sedimentological interpretation of the pure gravel layer as a prerequisite for further climatic interpretation. For this reason, we consider the assumption of a complete dry-down of the Dead Sea at this stage as an intriguing hypothesis that needs to be further investigated.

The transition from the Samra Fm. to the Lisan Fm. is marked by a major unconformity at about 80-70 ka in the shallow marginal lake areas, as identified from sediment outcrops (Stein, 2001) indicating a significant lake level decline at the MIS 5 to MIS 4 boundary (Waldmann et al., 2009). This period of a most likely rapid lake level drop is likely reflected by the ~11 m thick salt sequence at ~199-210 m (unit SU-II-e; Fig. 2-6). An U-Th age of ~75 ka obtained from a sample ~5 m above this salt sequence supports this correlation.

2.6.2.3 Lisan Formation

The Lisan Formation deposited during the last glacial from ~70 to 14 ka and has been intensively studied (e.g. Bentor, 1961; Neev and Emery, 1967; Begin et al., 1974; Katz et al., 1977; Niemi, 1997 and references therein; Machlus et al., 2000; Bartov et al., 2002; 2003) and well dated by radiocarbon and U-Th dating (e.g. Kaufman, 1971; Kaufman et al., 1992; Schramm et al., 2000; Stein et al., 2000; Haase-Schramm et al., 2004; Prasad et al., 2009; Torfstein et al., 2013a) on outcrops and short cores from the Dead Sea shorelines. Stein (2001) summarized the state of knowledge about the Lisan Formation as follows: the sediment formation encompasses a Lower, Middle and Upper Member that have been deposited during MIS 4, 3 and 2, respectively. The sediments of the Lower and Upper Member comprise mainly ***aad*** facies, intercalated by thick ***gd***

facies units suggesting occasional lake-overturn episodes and decrease in the freshwater supply. These massive gypsum units in the Lisan Fm. can be traced northward along the western (Torfstein et al., 2008) and eastern margins of the lake (e.g. Landmann et al., 2002; Abu Ghazleh and Kempe, 2009) all the way to the central Jordan valley, thus serving as important marker layers. Based on U-Th dating the formation of these gypsum layers has been related to North Atlantic Heinrich-events (Torfstein et al., 2013a; 2013b). The Middle Member of the Lisan Fm. (~55-30 ka) contains clastic layers deposited during lower lake stands and is sub-divided in two sections, one below and one above a hiatus between 47 and 43 ka (e.g. Machlus et al., 2000; Haase-Schramm et al., 2004). The highest Lake Lisan level of ~160 m below sea level (bsl) occurred during the last glacial maximum, at ~27-24 ka (Bartov et al., 2003; Torfstein et al., 2013b).

In the ICDP core from the deep basin the Lisan Formation is comprised in unit SU-III (Fig. 2-6) which is by a factor of three thicker (~112 m) than the corresponding sequence in the exposed marginal sediments (~30-40 m thick; e.g. Stein et al., 1997; Landmann et al., 2002; Torfstein et al., 2013a). The main reason for this enhanced sediment thickness is the large number of thick event deposits (***mtd*** facies) intercalated in the pelagic sediments. Nevertheless, a similar division into lower, middle and upper members as in the exposed Lisan Fm. is also observed in the deep basin sediment sequence. The predominant ***aad*** facies characterizes both the shallow and deep-water Lisan environments. Yet, the characteristic greenish color of some of the deep core sequences suggests a higher preservation of organic matter in the deep basin. An increase in the clastic material occurs between ~157 and 146 m, probably representing part of or the entire Middle Member, as confined by radiocarbon ages of >44 - ~55 cal ka BP (Fig. 2-5 and Table 2-2). Several massive primary gypsum layers occur at depths of ~198-196 m, ~186-185 m, ~175.4 m, ~170 m, ~144.5 m, ~124-121.5 m, ~101-99 m and ~96-91 m. We estimate that the latter two intervals can be correlated to the Upper and 'Additional' Gypsum Units, previously described in the shallower environment by Torfstein et al. (2013a; 2013b) and dated to ~17.1-15.5 ka and ~14.5 ka, respectively. These dates are in agreement with the initial radiocarbon ages of the 5017-1 core (Table 2-2). The Upper and 'Additional' Gypsum Units indicate a major lake level decline of about 100 m from ca 260-360 m bsl (Torfstein et al., 2013a).

2.6.2.4 Ze'elim Formation

The unit SU-IV is the equivalent of the Holocene Ze'elim Fm. (e.g. Yechieli et al., 1993; Bookman (Ken-Tor) et al., 2004; Migowski et al., 2006) deposited in the last ca 10,000 years and part of the Lateglacial (Fig. 2-6). In the exposures the Holocene part of the formation ranges in thickness between 20 and 30 m and mainly comprises lacustrine to fluvial sediments. Lacustrine sediments are characterized by detritus-aragonite-gypsum laminated sections (***ld*** facies) intercalated with thick detrital layers, with numerous depositional hiatuses and erosional unconformities during lower lake levels (Yechieli et al., 1993; Enzel et al., 2000; Stein, 2001; Bookman (Ken-Tor) et al., 2004; Migowski et al., 2006). Only in the southern basin of the Dead

Sea the Ze'elim Fm. has been found to span ca 80 m (Neev and Emery, 1995), which is about the same thickness as in the deep basin environment.

The base of the Ze'elim Formation is delineated by a massive (few meters up to ~25 m thick) halite unit that has been previously documented in near-shore shallow cores (Yechieli et al., 1993; Migowski et al., 2006; Stein et al., 2010). Radiocarbon dating of organic debris from many boreholes drilled along the Dead Sea shore placed the salt unit between 10.8 and 10.2 ka cal BP (Stein et al., 2010). In the Ein Gedi core the salt unit is overlain by a sequence with ***aad*** facies that marks a level rise ~ 10 ka cal BP (Migowski et al., 2006). In the DSIF borehole from Wadi Ze'elim at the western margin of the Dead Sea, a 'marl unit' (laminated detritus of the ***ld*** facies) was found below the salt for which radiocarbon dating yielded an age of ~13.2 ka cal BP, and which includes the Younger Dryas (Yechieli et al., 1993; Stein et al., 2010).

In the deep basin sediment record this salt interval is most likely represented by the ~16 m thick ***lh***, ***hh*** and ***hd*** facies in the lower sequence of unit SU-IV, which is interrupted by a ~2 m thick ***aad*** facies interval that might indicate a short-term lake level rise. A ^{14}C age of 11,440 ± 119 cal yrs BP (Table 2-2) from an ***aad*** facies unit 1 m below the halite unit is consistent with a very early Holocene age. Radiocarbon ages prove that the upper part of unit SU-IV (~72-0 m) covers the last ca 10,000 years, with alternating laminated marl and halite deposits (Fig. 2-4). During the last 10,000 years excluding the past decades lake levels showed only minor fluctuations of ± 30 m around 400 m bsl (Bookman (Ken-Tor) et al., 2004; Migowski et al., 2006; Bartov et al., 2007) as revealed from shoreline evidences.

2.7 Potential of the deep Dead Sea record for future paleoclimate research

The ICDP drilling in the northern deep basin of the Dead Sea has recovered, for the first time, a quasi-continuous sediment record from the deep DSB for the last two glacial-interglacial cycles. The lithological profile of the ~455 m long sediment sequence from the deepest part of the basin comprises four main sedimentary units (SU-I to SU-IV), thereby providing a firm stratigraphic framework to establish correlations with stratigraphic units and defined formations of the Dead Sea Group in the outcrops. The Dead Sea sediment record captures the upper part of the early to middle Pleistocene Amora Formation reflecting parts of or the entire MIS 7 and the penultimate glacial (MIS 6), the last interglacial Samra Fm. (broadly corresponding to MIS 5), the last glacial Lisan Fm. (MIS 4-2) and the Holocene Ze'elim Formation. Most importantly, the sediment record includes also the transitions between these main formations, which are mostly absent in the previously described outcrop sediments (e.g. Torfstein et al., 2009; Waldmann et al., 2009; Stein et al., 2010).

The recovery of sediments reflecting the glacial-interglacial and vice versa transitions (MIS 7/6, 6/5, 5/4 and 2/1) will aid a better understanding of the response mechanisms of the Dead Sea lake during periods of major re-organizations of the ocean-atmosphere system, such as the Younger Dryas cold interval at the end of the last glacial. The new sediment record from the Dead Sea

basin also includes sediments representing Greenland Interstadial 1 (GI 1a-e; Björck et al., 1998), which preceded the Younger Dryas cold period and which is not represented in the on-shore outcrops. These sediments potentially allow, for the first time, a transient reconstruction of hydro-meteorological conditions into and out of the Younger Dryas for the Dead Sea region.

Even more challenging is to understand the hydrological response in the Eastern Mediterranean region to the last interglacial climate. In the North Atlantic realm, this period was even warmer than the present interglacial (Fronval et al., 1998) and might thus serve as a potential scenario for future developments. However, perceptions of last interglacial Dead Sea lake levels so far still suffer from large uncertainties. On the one hand, Samra stage lake levels are considered higher compared to the Holocene Dead Sea (Waldmann et al., 2009; 2010) probably due to additional moisture supply from southern sources leading to intensive floods and sediment transport to the basin. On the other hand, preliminary interpretation of a gravel layer in the DSDDP 5017-1 profile as a beach deposit led to the formulation of a dry-down hypothesis and related extreme dry conditions in the later part of MIS 5 (Stein et al., 2011). This hypothesis has been criticized and obviously requires further verification by more detailed analyses of the sediment cores, which, however, is beyond the scope of this paper. In case that a very dry Levant in late MIS 5 could be verified, this would imply a major regional difference to the central Mediterranean climate. There, vegetation reconstructions from the Monticchio lake record indicate a rather moist later part of MIS 5 and seasonal moisture deficiency was only found during the early phase of the last interglacial (Brauer et al., 2007). Therefore, further detailed investigation and especially dating of the new sediment record from the Dead Sea has a great potential for an advanced reconstruction of Mediterranean hydroclimates during the last interglacial.

In addition to their paleoclimatic significance, Dead Sea sediments from marginal depositional environments have been demonstrated as valuable recorders of earthquakes (e.g. Marco and Agnon, 1995; Migowski et al., 2004). The abundance of mass transport deposits such as turbidites and slumping structures particularly during glacial intervals in the deep environment of core location 5017-1 will provide a more complete earthquake record than obtained from the marginal areas of the basin. The potential of the new sediment profile for establishing improved long earthquake time series is not only of scientific importance, but also of social relevance.

The long Dead Sea sediment record from the deep basin has a great potential in many other respects reaching from interglacial vegetation reconstruction through pollen analyses to emerging fields like investigating microbial processes in the past through modern geo-microbiological approaches (Vuillemin and Ariztegui, 2013). Fundamental for all future investigations of this sediment archive is the general lithological classification presented in this paper. The Dead Sea record is unique in terms of its highly diverse sediment facies, which exceptionally well records past climate and environment variability. The general sedimentological description and classification presented here is considered a first step towards more detailed investigations including modern analytical approaches combining micro-facies analyses and μXRF element scanning (Brauer et al., 2009; Dulski et al., in press).

Acknowledgments

We thank two anonymous reviewers for their constructive comments, which improved the quality of the manuscript substantially. Funding by the International Continental Scientific Drilling Program (ICDP), the German Research Centre for Geosciences (GFZ, Potsdam), the German Science Foundation (DFG; grants FR 1672/2-1 and BR 2208/10-1), the Israel Science Foundation (ISF; Center of Excellence Grant #1736/11 to YE and ZBA) and the US National Science Foundation (NSF; grant EAR 11-15312) is gratefully acknowledged. The ICDP Dead Sea Deep Drilling Project would not have been possible without the great commitment and initial project idea of Prof. Jörg F. W. Negendank. We thank DOSECC for performing the drilling operation, the Moti Gonen Marine Station in Ein Gedi for all issues related to the organizational support and the ICDP Operational Support Group (Uli Harms, Ronald Conze, Jochem Kück, Matxalen Rey Abasolo, Martin Töpfer and Christian Carnein) for downhole logging and assistance with the Drilling Information System. Further we want to cordially thank the numerous assistants, students and professionals during the drilling, core opening and sampling campaigns and Andreas Hendrich (GFZ Potsdam) for help with the figure design. This study is a contribution to the Helmholtz Association (HGF) climate initiative REKLIM Topic 8 `Rapid climate change derived from proxy data´.

3 Hydroclimatic variability during the early last glacial (~117-75 ka) derived from micro-facies analyses of the Dead Sea ICDP sediment record

I. Neugebauer[a], M.J. Schwab[a], N.D. Waldmann[b], R. Tjallingii[a], U. Frank[a], E. Hadzhiivanova[b], R. Naumann[c], N. Taha[b], A. Agnon[d], Y. Enzel[d], A. Brauer[a,e], and DSDDP Scientific Party[#]

a Helmholtz Centre Potsdam, GFZ German Research Centre for Geosciences, Section 5.2 – Climate Dynamics and Landscape Evolution, Telegrafenberg, 14473 Potsdam, Germany

b University of Haifa, Department of Marine Geosciences, Leon H. Charney School of Marine Sciences, Mount Carmel 31905, Israel

c Helmholtz Centre Potsdam, GFZ German Research Centre for Geosciences, Section 4.2 – Inorganic and Isotope Geochemistry, Telegrafenberg, 14473 Potsdam, Germany

d The Hebrew University of Jerusalem, The Fredy & Nadine Herrmann Institute of Earth Sciences, Givat Ram, Jerusalem 91904, Israel

e University of Potsdam, Institute of Earth and Environmental Science, Karl-Liebknecht-Str. 24-25, 14476 Potsdam-Golm, Germany

The complete list of scientists involved in the DSDDP can be found at http://www.icdp-online.org

Submitted manuscript to Climate of the Past (under review).

Abstract

A key region for deciphering hydrological responses to climate changes at the transition from interglacial to glacial climate conditions is the Levant. Recently a new sediment record from the Dead Sea provides a unique archive for hydroclimatic variability based on reconstructing lake level variations. Here we present high-resolution sediment facies analysis and elemental composition by µXRF scanning of core 5017-1 from the Dead Sea basin to trace hydroclimatic variability and lake levels in the time interval from ca 117-75 ka, i.e. the transition between the last interglacial and the onset of the last glaciation. We distinguished six different micro-facies types and interpreted these in terms of past lake level changes and associated hydroclimatic variability. The two end-members for highest and lowest lake levels are up to several meters thick, greenish sediments of alternating aragonite and detrital marl laminae (*aad*) and thick halite facies, respectively. Intermediate lake levels are characterised by detrital marl sediments with varying amounts of aragonite, gypsum or halite, reflecting higher levels, short-term drops or lower levels, respectively. Correlation of the deep-basin sediment facies to exposed sediments at the lake's margin allow a gross estimation of lake level fluctuations of at least 80 m, with stands below ~400 m below present-day mean sea level (bmsl) in the halite-dominated sections to stands at ~320 m bmsl in the greenish *aad* sections.

Applying a recently published chronology (Torfstein et al., 2015), two low lake level intervals occurred at ~110-108 ± 5 ka and ~93-87 ± 7 ka and likely coincide with stadial conditions in the central Mediterranean (Melisey I and II pollen zones in Monticchio) and low global sea levels related to MIS 5d and 5b, respectively. Two intervals of higher lake stands at ~108-93 ± 6 ka and ~87-75 ± 7 ka correspond to interstadial conditions in the central Mediterranean (St. Germain I and II pollen zones in Monticchio) and Greenland (GI 24+23 and 21) as well as to sapropels S4 and S3 in the Mediterranean Sea and MIS 5c and 5a. These apparent correlations suggest a close link of the climate in the Levant to North Atlantic and Mediterranean climates during the time of the build-up of Northern hemisphere ice shields in the early last glacial period. In particular, we present new petrographic data and facies analyses of a well-sorted gravel layer that contradicts with its interpretation as an indication for a major draw-down of the Dead Sea.

3.1 Introduction

The Dead Sea and its Pleistocene precursor lakes Amora, Samra and Lisan experienced major lake level fluctuations in the past as a sensitive response to changing hydroclimatic conditions in the lake's watershed (e.g. Enzel et al., 2008). The lakes expanded during glacial intervals, whereas interglacials are characterised by a general lake contraction due to reduced rainfall and runoff (Enzel et al., 2008; Rohling, 2013) and/or increased evaporation caused by higher temperatures. Hence, the last glacial Lake Lisan, which occupied the Dead Sea basin (DSB) between ~70 and 14 ka, reached up to ~270 m higher lake stands than the Holocene Dead Sea or the last interglacial Lake Samra (e.g. Bartov et al., 2002; 2007; Waldmann et al., 2007; Torfstein et al., 2013b). Since the global sea level was about 130 m lower during the last glacial maximum (e.g. Shackleton, 1987; Siddall et al., 2003), the Lisan lake level was at about sea level during that time compared to the present day ca 430 m lower elevation. Particularly strong lake level drops occurred at the transitions from glacial to interglacial climate conditions (e.g. Yechieli et al., 1993; Bartov et al., 2007; Waldmann et al., 2009; Stein et al., 2010). For example, the relatively fresher water body of Lake Lisan turned to the hypersaline Holocene Dead Sea during the last termination leading to the deposition of a thick halite sequence during the early Holocene (~11-10 ka; e.g. Stein et al., 2010).

In contrast, less information is available about lake level changes during the transition from interglacial to glacial climate conditions. Previous studies from exposed sediment sections of the Samra Formation at the south-western margin of the Dead Sea suggested a relatively shallow Lake Samra from ca 135 to 75 ka (Waldmann et al., 2007; 2009; 2010). The main lake level rise at the transition from Lake Samra to Lake Lisan was assumed from a sedimentological change from sand deposits to sediments of alternating fine laminae of aragonite and detritus at a major unconformity ~75-70 ka (e.g. Waldmann et al., 2009; Torfstein et al., 2013b). However, the early glacial time interval between the last interglacial low stand (Lake Samra) and the full glacial high stand (Lake Lisan), i.e. coinciding with MIS 5d to 5a, is not well represented in the outcropping sediment profiles (Waldmann et al., 2009).

Sediments from this time interval have been for the first time recovered by ICDP drilling project DSDDP from the deepest part of the DSB (Neugebauer et al., 2014). Based on a new chronology and interpretation of a well-sorted gravel deposit, Torfstein et al. (2015) inferred an almost complete drawdown of the Dead Sea leading to a sedimentary hiatus between 116 and 110 ka at around MIS 5d, which is considered the most extreme lake level drop during the last ~220 ka, i.e. the time period covered by the DSDDP sediment record. A trend towards drier conditions inferred from pollen and calcite data has also been reported from the northern Levant Yammoûneh sediment record in Lebanon (Gasse et al., 2015), although these dry conditions appear less extreme than assumed for the Dead Sea by Torfstein et al. (2015). Torfstein et al. (2015) suggest an African monsoon contribution to moisture supply in the southern Levant during more humid intervals in the early last glacial, which are considered to coincide with MIS 5c and 5a, whereas Gasse et al. (2015) propose that the northern Levant responded to long-term

orbitally induced temperature fluctuations, ice sheet waxing and waning in the northern hemisphere and climatic changes in the North Atlantic.

In this study, we apply a combination of petrographic, micro-facies and high-resolution XRF analyses to investigate in more detail the sedimentological changes in the new ICDP Dead Sea record between the last interglacial and the onset of the Lisan (~117-75 ka) as indicators for hydroclimatic variations in the southern Levant. One focus of our study is on the gravel layer in order to test the hypothesis of a major drawdown of the Dead Sea (Stein et al., 2011; Torfstein et al., 2015).

3.2 Regional setting

With a lake level of 428 m below mean sea level (m bmsl; in 2014) and water depth of ca 300 m the Dead Sea is located in one of the lowest continental depressions on earth. The basin is bounded by the Judean Mountains on the west and Jordan Plateau on the east, rising to heights of ~1000 m and ~1200 m above mean sea level, respectively (Fig. 3-1). The modern watershed of the lake, which is one of the largest in the Levant (~40,000 km²), experiences subhumid to semiarid Mediterranean climate in its north and arid to hyperarid conditions in the southern part typical of the Saharo-Arabian desert belt. These climate conditions combined with the particular steep topography of the basin margins create a hyperarid and extreme climate condition at the lake itself. The modern Dead Sea is a hypersaline Ca-chloride brine (e.g. Katz et al., 1977; Lensky et al., 2005) and a terminal lake, mainly fed by the Jordan River (Fig. 3-1). Precipitation primarily arrives in the watershed in fall to late spring (Oct-May) through eastern Mediterranean mid-latitude cyclones (Cyprus Lows; Ziv et al., 2006; Enzel et al., 2008) and tropical plumes in winter and spring (also termed subtropical jet storms by Kahana et al., 2002; Rubin et al., 2007). Occasionally, the region is influenced by the Active Red Sea Trough from the south during fall and winter (e.g. Enzel et al., 2008). The geology of the catchment is predominantly characterised by Cretaceous carbonate sedimentary rocks, with some Palaeozoic to Mesozoic sandstones and Pleistocene volcanic units (Bentor, 1961; Sneh, 1998).

3.3 Material and methods

3.3.1 Dead Sea deep-basin core 5017-1

The 5017-1 sediment core from the deep Dead Sea basin (31°30'29" N, E 35°28'16" E; ca 300 m water depth in 2010; sediment surface ~725 m bmsl; Fig. 3-1) was obtained during the drilling campaign of the ICDP Dead Sea Deep Drilling Project (DSDDP) in winter 2010-11. The record is ~455 m long and comprises two full glacial-interglacial cycles (Neugebauer et al., 2014; Torfstein et al., 2015). Here, we focus on a ~65 m long section from ~180 to ~245 mblf (m below lake floor). Sediment facies were described with an accuracy of 1 cm based on line-scanning images of the split sediment cores. Magnetic susceptibility data in 1 mm resolution were

routinely obtained for the entire 5017-1 record (see Neugebauer et al., 2014 for details) and are used here for further analyses.

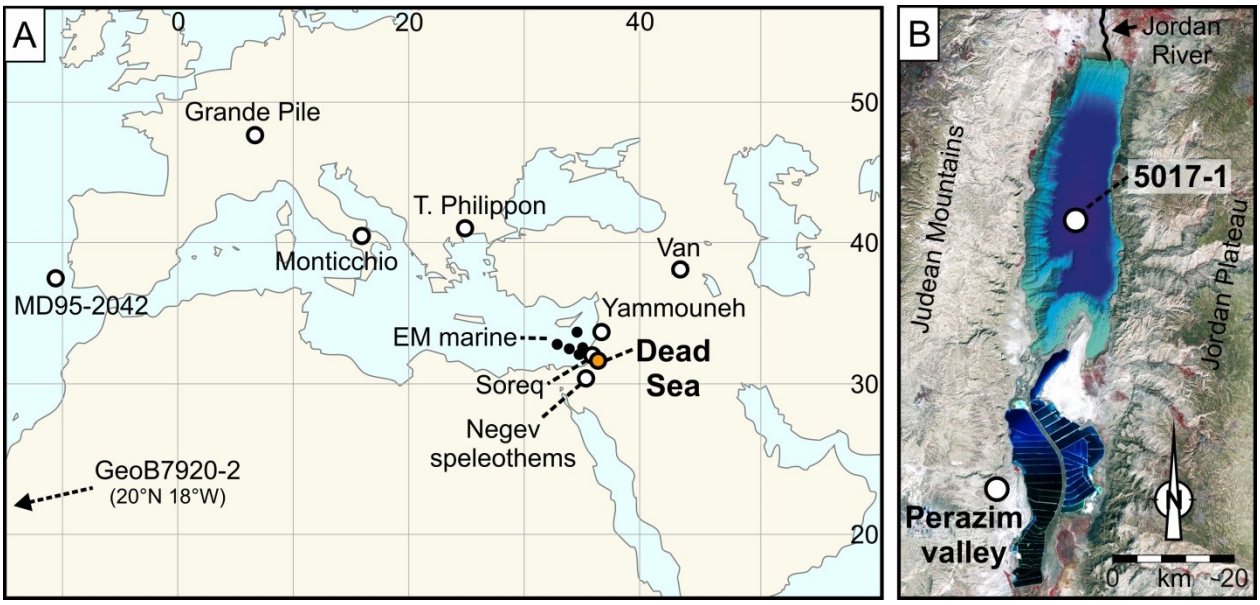

Figure 3-1: (A) Location of Mediterranean records discussed in the text; EM marine – eastern Mediterranean marine cores (Cheddadi and Rossignol-Strick, 1995; Almogi-Labin et al., 2009); Negev speleothems – various caves in the northern, central and southern Negev (see Vaks et al., 2006; 2007; 2010); for references of the other records the reader is referred to the text; (B) map of the Dead Sea (NASA image by R. Simmon using Landsat data (2011) from USGS, www.visibleearth.nasa.gov/), bathymetry of northern Dead Sea basin from Sade et al. (2014), 5017-1 coring location, Perazim valley Samra outcrop PZ-7 (Waldmann et al., 2009).

3.3.2 Micro-facies analyses

For micro-facies analyses we applied a combination of petrographic thin section microscopy and high-resolution µXRF element scanning. A total of 26 thin section samples (10 x 2 cm) were prepared representing changes in facies types along the section. Preparation largely followed the standard procedure for soft sediments (e.g. Brauer et al., 1999b). However, all steps were performed under dry conditions to avoid salt crystallization during the preparation process. Thin sections were analysed with a petrographic microscope (Leica DMLP) and images were taken with a digital camera (Olympus DP72). Fluorescence was analysed using a Nikon AZ100M microscope, operated with violet and polarised light conditions, and Nikon photo software (NIS Elements AR 4.3).

The µXRF measurements were acquired every 200 µm for 10 s using the ITRAX µXRF core scanner at GFZ-Potsdam, Germany. The core scanner is equipped with a Cr tube operated at 30 kV and 30 mA to irradiate the split-core sediment surface. This non-destructive method acquires element intensities of Si, S, Cl, K, Ca, Ti, Fe, Br and Sr (Neugebauer et al., 2014;

accepted), which are presented as count rates (counts per second – cps). The element intensity records reflect relative changes in the composition of the Dead Sea sediments, but are also influenced by physical sediment properties (e.g. density, water content, grain size) and the sample geometry. The easiest and most convenient way to minimize the physical and geometrical sample effects is by the transformation of element intensities into ratios or log-ratios (Weltje and Tjallingii, 2008).

3.3.3 Grain size analyses and gravel petrography

Laminated sediments were sampled for grain size measurements with 1 cm^3 sample volume, 1-3 cm resolution and a total number of samples of 363. Sample preparation included decomposing organic matter using 30 ml H_2O_2 (30%) and distilled water (1:1 concentration), and breaking aggregates with Calgon detergent ($(NaPO_3)_6$, 1%) and ultrasonic bath. The particle size distribution was measured using an LS 13 320 laser diffraction particle size analyzer for 1) the total sample and 2) the carbonate-free sample after dissolution through HCl (32%, dilution of 1:9 with distilled water). Less than 1 g of sediment was required for measurement.

From the ~455 m long core 5017-1, 22 gravel layers identified at various depths were sampled to analyse the petrography of these gravels. The samples were wet-sieved for five grain size fractions (>4 mm, 2-4 mm, 1-2 mm, 0.5-1 mm and <0.5 mm), for which strewn slides have been prepared for microscopic inspections. Here, we present results for two out of five gravel units that occur within the analysed core section (180-245 mblf). More detailed investigations are subject of ongoing work.

3.3.4 XRD and TOC/$CaCO_3$ measurements

For X-ray powder diffraction measurements 25 samples were collected from about the same depths as thin sections to support microscopic inspections. Powder X-ray patterns were collected using a PANalytical Empyrean powder diffractometer with Cu Kα radiation, automatic divergent and antiscatter slits and a PIXcel^{3D} detector. The diffraction data were recorded from 5° to 85° 2Θ via a continuous scan with a step-size of 0.013 and a scan time of 60 s per step. The generator settings were 40 kV and 40 mA.

Total organic carbon (TOC) and $CaCO_3$ contents have been determined from 19 of these samples using an elemental analyser (EA3000-CHNS Eurovector). First, for total carbon (TC) 5-10 mg of sample aliquots were weighed in Sn-capsules. Second, for TOC determination another 3-4 mg of the samples were decalcified in Ag-capsules in three steps through treatment with (1) 3% HCl, (2) 20% HCl and (3) drying at 75°C. Data were calibrated with standards (BBOT, Sulfanilamide, for TOC additionally Boden3) and empty Sn- and Ag-capsules. The relative standard deviation is <1%. $CaCO_3$ contents were calculated from the difference TC-TOC.

3.4 Results

3.4.1 Micro-facies, sedimentological and geochemical characterisation

The sediments of the analysed ~65 m long section of core 5017-1 mainly consist of laminated marl of the *aad* facies (alternating aragonite and detritus; Machlus et al., 2000), gypsum and massive halite deposits (Neugebauer et al., 2014). The detrital material is commonly composed of clay to silt-sized calcite, quartz, dolomite and minor feldspar and clay minerals. Thickness of detrital layers ranges from <1 mm to several cm and colour is usually greyish, black, if iron sulphides are present (pyrite or greigite) and brownish or greenish due to terrestrial organic or algal remains. Aragonite formed as 5-15 μm small stellate aggregates of orthorhombic crystals building ~0.1-4 mm thick white laminae. Monoclinic, euhedral ~10-60 μm gypsum crystals build ~0.2-3 cm thick beige layers. Larger, up to 1 mm gypsum crystals appear scattered within detrital layers. Cubic, ~1 mm to several cm long halite crystals are either embedded in predominantly detrital marl or build thick deposits. These thick halite deposits contain only minor detrital material and are often layered.

Six micro-facies types were identified (Fig. 3-2):

i) *green aad*: alternating white aragonite and greenish detrital marl laminae (~1 mm thick couplets; Fig. 3-2a), the greenish laminae exhibit some diatoms and very strong fluorescence pointing to a significant amount of chlorophyll preserved in the sediment (Fig. 3-2f);

ii) *aad-n*: alternating white aragonite and greyish detrital marl laminae (~1 mm thick couplets, occurrence as normal type; defined by Machlus et al., 2000);

iii) *aad-II*: alternating white aragonite and greyish detrital marl laminae with thicker aragonite layers than normal type (~1-5 mm thick couplets, Fig. 3-2b);

iv) *gd*: well-laminated to massive, cm-thick gypsum deposits and detrital marl (Fig. 3-2c);

v) *hd*: cubic halite crystals (mm-cm) scattered in detrital marl;

vi) *lh/hh*: layered or homogeneous consolidated halite; the layered type often alternates with thin detrital marl laminae (Fig. 3-2d).

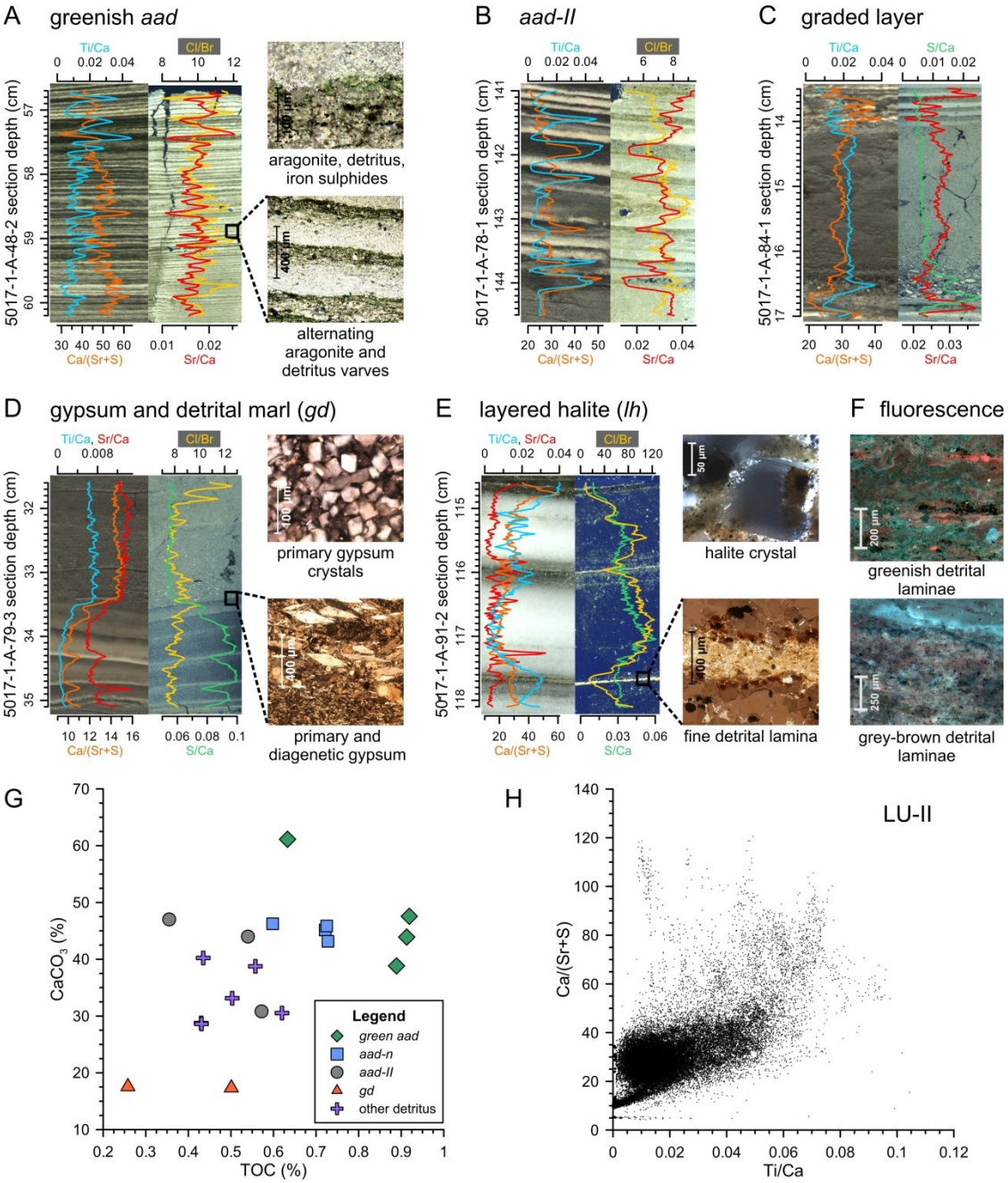

Figure 3-2: Micro-facies (core photos, polarised thin section scans and microscopic images with varying magnification and polarisation conditions) and µXRF characteristics (element ratios): (A) *green aad* facies with peaks in Sr/Ca typical for aragonite layers and peaks in Ti/Ca and Ca/(Sr+S) indicating detrital layers; (B) *aad-II* facies containing greyish detritus and thicker aragonite layers than the *green aad* facies; (C) example of a mass-movement deposit: graded layer with high Ti/Ca ratio and increased S/Ca at the base due to diagenetic gypsum; (D) *gd* facies characterised by high S/Ca ratio; (E) *lh* facies with high Cl/Br and positively correlated S/Ca, but peaks of all other elements only in the thin detrital laminae; (F) fluorescence (violet light) microscope images of greenish detrital laminae (upper photo, core section 5017-A-1-87-1, at ~72 cm) with very strong fluorescence (red colour) and greyish-brownish detrital laminae (lower photo, core section 5017-1-A-78-1, at ~140 cm) that are characterised by a weaker fluorescence; (G) correlation plot of TOC against $CaCO_3$ contents of 19 samples distinguished for different micro-facies types; (H) correlation plot of the two detrital fractions as derived from µXRF element scanning, exemplary for lithological unit (LU) II: Ti/Ca as proxy for the siliciclastic detrital fraction and Ca/(Sr+S) as proxy for the detrital carbonate fraction, $R^2 = 0.4$.

In addition, up to 1.7 m thick graded layers and up to 3 m thick slump deposits are frequently intercalated in the laminated sediments (see Neugebauer et al., 2014 for details). These deposits are predominantly associated to the *aad* micro-facies types, whereas they are less frequent and less prominent in the halite-dominated sections. Importantly, at their base or repeated within at least 22 slump deposits, matrix-supported ~2-8 mm gravels occur, commonly building some cm to tens of cm thick gravel units. These gravel particles are commonly angular to rounded limestone and dolomite clasts as well as cemented aragonite peloids, gypsum, anhydrite, halite and minor quartz (Fig. 3-3). These gravels associated to slump deposits occur at various depths in core 5017-1, of which four were identified within the section analysed here, at composite depths of ~233.5 m, ~192.8 m, ~183.5 m and ~183 m (Fig. 3-4). Fine and medium gravel fractions constitute ~40% of the total dry weight of an exemplary sample from ~233.5 m depth (Fig. 3-3b).

In one exceptional case at ~239 m composite depth a well-sorted ~35 cm thick gravel layer completely lacking fine-grained material occurred (Figs. 3-3 and 3-4). The petrographic composition of this gravel is the same as that of the other mud-supported gravels, but the fine and medium gravel fractions account for ~98% of the dry weight (Fig. 3-3). This gravel layer occurred in core 5017-1-A-92-1 with a major loss of core material. From a 130 cm core drive only 35 cm gravels and 10 cm mud, halite and gravel are recovered, so that the gravel is isolated and without any transition to over- and underlying sediments (Fig. 3-3).

Average grain size of the laminated sediments, excluding the halite-facies types *hd* and *lh/hh*, varies between ~11 µm including $CaCO_3$ and ~14 µm for the siliciclastics (i.e. after dissolution of $CaCO_3$; Supplement Table S 3-1). The sediment grain size distribution is mainly described by clay (~53% and ~41% with and without $CaCO_3$, respectively), very fine silt (~45% and ~56% with and without $CaCO_3$, respectively) and very little sand (~1.6% and ~2.5% with and without $CaCO_3$, respectively). Gypsum-detritus samples (*gd*-facies) revealed the coarsest mean grain size of ~26 µm (~30 µm without $CaCO_3$) and the highest sand fraction (~4% and ~7%, with and without $CaCO_3$, respectively). The *aad-n* and *aad-II* micro-facies show similar and low mean grain sizes of ~7 µm (~10 µm without $CaCO_3$), while the *green aad* type exhibits a slightly higher mean value of ~9 µm (~12 µm without $CaCO_3$). Also the silt and sand fractions of the *green aad* type are enhanced in comparison to the other two *aad* types (Supplement Table S 3-1).

The differentiation of the laminated micro-facies types *gd*, *aad-II*, *aad-n* and *green aad* is supported by total organic carbon and calcium carbonate contents (Fig. 3-2g). The *gd* facies is characterised by lowest values of 0.25-0.5% TOC and ~18% $CaCO_3$, followed by the *aad-II* facies (0.35-0.57% TOC, 30-47% $CaCO_3$) and the *aad-n* facies exhibiting higher values (0.6-0.7% TOC, ~47% $CaCO_3$). The *green aad* facies shows highest TOC (0.65 and ~0.9%) and $CaCO_3$ contents (~40-50 and 62%).

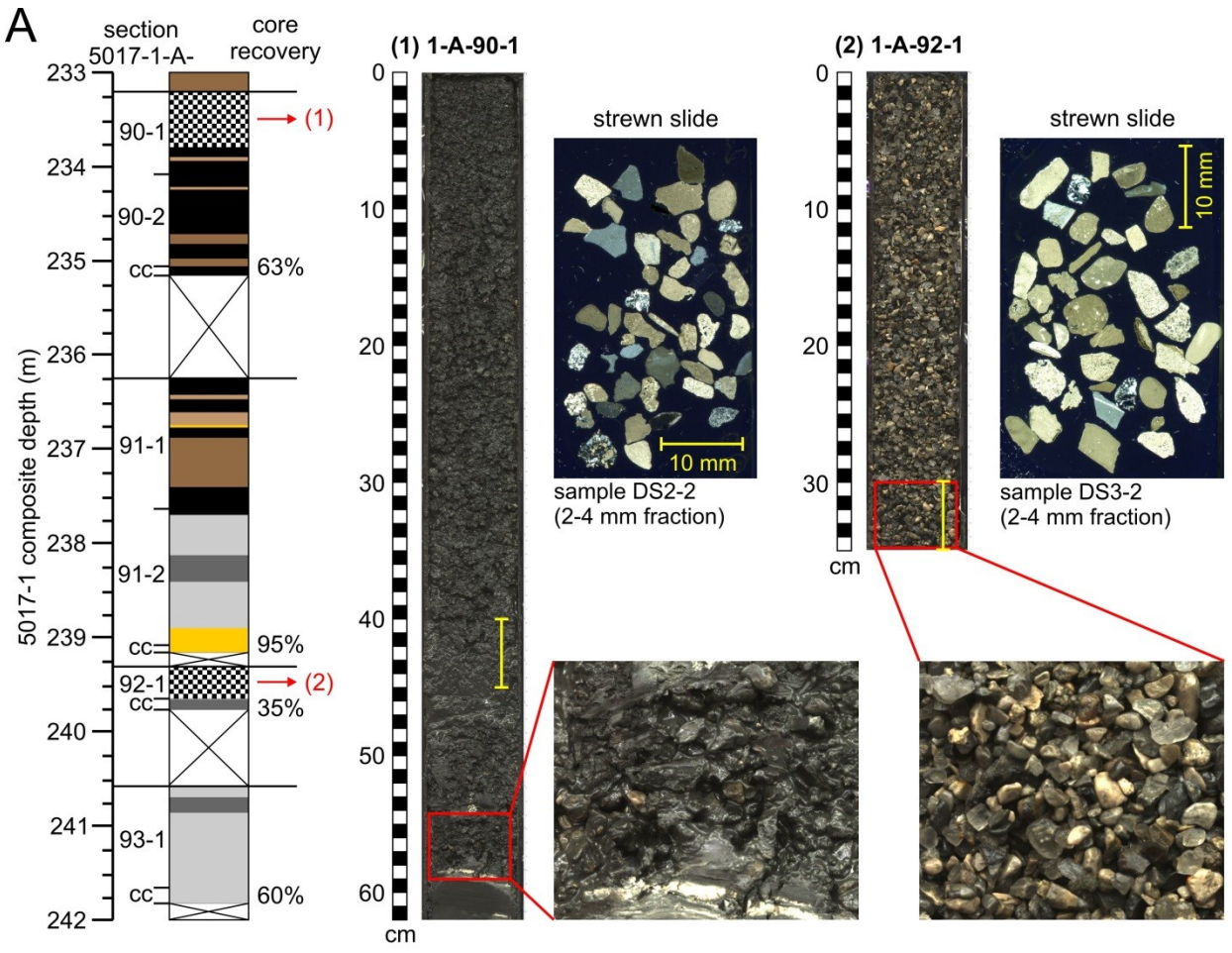

B

core section	lab ID	fraction (µm)		dry weight (g)	dry weight (%)
5017-1-A-90-1	**DS2**				
40-45 cm	DS2-1	> 4000	> FGr	2.014	3.54
	DS2-2	2000-4000	FGr	21.012	36.92
	DS2-3	1000-2000	CSa	5.102	8.96
	DS2-4	500-1000	MSa-CSa	0.169	0.30
	DS2-5	< 500	< MSa	28.622	50.29
5017-1-A-92-1	**DS3**				
30-35 cm	DS3-1	> 4000	> FGr	33.640	47.82
	DS3-2	2000-4000	FGr	35.110	49.91
	DS3-3	1000-2000	CSa	1.556	2.21
	DS3-4	500-1000	MSa-CSa	0.045	0.06
	DS3-5	< 500	< MSa	0	0

Figure 3-3: (A) Lithological profile from 233-242 m composite depth (cc – core catcher), two gravel deposits in core sections (1) 5017-1-A-90-1 (233.17 m composite depth) and (2) 5017-1-A-92-1 (239.27 m composite depth) and strewn thin slide scans (polarised light) of the 2-4 mm grain fractions; yellow bars indicate sampling positions in the two core sections. Both gravels are composed of carbonates (limestone, dolomite, with a presence of aragonite) in the form of sparite, (bio)micrite or peloid, and sulphates (gypsum, anhydrite) as well as halite and minor quartz; (B) table of grain size fractions after sieving for one example of a mud-supported gravel occurrence and the pure gravel layer, both as shown in (A).

The elements Si, S, Cl, K, Ca, Ti, Fe, Br and Sr were obtained by µXRF scanning and used to characterize the Dead Sea sediments (Fig. 3‑2; see also Neugebauer et al., 2014; accepted). Aragonite laminae are revealed by high Sr/Ca values, gypsum is represented by high S/Ca values and halite is best characterized by the Cl/Br ratio (Fig. 3-2). The elements Si, K, Ti and Fe are constrained to siliciclastics in the detrital sediment fraction. More ambiguous is the interpretation of Ca that occurs in aragonite, gypsum and detrital calcite. The Ca/(Sr+S) ratio indicates the detrital carbonate fraction because the authigenic Ca sources, i.e. aragonite and gypsum, are removed. The Ti/Ca ratio represents the relative siliciclastic fraction (Fig. 3-2). The sum of Ca/(Sr+S) and Ti/Ca ratios best represents the total amount of carbonate and siliciclastic detritus (Fig. 3-4). A correlation plot of these two element ratios shows significant correlation ($R^2 = 0.4$) for the carbonate and siliciclastic detrital fractions (Fig. 3-2h), but also indicates an additional Ca-bearing detrital fraction.

3.4.2 Lithostratigraphy

The analysed section of core 5017-1 is sub-divided into four main lithostratigraphic units (Fig. 3-4). Units I and III are predominantly composed of halite (controlled by *hd* and *lh/hh* facies), some gypsum and detrital marl. Units II and IV present primarily *aad* (*green aad*, *aad-n* and *aad-II*) and *gd* facies. These lithostratigraphic units are tied to the stratigraphic framework (Neugebauer et al., 2014) and the U-Th chronology (Torfstein et al., 2015) of the 5017-1 core.

The lowermost unit I (245-237.5 m composite depth) is the upper part of a ca 40 m thick halite sequence, the thickest halite in the entire core, and is part of the last interglacial Samra Formation (Neugebauer et al., 2014). This unit has very low magnetic susceptibility values and Sr/Ca ratios with high Cl/Br ratios (Fig. 3-4). A gravel layer, mainly composed of limestone and dolomite clasts and halite, was identified within this halite unit ~2 m below its top (Figs. 3-3 and 3-4). U-Th ages point to a sedimentary hiatus between ca 116-110 ± 3 ka marked by this gravel layer (Torfstein et al., 2015).

The ~25 m thick unit II (237.5-212.5 m) is mainly composed of *aad* and *gd* facies and can be divided into two sub-units. Sub-unit II-a (237.5-228 m) comprises *aad-II*, *aad-n* and *gd* facies and is characterized by low Sr/Ca and Cl/Br ratios and distinct peaks in magnetic susceptibility. Sub-unit II-b (228-212.5 m) differs from sub-unit II-a as in addition it presents three thick sequences of the *green aad* facies and partly high Sr/Ca ratios. Unit II is characterized by frequent, up to several m thick, graded detrital layers and slump deposits (Fig. 3-4). U-Th ages place unit II between ca 108 ± 5 and 93 ± 7 ka (Torfstein et al., 2015), i.e. an interval of ~3-27 thousand years. An initial varve counting on the core photographs of this unit reveals 4050 ± 250 varves, which is within the uncertainty of the U-Th ages. Unit II builds the upper part of the Samra Formation of core 5017-1 as defined by Neugebauer et al. (2014).

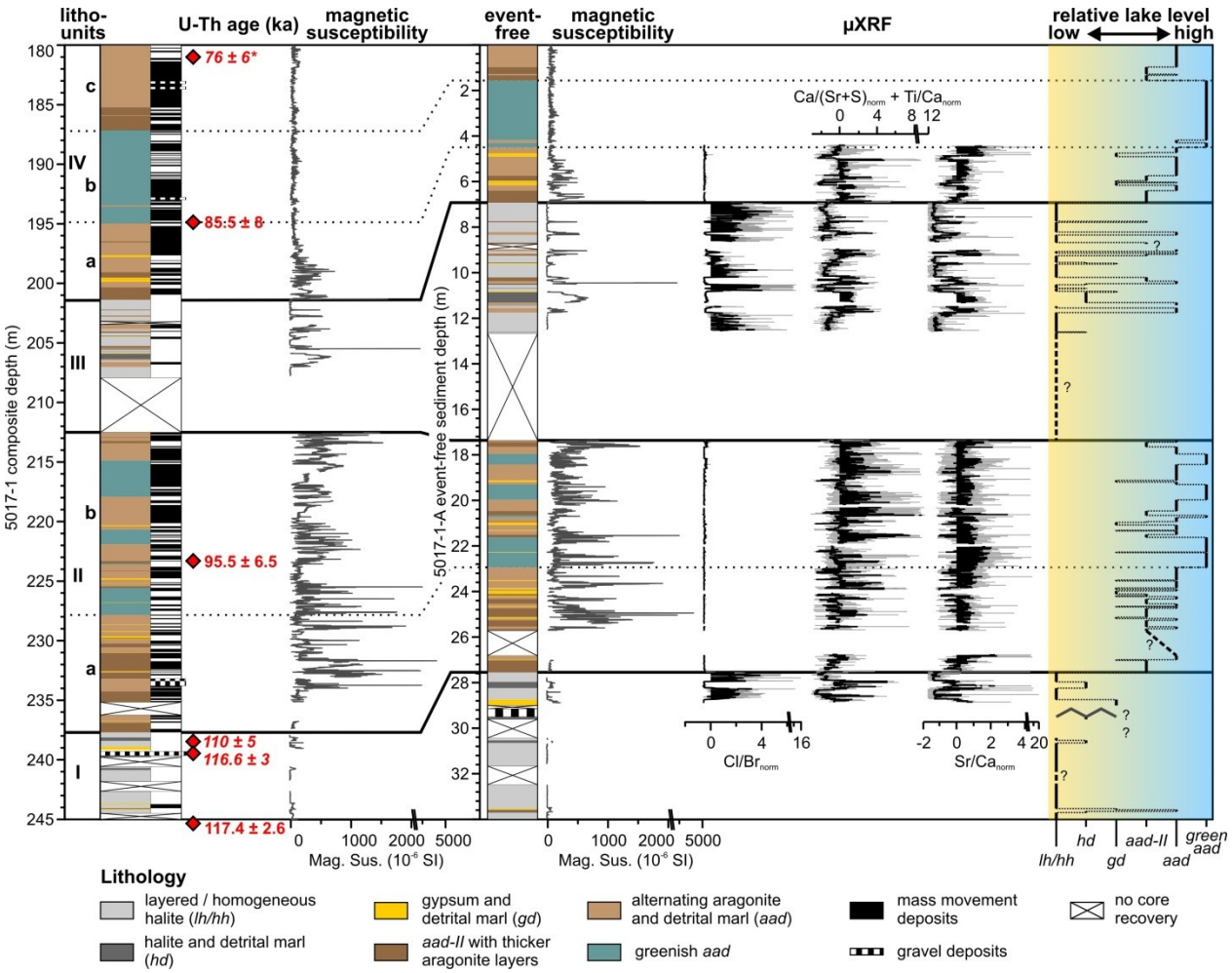

Figure 3-4: Lithology of the ~65 m long 5017-1 core section: lithostratigraphic units, U-Th ages (from Torfstein et al., 2015), with extrapolated ages in italic, * - interpolated age (see text for explanation), magnetic susceptibility (1 mm resolution, 10^{-6} SI); event-free lithology, µXRF data (grey: 200 µm steps, black: 101-steps running means of counts) and the relative lake level changes inferred from the changing micro-facies. All mass movement deposits thicker than 1 cm were excluded from the event-free lithological profile and data, event-free sediment depth starts with zero at 180 m below lake floor. µXRF data of normalized ratios: Cl/Br representing halite, Ca/Sr+S) + Ti/Ca indicating the total carbonate and siliciclastic detritus, Sr/Ca indicating aragonite.

Unit III (212.5-201.5 m) is dominated by halite deposits of the *hd* and *lh/hh* facies, which is well reflected in high Cl/Br ratios. The lower ca 4 m of this unit were not recovered due to the hard salt that was difficult to core (Neugebauer et al., 2014). Some cm- to dm-thick occurrences of *aad-n*, *aad-II* and *gd* facies are intercalated in the halite deposits, as reflected by higher magnetic susceptibility, Ca/(Sr+S) + Ti/Ca and Sr/Ca ratios. Unit III was deposited between ca 93-87 ± 7 ka BP (Torfstein et al., 2015) and marks the transition between the Samra and Lisan Formations in the deep-basin core 5017-1 (Neugebauer et al., 2014). When compared with the chronology at the lake's margins, this transition at ca 87 ka in the deep core is placed ca 15 thousand years

earlier than in the outcrops. There, the Samra-Lisan transition is marked by a sedimentary unconformity from 75-70 ka (Waldmann et al., 2009).

The uppermost unit IV (201.5-180 m) compares to unit II and is characterized by the three *aad* facies, as indicated by higher Ca/(Sr+S) + Ti/Ca and Sr/Ca ratios and the absence of halite (Fig. 3-4). In contrast to unit II, where magnetic susceptibility strongly fluctuates, constantly low magnetic susceptibility characterizes unit IV (Fig. 3-4). This unit can be divided into three sub-units: (1) sub-unit IV-a is composed of *aad-n*, *aad-II* and *gd* facies, (2) sub-unit IV-b is a *green aad* section, and (3) sub-unit IV-c is composed of *aad-n* and *aad-II*. Several cm- to m-scale thick slumped deposits and graded detrital layers occur in unit IV. At a composite core depth of ~195 m the sediment was dated to an age of ca 85.5 ± 8 ka. Six m above unit IV (i.e. at 174.5 m depth) the age is 70.5 ± 5 ka BP (Torfstein et al., 2015). The interpolated age of the upper boundary of unit IV at 180 m depth is ca 75 ± 6 ka BP. Unit IV builds the lowermost part of the Lisan Formation of core 5017-1 (Neugebauer et al., 2014).

3.5 Discussion

3.5.1 Micro-facies as relative lake level indicators

Lake levels of the water bodies occupying the DSB are sensitive responders to changing hydro-climatic conditions in the lake's catchment (Enzel et al., 2003; Bookman et al., 2006; Enzel et al., 2008). Lake level reconstructions based on on-shore sequences indicate a total amplitude of lake level fluctuation of at least ~270 m, with lowest levels of ~430 m bmsl occurring during parts of the last interglacial, the Holocene and during recent times (e.g. Bookman (Ken-Tor) et al., 2004; Bartov et al., 2007; Waldmann et al., 2009; Stein et al., 2010). The highest lake level of Lake Lisan of ~160 m bmsl was reached during the last glacial maximum (Bartov et al., 2003). These exposed sediments at the Dead Sea margins also showed that different lake levels resulted in different sediment facies (e.g. Machlus et al., 2000; Migowski et al., 2006). We can, hence, use facies types as proxies for changing trends in lake level that, in turn, reflect changing climatic conditions (Figs. 3-4 and 3-5). These trends are important for climatic inferences as they point to the net lake budget over decades to millennia. In this research, we avoided inferences of the highest resolution changes in lake budget due to the relatively large age uncertainties of U-Th ages and concentrated the effort in reconstructing changes at centuries-millennia temporal scales, hence keeping conservative inferences.

The sediment facies characteristic for high-stands and rising levels of the last glacial Lake Lisan and Holocene Dead Sea are rich in the so-called *aad* facies that is composed of alternating aragonite and detritus (Machlus et al., 2000; Bookman (Ken-Tor) et al., 2004). Deposition of *aad* requires sufficient freshwater and the bicarbonate it supplies through runoff during the rainy season to trigger precipitation of primary aragonite during the subsequent dry season (Stein et al., 1997). Three different micro-facies of *aad* were distinguished in the investigated sediment section of core 5017-1. (i) *Green aad* (Fig. 3-2) comprises greenish detrital laminae containing

green algae remains and is interpreted to represent highest lake levels or fresher limnological conditions, as this facies also depicts the sediments deposited in core 5017-1 during the Last Glacial Maximum highest stands (Neugebauer et al., 2014), when Lake Lisan reached its maximum extent (e.g. Begin et al., 1974; Bartov et al., 2002). (ii) The *aad-n* and (iii) the *aad-II* facies are similar, except that *aad-II* is characterised by commonly thicker, but irregularly spacing aragonite laminae (Fig. 3-2). This may indicate insufficient supply of bicarbonate to support annual aragonite formation. Therefore, the *aad-II* facies is interpreted to be deposited during episodes of lower lake levels compared to the *aad-n* facies. The *aad-II* facies also differs from the *ld* facies-type (laminated detritus), which exhibits significantly coarser mode of the detritus (50-60 μm) than *aad* (8-10 μm; Haliva-Cohen et al., 2012) and which is a characteristic facies for intermediate lake levels of the interglacial Samra and Ze'elim Formations (e.g. Migowski et al., 2006; Waldmann et al., 2009; Neugebauer et al., 2014). The *ld* facies-type was, however, not detected in the core section analysed here, which is supported by the continuously fine grain sizes of ~10 μm for all three *aad* facies (Supplement Table S 3-1).

The deposition of well-laminated or massive gypsum (*gd* facies, Fig. 3-2) is associated with mixing of the water body due to lake level fall and a thinning of the upper freshwater layer (Torfstein et al., 2008). Halite deposition is related to a negative water balance during times of decreased lake levels (as in today's Dead Sea). Here, we distinguish between a mixed halite-detritus facies (*hd*) and massive or layered, consolidated halite (*lh/hh* facies, Fig. 3-2). Whereas the presence of detritus suggests some freshwater influx, deposition of thick halite indicates episodes of lowest lake levels.

The μXRF element scanning data greatly support lake level trends inferred from micro-facies analysis in terms of water balance (Figs. 3-4 and 3-5). Halite sequences are expressed in the Cl/Br ratio and are associated with a negative water balance. The detrital input depends on the erosion in the catchment, aeolian deposition over lake and catchment, and freshwater supply to the lake. The relative detrital input can be estimated using the Ca/(Sr+S) ratio (for carbonate fraction) and the Ti/Ca ratio (for siliciclastic fraction). The Sr/Ca ratio resembles the aragonite amount that increases with enhanced supply of freshwater. The combination of these ratios by summing up both detrital fractions and aragonite and subtracting halite, results in a curve that can be interpreted as proxy for water balance (Fig. 3-5), with negative values for halite and gypsum deposits and positive values for detritus and aragonite.

3.5.2 Gravel deposits in the deep basin

The well-sorted, 35 cm thick gravel layer found at ~239 m composite sediment depth (Figs. 3-3 and 3-4) is a unique deposit and has played a major role for inferring an extreme lake level change. This gravel was interpreted as beach deposit and as such the main argument for suggesting a major drawdown of the lake or even almost desiccation at the end of the last interglacial (Stein et al., 2011; Torfstein et al., 2015). At the position of this gravel layer, a sedimentary hiatus was suggested from ~116 to 110 ka based on combined U-Th dating and

oxygen isotope stratigraphy of the 5017-1 core (Torfstein et al., 2015). However, the interpretation of a beach layer is not unambiguous and must be questioned if the gravel deposit is examined in more detail. First of all, it is suspicious that no information about the in-situ contacts of the gravel to over- and underlying sediment units is available (Fig. 3-3a). This is due to a coring problem resulting in only 0.35 m of gravel revealed from a 1.3 m core run (35% core recovery, including core catcher; Fig. 3-3a). Such low core recoveries often occurred in sediment sections where hard halite deposits alternate with soft mud (Neugebauer et al., 2014). Thus, it is very likely that the presumably fine-grained sediment components were washed out during the drilling process. This assumption is supported by the sediment found in the 10 cm-long core catcher of this core run, which is composed of a mixture of fine-grained mud, some gravel and halite. From this we conclude, that the well-sorted gravels are the result of a drilling artefact and should not be interpreted as an in-situ deposit in its primary sedimentological context.

Instead, we interpret the gravel deposit as the washed-out relict of the basal sediments of a major mass waste deposit. Up to several meter thick turbidites related to mast wasting events are characteristic for *aad* facies in the deep basin and most likely triggered by high-amplitude lake level fluctuations during transgressions and/or by earthquakes (Kagan and Marco, 2013; Neugebauer et al., 2014; Waldmann et al., 2014). We have identified at least 22 of such turbidites including matrix-supported gravel in their basal sediments. One prominent example occurred in core 5017-1 only 6 m above the well sorted gravel discussed above (Fig 3-3). Comparison of the petrographic composition of the well-sorted gravel with the gravel components of turbidites that we have washed out in the lab reveals an identical composition of carbonate, sulphate, halite and minor quartz clasts suggesting the same origin of these gravels. Deposition of a thick turbidite might also explain the supposed hiatus although the length might be critically tested.

Our re-interpretation of the well-sorted gravel as a drilling relict of a turbidite implies that the Dead Sea not necessarily desiccated at the end of the last interglacial. This consideration is in accord with thermodynamic calculations concluding that the exceptional geochemistry of the brine and the geometry of the basin would not allow a dry down of the lake (Yechieli et al., 1998; Krumgalz et al., 2000). According to these calculations a nearly complete desiccation of the water body as suggested by Torfstein et al. (2015) would require a very different geochemical composition of the brine.

3.5.3 Lake level fluctuations between ~117 and 75 ka

Based on interpretation of the six micro-facies detected above, relative lake levels have been reconstructed for the ~117-75 ka interval (Figs. 3-4 and 3-5). Lowest lake levels are assumed in the halite-dominated units I and III, i.e. from ~117-108 ka and ~93-87 ka, respectively. Intermediate to higher lake levels as a result of high inflow are inferred for units II and IV, ~108-93 ka and ~87-75 ka, respectively. These units are characterised predominantly by *aad* facies indicating a continuous positive trend of runoff inflow into the lake.

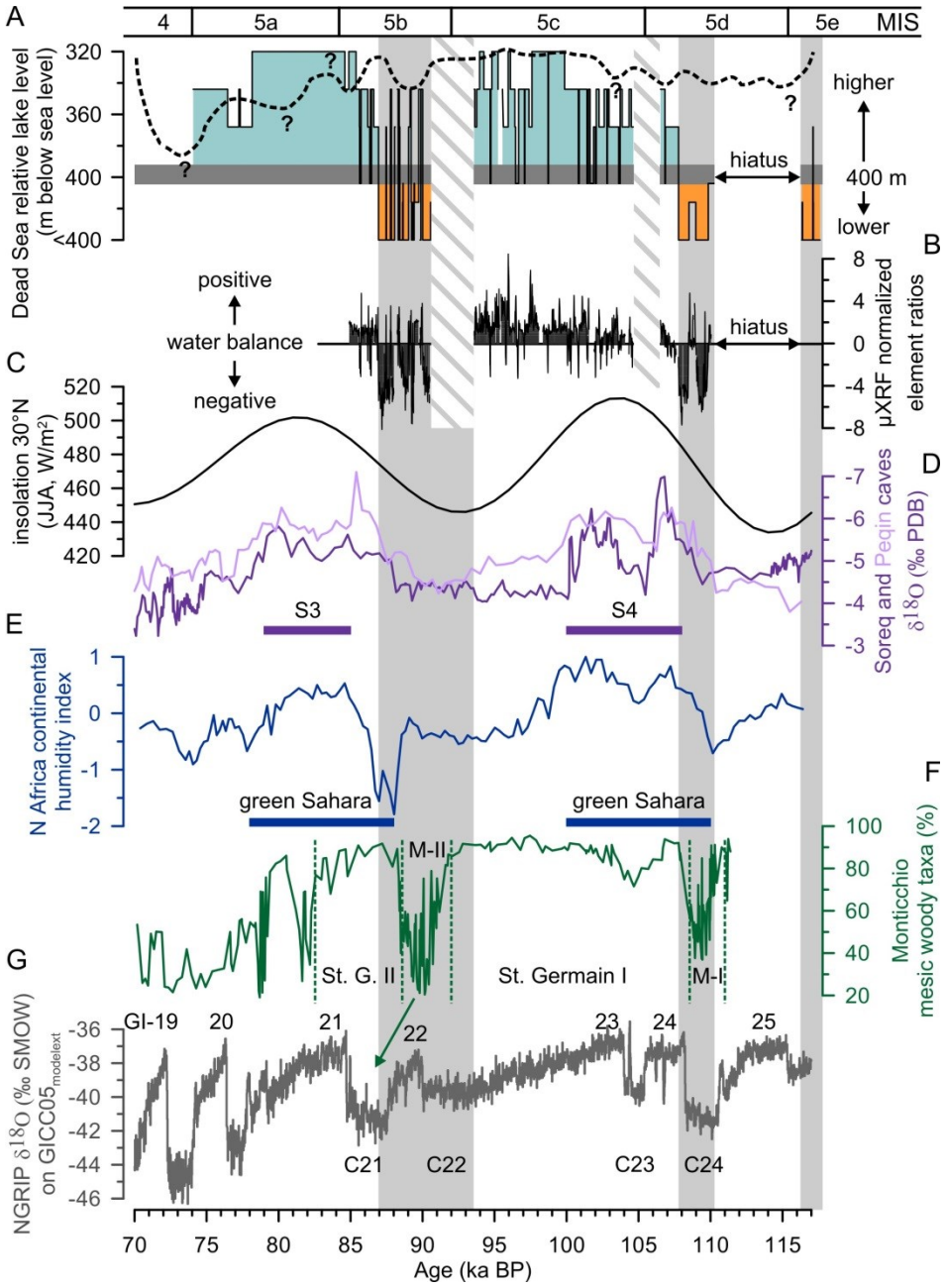

Figure 3-5: Comparison of the Dead Sea to other records: (A) The relative Dead Sea lake level curve inferred from micro-facies analysis of the deep-basin core 5017-1 (this study) and from site PZ-7 from the Perazim valley (dashed line) (Waldmann et al., 2009); (B) sum of normalized ratios of Ca/(Sr+S) and Ti/Ca as proxies for carbonate and siliciclastic detritus, respectively, and of Sr/Ca, proxy for aragonite, subtracted by the Cl/Br ratio, which is a proxy for halite, [Ca/(Sr+S) + Ti/Ca + Sr/Ca – Cl/Br] indicating the water balance of the lake and agreeing well with the relative lake level curve; (C) mean summer (JJA) insolation at 30°N (after Laskar et al., 2004); (D) $\delta^{18}O$ of Soreq and Peqin speleothems, Israel (Bar-Matthews et al., 2003) and eastern Mediterranean sapropel events S3 and S4 (according to Bar-Matthews et al., 2000); (E) humidity index of continental North Africa (core GeoB7920-2) and "green Sahara" phases (Tjallingii et al., 2008); (F) Monticchio (southern Italy) pollen record of mesic woody taxa and Mediterranean pollen zones Melisey (M) I and II, and St Germain I and II (Brauer et al., 2007; Martin-Puertas et al., 2014); (G) Greenland ice core $\delta^{18}O$ record on $GICC05_{modelext}$ timescale (Wolff et al., 2010), indicated are also Greenland interstadials (GI) after Rasmussen et al. (2014) and North Atlantic ice rafting events C21 to C24 (Chapman and Shackleton, 1999). Marine isotope stages are given according to Wright (2000). Grey vertical bars indicate periods of negative water balance in the Dead Sea; obliquely banded bars: no core recovery.

The chronology of unit I indicates that the low stand of Lake Samra commenced as part of the last interglacial corresponding to the later MIS 5e and may have continued until ~108 ± 5 ka BP (Fig. 3-5). However, there is no reliable information for the time interval from ~116 to 110 ± 4 ka, as this is not represented in the record due to the major erosional unconformity related to a gravel unit. The deposition of ca 2 m of halite above this gravel layer indicates that low levels of the lake continued from ~110 to 108 ± 5 ka. During times of halite deposition in the DSB a lake level below 400 m bmsl can be assumed (Neev and Emery, 1967; Bookman (Ken-Tor) et al., 2004; Waldmann et al., 2009; Stein et al., 2010).

During ~108-93 ± 6 ka (unit II) a general increase in lake level can be assumed from the succession of *aad-II* to *aad-n* facies and finally to the *green aad* facies (Fig.3-4). Frequently occurring gypsum deposits from ~108-100 ka indicate short-term drops in lake level. In the last glacial Lisan Formation such gypsum deposits were associated with intensified winds and evaporation during Heinrich events (Bartov et al., 2003; Torfstein et al., 2008; Rohling, 2013; Torfstein et al., 2013b). A following high-stand of Lake Samra ~100-93 ka BP is consistent with studies from exposures at the lake's margins, where a relatively high level of ~320 m bmsl was proposed for that interval (Fig. 3‑5; Waldmann et al., 2009; 2010).

An abrupt lake level decline and millennial-scale low stand, probably below 400 m bmsl, is inferred from the several-meter thick halite deposit during the ~93-87 ± 7 ka interval (unit III, Figs. 3-4 and 3-5). Some *aad-n, aad-II* and *gd* facies alternate with the thick and mainly layered halite deposits. This indicates superimposed, probably decadal-scale lake level fluctuations. In core 5017-1 this halite sequence is defined as the final stage of the Samra Formation. In the exposed sediment sections this final Lake Samra low stand is characterised by coarser clastic deposits (Waldmann et al., 2009). This halite sequence in the deep core marks the last appearance of halite for the next ~70,000 years (Neugebauer et al., 2014) appearing again during the early Holocene (e.g. Yechieli et al., 1993; Stein et al., 2010). Only a minor lake level decline from ~320 to 340 m bmsl was assumed from the margin exposures (Fig. 3‑5; Waldmann et al., 2009). However, the deposition of halite in the deep basin during the last phases of Lake Samra indicates a lengthier and possibly more pronounced low-stand.

From ~87 to 79 ± 7 ka (units IV-a and IV-b) lake level increased again. This is evident from the sediment succession from *aad-II* and *aad-n* facies, intercalated by some *gd* facies, to *green aad* facies (Fig. 3-4). At ~79 ka (unit IV-c) the lake probably declined slightly before continuing to rise at ~77 ± 6 ka BP and thereafter (Fig. 3-5). Earlier studies of the exposed sediments of the Samra and Lisan Formations suggested that a depositional unconformity, ~75 to 70 ka, separated these two formations at the lake's margins (Bartov et al., 2003; Waldmann et al., 2009; Torfstein et al., 2013b). In these exposures, overlying the proposed unconformity, sediments present *aad* facies characterising the lower and upper members of the Lisan Formation (e.g. Bartov et al., 2002). Below the unconformity, the on-shore Samra Formation is composed of reddish *ld* facies, sands and gravels (Waldmann et al., 2009). In the deep core there is, however, no sedimentological hint for a low stand of the lake from ~75-70 ka and the sediments do not change

significantly, continuously presenting *aad* facies from ~87 ka onwards. This suggests that Lake Lisan already commenced ca 10-15 kyr earlier than was proposed from the exposures. This difference between shallow- and deep-basin sediments might be explained by the abundant occurrence of slumping deposits and graded layers (Fig. 3-4) that occasionally contain some gravel material at their base. These deposits might indicate transgressive erosion at the outcrop locations during lake level rise of the early Lake Lisan (Bartov et al., 2007), causing unconformities in the shallower areas further leading to deposition of coarse gravel material in the deep basin. A total lake level rise of at least ~80 m, from <400 m bmsl to ≥320 m bmsl, is estimated for the time period from ~87 to 70 ± 6 ka (Fig. 3-5). As this lake is terminal, we anticipate numerous fluctuations during this minimal net level rise. These fluctuations can explain the many slumps observed in the core during this interval.

3.5.4 Hydroclimatic implications

The core section analysed here records ca 40,000 years of climate history, starting at the demise of the last interglacial (MIS 5e) and covering the early last glacial period until ca 75 ka (Fig. 3-5). Following the chronological framework of the deep Dead Sea core by Torfstein et al. (2015), two dry periods in the Dead Sea region at ~110 to 108 ± 5 ka and ~93-87 ± 7 ka coincide with MIS 5d and 5b and correspond to cold stadial conditions in the North Atlantic, as reflected in Greenland ice cores (Fig. 3‑5; Wolff et al., 2010) and North Atlantic ice rafting events C24 and C22+C21, respectively (Chapman and Shackleton, 1999). Cold and dry conditions during these times also influenced the Mediterranean region, as demonstrated, for example, in the reversal from forested back to steppic vegetation in the Monticchio pollen record, southern Italy, during Melisey I and II (Fig. 3‑5; Brauer et al., 2007; Martin-Puertas et al., 2014). These cold and dry events are recognized in other pollen records from the Mediterranean region, such as in marine core MD952042 off the Iberian margin (Sánchez Goñi et al., 1999), Tenaghi Philippon, NE Greece (Tzedakis, 2005), Lake Van, NE Turkey (Litt et al., 2014), eastern Mediterranean marine cores (Cheddadi and Rossignol-Strick, 1995) and Lake Yammoûneh, Lebanon (Develle et al., 2011; Gasse et al., 2015). Information from speleothem records from the Levantine arid regions is lacking probably due to the prevailing aridity that prevented speleothem growth during these time intervals (Vaks et al., 2006; 2007; 2010). The Soreq and Peqin caves (Fig. 3‑5; Bar-Matthews et al., 1999; 2000; 2003), which are currently located under wetter (>550 mm yr^{-1}) Mediterranean climate, continuously received precipitation during these intervals. Excursions to higher $\delta^{18}O$ values at Soreq and Peqin caves during MIS 5d and the later MIS 5c to 5b indicate drier climatic conditions in the eastern Mediterranean region and, hence, support our observations (Fig. 3-5), but these records might be also influenced by the source effect (e.g. Kolodny et al., 2005).

Two intervals of positive water balance and inferred higher lake levels of the Dead Sea at ~108-93 ± 6 ka and ~87 to 75 ± 6 ka broadly corresponding to MIS 5c and 5a (Fig. 3-5) coincide with Greenland interstadials (GI) 24+23 and GI 21, respectively (Rasmussen et al., 2014), which are associated with warming in the North Atlantic region. In the Mediterranean pollen records

more humid climatic conditions during these interstadials are expressed in the returning of arboreal taxa during the St. Germain I and II pollen phases (Woillard, 1978), e.g. in the Monticchio record (Fig. 3‑5; Brauer et al., 2007; Martin-Puertas et al., 2014). Positive excursions of orbital insolation in the northern hemisphere (Fig. 3‑5; Laskar et al., 2004) correlated with the early MIS 5c and 5a led to a strengthening of the African summer monsoon and widespread vegetation cover in the Sahel and at least in the southern Sahara regions (Fig. 3‑5; Tjallingii et al., 2008). Enhanced precipitation in tropical eastern Africa induced the formation of organic-rich sapropel layers in the eastern Mediterranean basin due to enhanced Nile River runoff (e.g. Rossignol-Strick, 1985). The sapropel events S4 and S3 are recognized in eastern Mediterranean marine cores (Cheddadi and Rossignol-Strick, 1995; Almogi-Labin et al., 2009; Langgut et al., 2011) and indirectly from Mediterranean water into the isotopic composition of Soreq and Peqin speleothems (Fig. 3‑5; Bar-Matthews et al., 2000; 2003), i.e. monsoonal influence over the eastern Mediterranean is manifested indirectly in the continental records of the Levant during these time intervals.

Contrary suggestions have been made addressing the question, whether enhanced moisture supply to the DSB during early last glacial originated from the North Atlantic-Mediterranean or from southern sources related to the African monsoon system. Based on the sedimentary and oxygen isotopic signatures of the deep Dead Sea drill core, Torfstein et al. (2015) hypothesised that summer monsoonal rainfall arrived as far north as the southern Levant during the last interglacial (MIS 5e). Torfstein et al. (2015) furthermore argued for a possible contribution of these summer rains also for the moderately high lake level periods at the Dead Sea during the early glacial, corresponding to MIS 5c and 5a and the formation of S4 and S3, respectively (Fig. 3-5). However, it was concluded from many studies focussing on the last interglacial (S5) period and on the early Holocene African Humid Period (S1), when the monsoon was even more intense than during S4 and S3, that the monsoonal rain belt did not reach the North African coastal latitudes (Tzedakis, 2007 and references therein). This is supported by (a) $\delta^{18}O$ records of northern, central and southern Negev speleothems and (b) the occurrence of speleothems that diminish in a southern direction in the Negev, suggesting the Atlantic-Mediterranean as the dominant source of winter precipitation in the Negev during intervals also characterised by maxima of the African monsoon and sapropel events (Vaks et al., 2007; 2010). Furthermore, based on climate model simulations Kutzbach et al. (2014) suggested that either increased winter storm track precipitation or a combination of increased summer and winter rainfall may account for wetter climate in the Levant during these intervals of maximum northern hemisphere seasonality.

A plausible alternative to these two atmospheric circulation patterns, i.e. the Atlantic-Mediterranean causing winter rains and the African summer monsoon, respectively, are the winter-spring tropical plumes (e.g. Rubin et al., 2007). In modern times, these act as over-the-continent atmospheric rivers that bring tropical eastern Atlantic-western Africa moisture across the Sahara into the southern Levant deserts, and precipitate usually when the sub-tropical jet is at

a southern latitudinal position (e.g. Kahana et al., 2002; Rubin et al., 2007; Tubi and Dayan, 2014). The rainfall associated with these types of storms is widespread, long-duration and causes large floods. Based on studies of the exposed Samra Formation at the margins of the Dead Sea and travertines in the Arava Valley, Waldmann et al. (2010) concluded that these low-latitude tropical plumes and potentially also the mid-latitude Red Sea Troughs, which are both autumn to spring phenomena, may have supplied some moisture to Lake Samra from southern directions during times of insolation maxima in the northern hemisphere and sapropel formation in the eastern Mediterranean Sea. Waldmann et al. (2009; 2010), however, associate these southern rain contributions with low lake level phases of Lake Samra, which is contrary to our results from the deep-basin core, but this might be attributed to missing sediments and/or dating uncertainty of the on-shore deposits.

Whereas a monsoonal impact on the Dead Sea level during the last peak interglacial, as suggested by Torfstein et al. (2015), cannot be ruled out here, we propose a persistent source of moisture from the Atlantic-Mediterranean system to the Dead Sea during the early last glacial period, based on the striking evidence by speleothem studies from the Negev (Vaks et al., 2007; 2010). These winter rains might have been accompanied by a more frequent occurrence of tropical plumes from southern sources during the same season.

3.6 Conclusions

Investigation of a ~65 m long sediment section of the 5017-1 core from the deep Dead Sea basin demonstrated the exceptional sensitivity of sediment deposition to lake level variations. This enabled using micro-facies types as indicator for different lake levels and water balance and, hence, changing hydroclimatic conditions in the southern Levant during the early last glaciation from ~117 to 75 ka.

The lake rose from a level below ~400 m bmsl at ~108 ka to levels of ~320 m bmsl at ~100 to 95 ka. Thereby, frequent occurrence of gypsum deposits indicates short-term lake level drops and alternation of different manifestations of the *aad* facies type suggests millennial-scale fluctuations of the lake. Subsequently, a sharp lake level decline at ~93 ka and following millennial-scale low-stand, again below ~400 m bmsl, is indicated by a thick halite sequence that was deposited from ~93 to 87 ka corresponding to MIS 5b and which marks the transition from the Samra to the Lisan Formations in the deep core. Thereafter, the lake rose again to ~320 m bmsl between ~87 and 75 ka and probably further increased at the MIS 5-4 transition and thereafter, accompanied by short-term intense lake level fluctuations.

The major findings of this study are:

- Our high-resolution sedimentological study from the deep core indicates that Lake Lisan already commenced ca 15 kyr earlier than was proposed from exposed sediments at the margins. The major system shift occurs with the beginning of Lake Lisan at ~87 ka, but Lisan-type sediments, i.e. *aad*, were deposited in the deep basin already earlier from

~108-93 ka during the early last glacial. These were interrupted by a final period of halite deposition marking the end of Lake Samra at ~87 ka.

- Moisture contributing to higher lake levels of the Dead Sea during the early last glacial (MIS 5d-5a), excluding the last interglacial (MIS 5e), most likely arrived from Atlantic-Mediterranean winter storms, presumably accompanied by tropical plumes from southern sources during the autumn to spring seasons.
- Our results disagree with previous climate interpretations (Torfstein et al., 2015) as we do not suggest an extreme drawdown or almost complete desiccation of the lake at the end of the last interglacial. Instead of a beach interpretation as proposed by Torfstein et al. (2015), we show that the pure gravel layer likely derived from slumping and artificial draining out of the finer fractions during the drilling. This gravel layer might have even resulted from an increasing lake level, as higher slumping frequency is associated with lake level rise or at least rapid lake level fluctuations.

Acknowledgements

Funding by the International Continental Scientific Drilling Program (ICDP), the German Science Foundation (DFG grants FR 1672/2-1 and BR 2208/10-1), the GFZ German Research Centre for Geosciences and the Israel Science Foundation (ISF) Dead Sea Core-Center of Excellence Research (Grant # 1436/14 to Y.E.) is gratefully acknowledged. We thank G. Arnold, D. Berger and B. Brademann for preparing excellent thin sections and for technical support, P. Dulski and F. Ott for help with μXRF, B. Plessen and P. Meier for TOC and $CaCO_3$ measurements, J. Mingram for support with the fluorescence microscope, G. Schlolaut (all GFZ German Research Centre for Geosciences) and K. Schorling (HU Berlin) for grain size sampling, S. Baltruschat (TU Darmstadt) for assistance with XRD samples and all people that have been involved in the drilling, core opening and sampling campaigns. This study is a contribution to the Helmholtz Association (HGF) climate initiative REKLIM Topic 8 ”Rapid climate change derived from proxy data“.

Supplementary material

Table S 3-1: Table of grain sizes of all samples and distinguished after micro-facies types before and after dissolution of $CaCO_3$; n - number of samples, stdv. – standard deviation.

facies	$CaCO_3$ included										
	n	clay (%)	stdv.	silt (%)	stdv.	sand (%)	stdv.	mean (µm)	stdv.	clay/ silt	stdv.
all samples	363	53.01	10.21	45.42	8.67	1.55	5.92	10.66	34.17	1.24	0.43
green aad	108	48.13	9.05	50.51	7.64	1.37	4.17	8.85	7.60	0.99	0.29
aad-n	157	56.24	8.29	42.92	7.27	0.84	2.01	6.72	3.11	1.38	0.41
aad-II	36	56.64	8.03	42.46	6.33	0.90	2.38	7.17	4.18	1.39	0.36
gd	62	51.25	13.48	44.59	10.84	4.01	12.50	25.79	80.67	1.25	0.54
facies	$CaCO_3$ dissolved										
	n	clay (%)	stdv.	silt (%)	stdv.	sand (%)	stdv.	mean (µm)	stdv.	clay/ silt	stdv.
all samples	355	41.28	8.56	56.08	7.49	2.51	6.73	13.81	25.52	0.76	0.23
green aad	105	39.12	7.52	58.30	6.81	2.13	3.22	11.69	5.03	0.70	0.22
aad-n	156	43.92	7.10	54.77	6.26	1.31	1.78	10.09	3.41	0.83	0.21
aad-II	36	44.03	6.99	54.77	6.16	1.19	1.27	9.94	3.05	0.83	0.21
gd	58	36.36	11.32	56.37	10.91	7.27	14.98	30.09	60.31	0.67	0.24

4 Evidences for centennial dry periods at ~3300 and ~2800 cal yr BP from micro-facies analyses of the Dead Sea sediments

Ina Neugebauer[a], Achim Brauer[a], Markus J. Schwab[a], Peter Dulski[a], Ute Frank[a], Elitsa Hadzhiivanova[b], Hiroyuki Kitagawa[c], Thomas Litt[d], Vera Schiebel[d], Nimer Taha[b], Nicolas D. Waldmann[b], and DSDDP Scientific Party [#]

a Section 5.2 – Climate Dynamics and Landscape Evolution, GFZ German Research Centre for Geosciences Potsdam, Germany

b Dr. Strauss Department of Marine Geosciences, Leon H. Charney School of Marine Sciences, University of Haifa, Israel

c Graduate School of Environmental Studies, Nagoya University, Japan

d Steinmann Institute of Geology, Mineralogy and Paleontology, University of Bonn, Germany

[#] The complete list of scientists involved in the Dead Sea Deep Drilling Project can be found at http://www.icdp-online.org

Accepted manuscript in The Holocene (after minor revisions).

Abstract

Laminated lake sediments from the Dead Sea basin provide high-resolution records of climatic variability in the eastern Mediterranean region, which is especially sensitive to changing climatic conditions. In the study presented here, we aim on detailed reconstruction of climatic fluctuations and related changes in the frequency of flood and dust deposition events at ca 3300 and especially at 2800 cal yr BP from high-resolution sediment records of the Dead Sea basin. A ca 4 m thick, mostly varved sediment section from the western margin of the Dead Sea (DSEn - Ein Gedi profile) was analysed and correlated to the new ICDP Dead Sea Deep Drilling Project core 5017-1 from the deep basin. To detect even single event layers, we applied a multi-proxy approach of high-resolution microscopic thin section analyses, μXRF element scanning and magnetic susceptibility measurements, supported by grain size data and palynological analyses. Based on radiocarbon and varve dating two pronounced dry periods were detected at ~3500-3300 cal yr BP and ~3000-2400 cal yr BP which are differently expressed in the sediment records. In the shallow-water core (DSEn), the older dry period is characterised by a thick sand deposit, whereas the sedimentological change at 2800 cal yr BP is less pronounced and characterised mainly by an enhanced frequency of coarse detrital layers interpreted as erosion events. In the 5017-1 deep-basin core both dry periods are depicted by halite deposits. The onset of the younger dry period coincides with the Homeric Grand Solar Minimum at ca 2800 cal yr BP. Our results suggest that during this period the Dead Sea region experienced an overall dry climate, superimposed by an increased occurrence of flash-floods caused by a change in synoptic weather patterns.

Keywords

ICDP Dead Sea drilling; Levant palaeoclimate; varve chronology; micro-facies; dry periods; extreme events.

4.1 Introduction

Annually laminated lake sediments provide independently datable and high-resolution records of climate dynamics (e.g. Brauer et al., 1999b; 2008; 2009; Martin-Puertas et al., 2009; Ojala et al., 2012). A particular interest is in records that are located at major climatic transition zones affected by different regional climate regimes. At these locations small-scaled shifts in atmospheric circulation patterns are expected to considerably impact on the sedimentation. Possible sedimentation changes include variations in the seasonal succession of autochthonous and allochthonous components and in the frequency of detrital layers reflecting extreme hydro-meteorological events like dust storms or floods (e.g. Brown et al., 2000; Sirocko et al., 2005; Swierczynski et al., 2013; Schlolaut et al., 2014). Long time series of event layers thus can be used to reconstruct past changes in atmospheric circulation, wind trajectories and hydrological conditions.

Centennial and decadal-scale climatic fluctuations during the Holocene have been commonly related to changes in solar irradiation and, in particular, extended periods of solar minima, also termed as Grand Solar Minima (GSM) (e.g. van Geel et al., 1999; Bond et al., 2001; Solanki and Krivova, 2007). One pronounced GSM is the Homeric Minimum at ca 2800 cal yr BP (van Geel et al., 1999; Martin-Puertas et al., 2012). This GSM has been associated with cooling and increased humidity in large parts of Europe and even the central Asian plains (van Geel et al., 1996; Mauquoy et al., 2004; van Geel et al., 2004; Holzhauser et al., 2005; Martin-Puertas et al., 2009; 2012), higher lake levels in Western Europe (Magny, 2004) and the Caspian Sea (Kroonenberg et al., 2007) as well as intensified cyclones leading to more extreme flood events (Czymzik et al., 2013) in alpine and pre-alpine lakes. Whereas cooler and wetter conditions prevailed in large parts of the subtropical and temperate climate regions during that time, tropical regions apparently became drier (van Geel et al., 1996 and references therein). However, so far little is known about climatic changes and environmental responses during this time interval from transitional areas such as the eastern Mediterranean (EM). In this region, the Dead Sea provides an important long sediment record of past climate variability (e.g. Neugebauer et al., 2014).

The hypersaline Dead Sea is situated at the transition between subtropical Mediterranean climate and the Saharo-Arabian deserts. Earlier investigations of exposed sediments along the Dead Sea shore and the adjacent tributary valleys (e.g. Begin et al., 1974; Bartov et al., 2002; Bookman (Ken-Tor) et al., 2004 among others) and of drill cores from the lake (Yechieli et al., 1993; Heim et al., 1997; Migowski et al., 2006) have proven the sediments from the Holocene Dead Sea and its Pleistocene precursors as excellent archives of lake level fluctuations. Evidences for regional climate changes are mirrored in the laminated sedimentary record (Bartov et al., 2003; Kushnir and Stein, 2010; Stein et al., 2010; Waldmann et al., 2010). Since some of the finely laminated sediment facies from the last glacial Lake Lisan and the Holocene Dead Sea have been suggested to be of annual nature (Heim et al., 1997; Prasad et al., 2004), they are particularly suited for establishing high-resolution time series of climatic change and earthquakes (Migowski et al., 2004; Leroy et al., 2010). Most previous studies focussed on glacial-interglacial climatic changes

on millennial time scales (Stein, 2014 and references therein) and high-resolution studies of Holocene climate variability and time series of past extreme floods or dust storms are still lacking.

In this study, we present the first annually resolved, ca 1500-years comprising time series of erosion and dust deposits in the Dead Sea basin during the late Holocene in order to investigate the impact of the Homeric GSM in the southern Levant. This record was established by high-resolution micro-facies analyses of a varved interval identified in both, a shallow-water core from the western margin of the Dead Sea and from a deep core drilled as part of an ICDP project in the deep area of the lake at a water depth of ~300 m (Stein et al., 2011; Neugebauer et al., 2014).

4.2 Regional setting of the Dead Sea

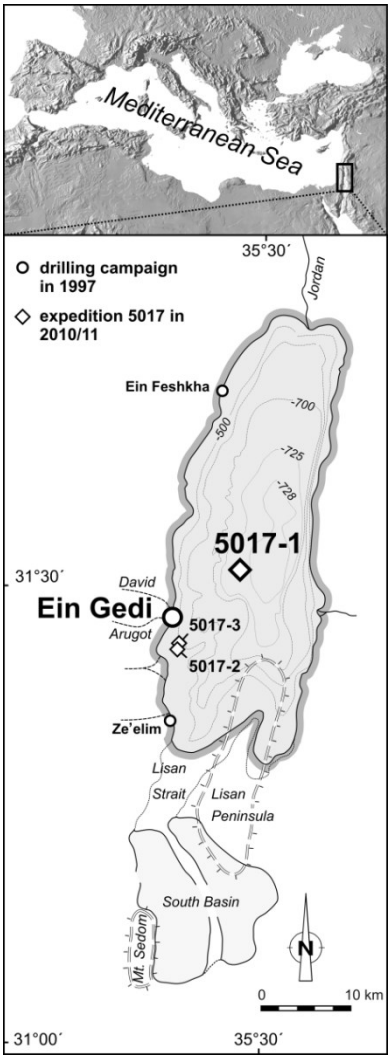

Figure 4-1: Map of the Dead Sea in the eastern Mediterranean region and drilling locations of the shallow-water DSEn (Ein Gedi) and deep-basin 5017-1 cores.

The hypersaline Dead Sea (Fig. 4-1) is the terminal lake of the Jordan River system and presently (in 2014) has a lake level of 428 m below mean sea level (bmsl). The lake's watershed of ~40,000 km² (Bentor, 1961) is one of the largest in the Levant and is located along the boundary between semiarid and arid climate. It is under the influence of Mediterranean climate in its northern part, characterised by wet winters and dry summers, while the southern areas are influenced by the dry climate of the Saharo-Arabian desert belt. Most of the fresh water entering the lake originates from the perennial upper Jordan River (annual precipitation >600 mm; Enzel et al., 2003), while only minor fresh water contributions arrive from the eastern and western escarpments of the basin and from the southern part of the drainage area mainly during extreme runoff events. Annual precipitation over the Dead Sea itself does not exceed ~75 mm so that lake level fluctuations mainly reflect precipitation changes in its much wetter headwaters (Enzel et al., 2003). Mediterranean mid-latitude cyclones (Cyprus Lows) are the main driving mechanisms promoting rainfall in the northern and western parts of the watershed, whereas the southern part is influenced by occasional incursions of the Active Red Sea Troughs, triggering flash floods usually during the autumn season (Dayan and Morin, 2006).

Lake levels of the Dead Sea and its Pleistocene precursors strongly fluctuated in the past. The glacial Lake Lisan reached a maximum level ca 270 m higher than the present-day level, reaching ~160 m bmsl during the last glacial maximum (e.g. Begin et al., 1974; Torfstein et al., 2013b). For the last ca 10,000 years comparably stable lake levels of ~400 ± 30 m bmsl have been reconstructed from exposed sediments and sediment cores retrieved from the marginal zone of the Dead Sea (Bookman et al., 2006 and references therein).

Most of the clastic-detrital material brought into the Dead Sea basin is transported by ephemeral streams flowing from the western rims of the catchment made up of Cretaceous carbonates (Bentor, 1961). The eastern fluvial systems discharge from a geologically more complex catchment consisting of Palaeozoic to Mesozoic sandstone and Cretaceous carbonates with some Pleistocene volcanic units. Commonly, fluvial systems form fan delta structures, which are influenced by both, lake level fluctuations and variations in the upstream precipitation.

The vegetation in the Dead Sea watershed depends on the topography and precipitation gradient, with a clear rainfall decrease from North to South and from West to East. The main geobotanical regions are classified as (1) Mediterranean (e.g. *Olea,* evergreen and deciduous oaks), (2) Irano-Turanian steppe (e.g. *Artemisia*), (3) Saharo-Arabian desert (mainly Chenopodiaceae) around the Dead Sea and in the Negev, and (4) Sudano-Deccanian oasis vegetation (e.g. *Acacia* and *Phoenix*) in the Jordan valley (e.g. Danin, 1988; Neumann et al., 2010; Litt et al., 2012).

4.3 Material and methods

4.3.1 Sediment cores DSEn and 5017-1

The 21 m long DSEn sediment core has been retrieved from the western shore of the Dead Sea (31°27’55” N, 35°23’39” E; 413 m below mean sea level – bmsl; Fig. 4-1; Migowski, 2001). A Holocene age is well constrained by 20 radiocarbon dates and varve counting of the upper part of the record (Migowski et al., 2004). Here, we analyse a 3 m long interval of the DSEn core (5.10-2.10 m sediment depth) that partly overlaps with the varve chronology by Migowski et al. (2004). The composite depths were corrected for this study and slightly differ from the depths given by Migowski (2001) due to improved correlation of the parallel cores.

Core DSEn has been correlated and compared to the new sediment core 5017-1 obtained from the Dead Sea basin at 300 m water depth (31°30'29" N, E 35°28'16" E; ~725 m below mean sea level (bmsl) sediment surface; Fig. 4-1) by the ICDP Dead Sea Deep Drilling Project (DSDDP). This sediment record is ~455 m long and comprises two full glacial-interglacial cycles (Neugebauer et al., 2014). Here, we focus on a 13 m long interval of the 5017-1 composite core (28-15 m below lake floor (mblf)) that correlates to the investigated 3 m long DSEn sequence from the present-day shore location. Details about the 5017-1 composite core are provided by Neugebauer et al. (2014).

4.3.2 Radiocarbon dating

AMS radiocarbon dating on terrestrial plant remains was carried out at the University of Kiel, Germany (DSEn samples, lab code: KIA) as reported earlier by Migowski et al. (2004), Nagoya University, Japan (5017-1 samples, lab code: NUTA2) and University of California-Irvine (5017-1 samples, lab code: UCIAMS). Radiocarbon dating of core 5017-1 has been described in detail by Neugebauer et al. (2014). Here, we used nine ^{14}C dates from the DSEn profile and ten dates from the 5017-1 profile both calibrated with the IntCal13 atmospheric calibration curve (Reimer et al., 2013) using OxCal 4.2 (Bronk Ramsey, 2009). The applied P_Sequence (1,0.05,U(-2,2)) deposition model allows a random deposition process (Bronk Ramsey, 2008). The results are summarised in Table 4-1.

4.3.3 Micro-facies analyses

4.3.3.1 Thin section microscopy and grain size

Varve counting and layer thickness measurements were carried out on 37 overlapping large-scale petrographic thin sections (10 x 1.5 cm) from the DSEn profile. The corresponding sequence in the 5017-1 profile was varve-counted and systematically scanned for marker correlation layers in 82 thin sections. Varve counting was performed two times for both profiles, but layer thickness was measured only for the DSEn profile. The preparation process largely followed the standard procedure for soft sediments (e.g. Brauer and Casanova, 2001) including freeze-drying and impregnation with epoxy resin (Araldite 2020), except that sawing and polishing of impregnated sediment blocks has been performed manually at dry conditions due to the salt content of the sediments and pore waters. Thin sections were analysed with a petrographic microscope (Leica DMLP). Layer thickness was measured with 50x magnification under partly polarised light conditions. Microscopic images were taken with digital cameras (Olympus DP72, Zeiss AxioCam). For demonstration of grading pattern, some detrital layers of core 5017-1 were measured for grain size distribution in 1-cm steps using an LS 13 320 laser diffraction particle size analyzer in the Sedimentology Laboratory of the University of Haifa.

4.3.3.2 Continuous split-core µ-XRF and magnetic susceptibility logging

The elemental composition of the sediments was measured on the split core surface using an ITRAX µXRF spectrometer (Croudace et al., 2006). We applied a Chromium tube, which is sensitive for lighter elements, with 30 kV voltage and 30 mA current; step size was 200 µm and exposure time 10 seconds per step. The main elements representing the lithology of the Dead Sea sediments (Br, Ca, Cl, Fe, K, S, Si, Sr and Ti) were selected for interpretation. The µXRF data are presented as count rates (counts per second – cps) or as element ratios. The magnetic susceptibility was determined on the split core surface with a Bartington MS2E sensor (Nowaczyk, 2001) in 1 mm steps.

4.3.4 Pollen analysis of the DSEn core

Previously published pollen data from the DSEn profile have a temporal resolution of ~150-200 years (Litt et al., 2012). For higher resolution pollen analyses of the sediment section investigated here mainly to support our abiotic proxies, we complemented the existing data set with 27 additional samples to a total of 43 samples. The additional samples were taken from 3.48 to 5.62 m composite depth in 2-5 cm steps and with a 10-40 year resolution. Sample preparation and counting followed the procedure described in Faegri and Iversen (1989). At least 500 pollen grains were counted in each sample for the terrestrial pollen sum, i.e. excluding aquatics. *Lycopodium* tablets were added to calculate the pollen concentration per cm^3. For further details see also Litt et al. (2012).

4.4 Results

4.4.1 Lithology

4.4.1.1 DSEn

The base of the analysed 3 m long DSEn sediment section (Fig. 4-2) lies within the 'Upper clastic sequence' (Migowski, 2001) characterised by dark grey clayey-silty marl layers and few white aragonite and greyish or beige gypsum layers. This mainly clastic sequence is topped by a ~20 cm thick carbonatic sand layer at 4.55-4.35 m depth overlain by the 'Uppermost aragonite sequence' as described by Migowski (2001). This sequence continues until the top of the profile and consists of alternations of aragonite and/or gypsum and detrital layers that have been interpreted as varves (Migowski et al., 2004). Intercalated within the regular aragonite laminations are black and brown detrital layers.

4.4.1.2 5017-1

The studied 13 m long sequence from core 5017-1 is subdivided into five sediment units (Fig. 4-2). The basal unit (28-26.75 m depth), the middle section (24.30-22.70 m) and the top unit (19.05-15 m) are composed of grey, brown or black marl layers, alternating with aragonite and/or gypsum laminae. The laminated sediments are intercalated by up to ~80 cm thick and commonly graded layers. The second (26.75-24.30 m) and fourth (22.70-19.05 m) units are characterised by mixed halite and marl sediments and only short laminated sediment intervals containing small halite crystals. In the halite-dominated sediment units coring gaps may occur due to the coring process (Neugebauer et al., 2014).

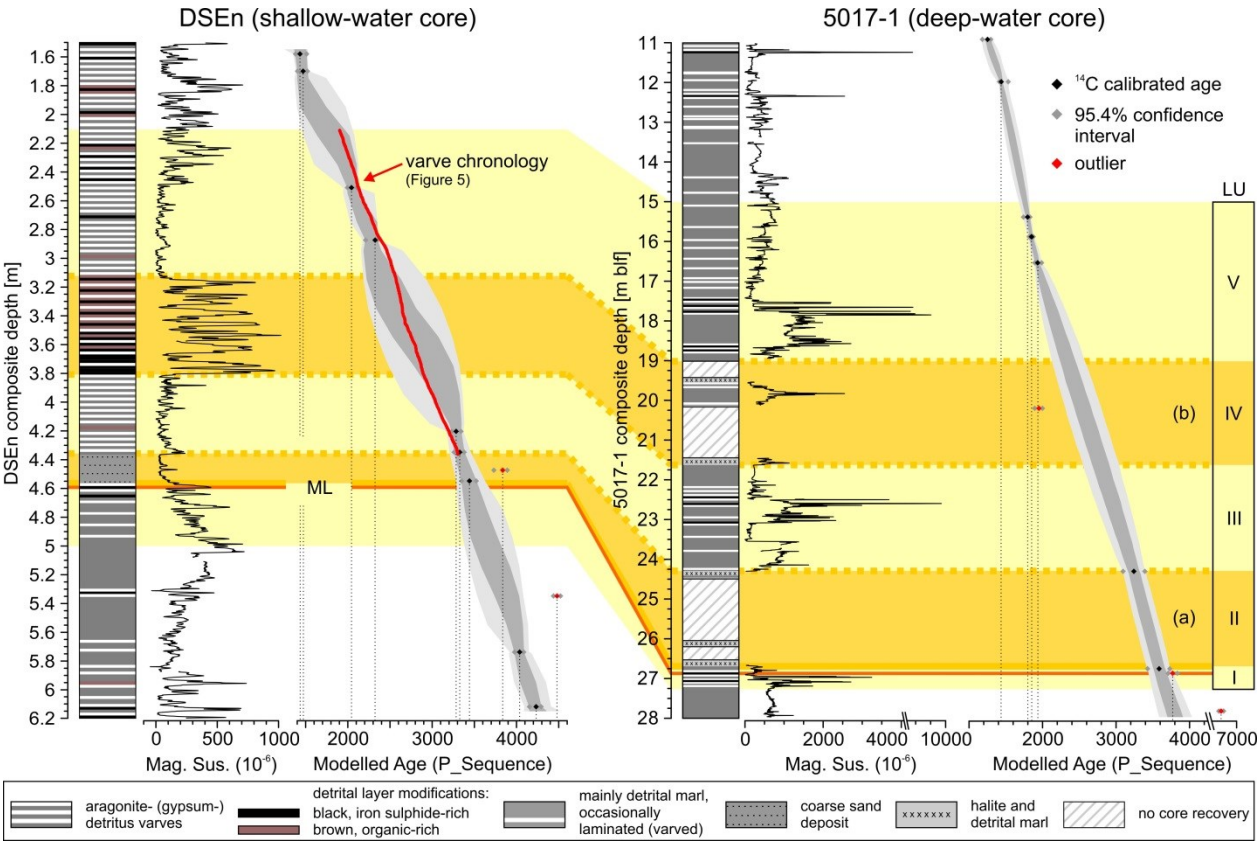

Figure 4-2: DSEn and 5017-1 sediment profiles, magnetic susceptibility data (Mag. Sus.) and modelled ^{14}C age-depth plots with 68.2% (dark grey; ~1σ error) and 95.4% (light grey; ~2σ error) confidence intervals; note that for 5017-1 the lowermost age included in the model (4673 ± 85 cal yr BP at 32.36 m; Table 4-1) is not shown here for better readability of the figure; highlighted intervals: (a) ~3500-3300 cal yr BP and (b) ~3000-2400 cal yr BP; ML: marker layer; LU: lithological units (I to V) as in Fig. 4-4.

4.4.2 Dating and varve counting results

4.4.2.1 Radiocarbon dating

From the DSEn core nine ^{14}C dates from 6.12 m to 1.58 m depths with ages ranging from 4245 ± 78 to 1422 ± 55 cal yr BP have been used to construct the age-depth model (Table 4-1; Fig. 4-2). Two dates are considered as outliers and not included in the age model: sample KIA11630 and sample KIA9123. For the latter, obtained from the coarse sand deposit at 4.55-4.35 m depth, an age overestimation by ca 400 yrs has been proven by correlation of the sand deposit to a beach ridge in the nearby Ze'elim outcrop (Fig. 4-1) with well-constrained ages supported by palynological and archaeological evidences (Bookman (Ken-Tor) et al., 2004; Langgut et al., 2014; Kagan et al., in press).

The age model of the studied interval of core 5017-1 is based on ten radiocarbon dates between 32.36 m and 10.92 m depths (Table 4-1; Fig. 4-2) with ages ranging from 4673 ± 85 to

1232 ± 44 cal yr BP. Three outliers were identified and excluded from the age model: (1) sample NUTA2-19884, (2) sample UCIAMS-110343 and (3) sample UCIAMS-110342.

Table 4-1: Radiocarbon dates from the shallow-water DSEn core (Migowski et al., 2004; re-calibrated) and the deep-water core 5017-1. Age modelling was performed with OxCal 4.2 (Bronk Ramsey, 2009) using the deposition model P_Sequence(1,0.05,U(-2,2)) (Bronk Ramsey, 2008) and the atmospheric calibration curve IntCal13 (Reimer et al., 2013).

Sample	Lab-Code	Depth	^{14}C Age	Calibrated Age Range		Median	Modelled Age Range	
Core_cm		(m)	BP ± 1σ	68.2%	95.4%	cal yr BP ± 1σ	68.2%	95.4%
DSEn (shallow-water core)								
A2_49	KIA11627	1.58*	1528 ± 39	1365-1518	1343-1525	1422 ± 55	1380-1512	1357-1520
A2_61	KIA9122	1.70*	1555 ± 30	1406-1521	1381-1529	1464 ± 43	1404-1521	1390-1527
A3_40	KIA5842	2.51	2070 ± 30	1994-2104	1950-2123	2039 ± 45	1996-2108	1951-2125
B3_21	KIA11628	2.875	2293 ± 29	2310-2350	2181-2355	2327 ± 53	2211-2350	2180-2355
A5o_7	KIA11629	4.205	3065 ± 40	3225-3345	3171-3369	3278 ± 55	3234-3342	3180-3365
Boundary (coarse sand-top)***		4.35				3327 ± 61	3261-3380	3209-3454
B4_78	KIA9123	4.475	3545 ± 35	3730-3890	3715-3958	3836 ± 60	outlier	
Boundary (coarse sand-bottom)***		4.55				3442 ± 86	3349-3522	3288-3622
B5o_70	KIA11630	5.35	4018 ± 31	4438-4522	4419-4568	4480 ± 45	outlier	
B5u_13	KIA5843	5.74	3680 ± 30	3974-4083	3914-4139	4024 ± 51	3977-4085	3925-4143
A6u_2	KIA11631	6.12*	3836 ± 40	4154-4345	4100-4410	4245 ± 78	4153-4291	4097-4405
5017-1 (deep-basin core)								
E-5-H-1_61**	NUTA2-19875	10.915*	1290 ± 40	1184-1280	1090-1298	1232 ± 44	1227-1288	1181-1295
E-5-H-3_11.2	UCIAMS-110339	11.987	1600 ± 15	1419-1534	1415-1543	1457 ± 40	1418-1450	1411-1531
E-6-H-2_43	UCIAMS-110340	15.39	1850 ± 15	1739-1821	1720-1860	1781 ± 33	1778-1822	1738-1827
E-6-H-2_92.6	UCIAMS-110341	15.881	1870 ± 15	1743-1867	1736-1870	1822 ± 38	1819-1864	1816-1869
A-7-H-2_31	UCIAMS-110344	15.89	1885 ± 15	1822-1865	1743-1881	1844 ± 26	1821-1866	1818-1869
A-7-H-2_96**	UCIAMS-110316	16.54	1985 ± 15	1898-1949	1892-1988	1931 ± 25	1900-1949	1893-1985
E-8-H-1_74.5	UCIAMS-110342	20.20	2000 ± 25	1925-1989	1891-1998	1949 ± 31	outlier	
Boundary (salt-top)***		24.30				3242 ± 74	3167-3314	3095-3392
Boundary (salt-bottom)***		26.75				3587 ± 75	3512-3662	3429-3733
E-19-A-1_18.3**	UCIAMS-110343	26.863	3500 ± 15	3724-3829	3710-3835	3770 ± 36	outlier	
E-19-A-1_113.5	NUTA2-19884	27.815	5350 ± 40	6020-6261	6001-6272	6132 ± 76	outlier	
A-20-A-2_62	NUTA2-19857	32.36*	4130 ± 40	4574-4811	4530-4821	4673 ± 85	4526-4691	4447-4814

* sample is from above or below the analysed section
** samples from Neugebauer et al. (2014)
*** coarse sand deposit in DSEn and salt sequence in 5017-1 correlated to beach ridge at Ze´elim outcrop (Langgut et al., 2014; Kagan et al., in press)

4.4.2.2 Varve counting

For core DSEn, a 1351 ± 53 varves comprising floating varve chronology was created from 4.35 m to 2.10 m depth. This chronology was anchored to three ^{14}C ages (Table 4-1; Fig. 4-2) revealing an absolute age from 3286 ± 61 to 1882 ± 166 cal yr BP. Below 4.35 m depth continuous varve counting was prevented by a lack of varve preservation (Table 4-2). Varve numbers in intraclast breccias were determined by linear interpolation using the average varve thickness of 30 varves above and below the intraclast breccia corrected by multiplication with a factor of 1.61 that has been calculated from varve-count to interpolation comparison in five intraclast breccia with sufficient varve preservation. Varve counting of lithological units III to V in core 5017-1 revealed a 45% lower number (781 ± 50 varves) than in the corresponding intervals of the DSEn varve chronology (Table 4-2).

Table 4-2: Radiocarbon dating and varve counting results of cores DSEn and 5017-1, divided in defined lithological units V to I; the total number of varves counted in DSEn and 5017-1 is given only for lithological units V to III because in units II and I varves are absent or discontinuous, respectively. N.a. – not applicable; vyrs – varve years.

litho -unit	DSEn (shallow-water core)						5017-1 (deep-basin core)			
	sediment depth (m)	^{14}C age (cal yr BP, bottom)	counted varves	varve age (cal yr BP, bottom)	coarse detrital layers (per 100 vyrs)	mean thickness coarse detrital layers (mm)	sediment depth (m)	event-free sediment depth (m)	^{14}C age (cal yr BP, bottom)	counted varves
top	2.10	1751 ± 166		1882			15.05	0.00	1760 ± 34	
V	2.10-3.15	2455 ± 199	657 ± 9	2548	16	0.59	15.05-18.98	0.00-1.19	2340 ± 106	430 ± 27
V-b	*2.10-2.48*	*2030 ± 63*	*203 ± 7*	*2092*	*18*	*0.83*	*15.05-17.46*	*0.00-0.62*	*2082 ± 76*	*285 ± 21*
V-a	*2.48-3.15*	*2455 ± 199*	*454 ± 2*	*2548*	*15*	*0.46*	*17.46-18.98*	*0.62-1.19*	*2340 ± 106*	*145 ± 6*
IV	3.15-3.81	3022 ± 218	296 ± 30	2874	25	2.00	18.98-21.67	1.19-2.14	2799 ± 116	37 ± 3
III	3.81-4.35	3327 ± 61	398 ± 14	3286	7	0.51	21.67-24.30	2.14-3.00	3242 ± 74	314 ± 20
II	4.35-4.55	3442 ± 86	coarse sand	n.a.	n.a.	n.a	24.30-26.75	3.00-3.68	3587 ± 75	salt
I	4.55-5.10	3717 ± 155	135 ± 9	n.a.	n.a.	n.a.	26.75-27.31	3.68-4.00	3689 ± 93	105 ± 2
total			**1351 ± 53 (LU III-V)**							**781 ± 50 (LU III-V)**

4.4.3 Correlation of the shallow- and deep-water cores

The correlation of the DSEn and 5017-1 core sequences relies on (1) the radiocarbon-based age models and (2) a distinct marker layer appearing in both cores (Fig. 4-2; Supplement S 4-1). This marker is a ~2 mm thick black detrital layer within a laminated marl section at 4.58 m depth in DSEn and at 26.88 m depth in 5017-1. Radiocarbon ages from a few cm above this layer in both cores confirm this correlation (3836 ± 60 cal yr BP in DSEn-B4, 3770 ± 36 cal yr BP in 5017-1-E-19-A-1; Table 4-1; Supplement S 4-1).

4.4.4 Sediment micro-facies

4.4.4.1 Evaporitic facies

Aragonite and gypsum layers as well as halite reflect evaporation processes. Aragonite crystals appear as small needles (5-10 µm) building stellate aggregates (Fig. 4-3c). The white aragonite laminae are 0.5-5 mm thick. Gypsum mostly forms as euhedral monoclinic crystals (20-50 µm) and builds 1-5 mm thick greyish to beige laminae. Up to ~ 1 mm sized, often twinned, elongated gypsum crystals (Fig. 4-3c) occasionally formed post-depositionally within detrital laminae. Halite appears as euhedral cubic, mostly 100-500 µm sized transparent crystals commonly scattered within detrital laminae. In core 5017-1 larger, up to ~4 cm big, halite crystals and aggregates formed within fine-grained detrital marl layers.

4.4.4.2 Detrital facies

Clastic sediment components transported from the catchment into the basin either by fluvial or aeolian processes are summarised as detrital facies: (a) ~0.5-3 mm thick detrital laminae (Fig. 4-3a and c) consisting of clay- to silt-sized calcite, clay minerals and minor amounts of quartz, dolomite and feldspar. Silt-sized grains are sub-angular to rounded and suggest fluvial transport. Typically, these layers are grey, brown or black, but if aragonite is present, a lighter grey colour appears. Brown colours are due to well preserved organic material mixed with minerogenic detrital components. Black detrital laminae contain iron sulphides (pyrite or greigite), which build spheroidal, fine dispersed or aggregated concretions. In these laminae, often macroscopic plant remains are scattered. (b) Graded detrital layers (Fig. 4-3b) show similar characteristics as detrital laminae, but they contain a coarse, lighter base made of sand-sized calcite and quartz and show grading as well as darkening towards the top. Graded layers can get up to ~25 mm thick in the analysed DSEn section and up to ~80 cm in core 5017-1. (c) In core 5017-1, up to several cm thick, dark brown or grey homogenites (Fig. 4-3b) appear, consisting of clay- to silt-sized calcite and clay minerals, scattered coarse grains (quartz, calcite) and often macroscopic plant remains. (d) Frequently in both cores, light-coloured material of clay-sized calcite and clay minerals (Fig. 4-3c) forms a cloud-like component mostly within aragonite laminae and less often within detrital laminae. Rarely, this material builds discrete, very thin (<0.2 mm) light laminae.

4.4.4.3 Post-depositionally mixed facies

Occasionally, evaporitic layers are mixed with clastic-detrital deposits from the catchment. These mixed layers have different manifestations: (a) in core DSEn, ~3-12 mm thick mixed layers consisting of fine- to coarse-grained chaotically arranged detrital material (mostly calcite, clay and organic material) in an aragonite matrix or with aragonite lenses occur in few cases. (b) A specific mixed facies commonly observed are intraclast breccias (Fig. 4-3a) consisting of aragonite (or gypsum) lamina fragments within a fine-grained detrital matrix. The formation of these intraclast breccias has been demonstrated to be triggered by earthquakes (e.g. Agnon et al., 2006 and references therein). In core DSEn these breccias are few mm to ~7 cm thick. In core 5017-1 they are mostly incorporated in the coarse base of graded layers or even replacing these.

4.4.5 Varve model

A typical varve can be composed of either two or three sublaminae (Fig. 4-3c). A detrital layer reflects catchment runoff during winter floods also carrying bicarbonate which favours aragonite formation in the upper layer of the water body during the following dry season (e.g. Begin et al., 1974; Katz et al., 1977; Stein et al., 1997). In some years a primary gypsum layer forms instead of or additionally to the aragonite sublayer during the dry season (Stein et al., 1997; Torfstein et al., 2008).

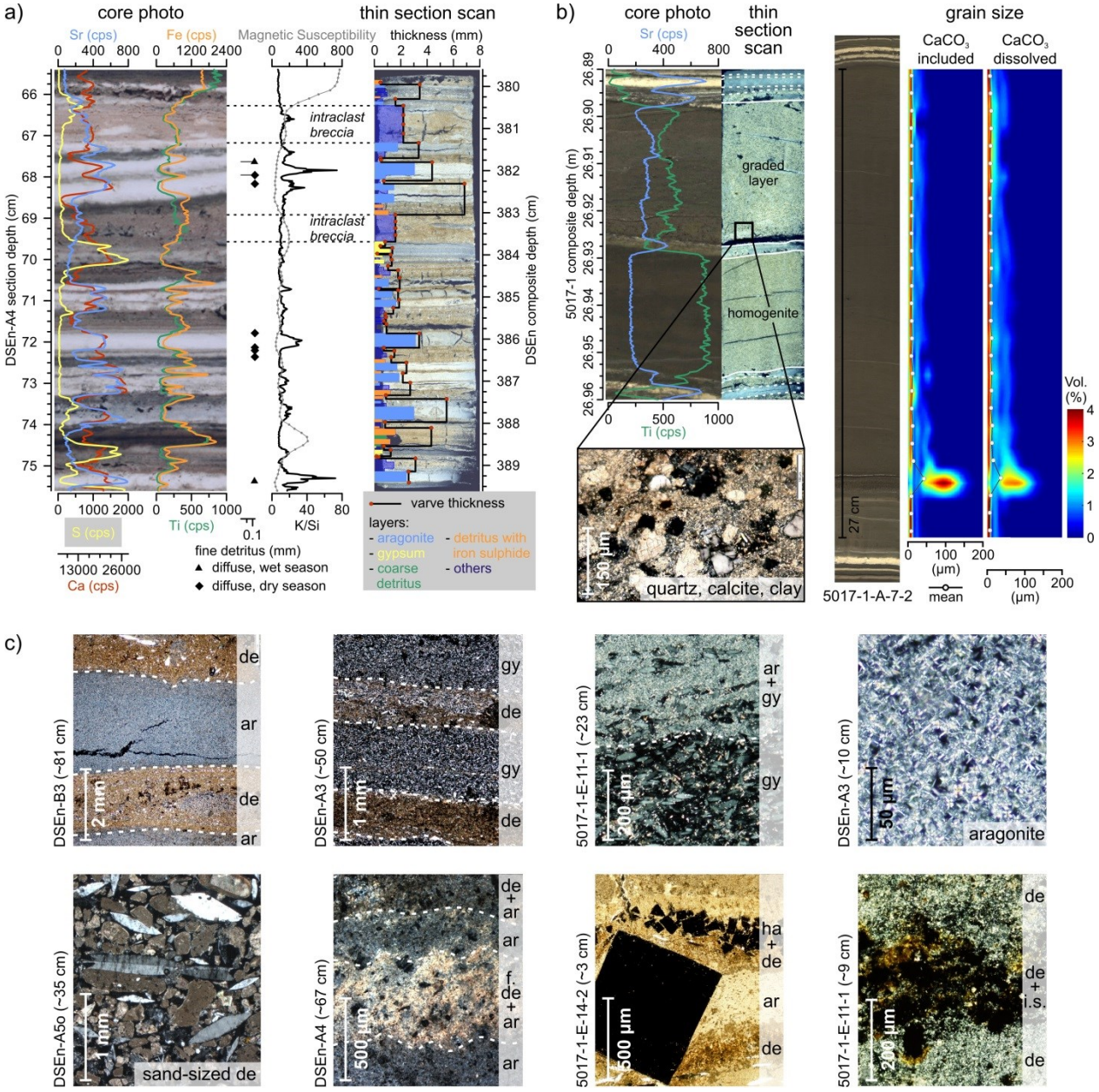

Figure 4-3: Micro-facies of the Dead Sea sediments: (a) selected 10 cm long varved sediment section from the shallow-water DSEn core, respective µXRF data of Sr, S, Ca, Fe, Ti and the K/Si ratio, magnetic susceptibility data (10^{-6} SI), layer and varve thicknesses, fine light detritus lamina, either diffuse within aragonite (dry season) or within detritus (wet season); (b) example for graded and homogeneous detrital layers from core 5017-1, including zoomed thin section image of the coarse-grained base of a graded layer; grain size results for an exemplary graded layer were plotted using the MATLAB built in function 'contour'; (c) microscope images of different layer types or components, de: detritus, ar: aragonite, gy: gypsum, f.de: fine detritus, de + i.s.: detritus and iron sulphide (black).

4.4.6 Magnetic susceptibility

In the DSEn core section magnetic susceptibility data range from very low to high values of up to ~1000 x 10^{-6} SI (Fig. 4-2) in black detrital layers. In core 5017-1 very low values indicate the presence of halite, while highest values of up to ~10,000 x 10^{-6} SI occur in few distinct peaks related to black detrital layers.

4.4.7 µXRF element scanner data

Micro-XRF element scanning data fingerprint the mineralogical composition of the sediments (Fig. 4‑3a; Neugebauer et al., 2014). Ca, Sr, S and Cl are characteristic for the evaporitic minerals aragonite (Ca, Sr), gypsum (Ca, S) and halite (Cl). Chlorine also occurs in the pore water of the sediments, but this can be distinguished from the halite signal using the Cl/Br ratio since Br only occurs in the pore water. Ca cannot be unambiguously interpreted as a proxy for evaporitic processes because it not only occurs in aragonite and gypsum but also in detrital calcite that forms the major component of the detrital layers. The terrestrial siliciclastic component (clay minerals, quartz, feldspar) is indicated by K, Ti, Fe and Si. Fe is also a proxy for post-depositionally formed Fe-sulphides within black detrital layers, where Fe counts reach maximum values. Furthermore, the µXRF data show characteristic patterns for graded and thick homogeneous sediment layers (Fig. 4-3b). The occurrence of fine light detritus deposits coincides with peaks in the K/Si ratio (Fig. 4-3a).

4.4.8 Micro-facies of lithological units

Both sediment sequences are subdivided into five sediment units, based on macroscopic description, thin section analysis, magnetic susceptibility and µXRF scanning data (Figs. 4-4 and 4-5; Table 4-2).

The lowermost lithological unit I mainly consists of clastic detrital sediments and is partly varved in both, core DSEn (135 ± 9 varves) and core 5017-1 (105 ± 2 varves; Table 4-2). In core 5017-1, unit I (4.00-3.68 m event-free sediment depth; Fig. 4-4) is characterised by up to one order higher magnetic susceptibility values than in core DSEn. In both cores, light fine-grained detritus is frequently observed in thin sections (black diamonds in Fig. 4-4), coinciding with peaks in the K/Si ratio. This unit can be unambiguously correlated in both cores through the identification of a marker layer (black detrital layer) and a characteristic succession of gypsum layers below this marker layer (Supplement S 4-1).

Unit II is a clastic detrital deposit in core DSEn and a halite-dominated section in core 5017-1. DSEn-unit II (4.55-4.35 m; Fig. 4-4) comprises an intraclast breccia including silt- to sand-sized clastic material followed by pure silt- to sand-sized clastic deposits. The coarse material consists of carbonate lithoclasts, calcite, halite and minor quartz minerals, aggregates of aragonite crystals and large gypsum crystals. The subangular to well-rounded clastic grains commonly have micritic coatings, which explain the low Ti/Ca ratio values of these deposits. Highest Cl/Br ratios

in this interval suggest a substantial halite component. In core 5017-1 unit II (3.68-3.00 m) mainly consists of salt in form of up to 3 cm big halite aggregates, partly embedded in clayey to silty marl.

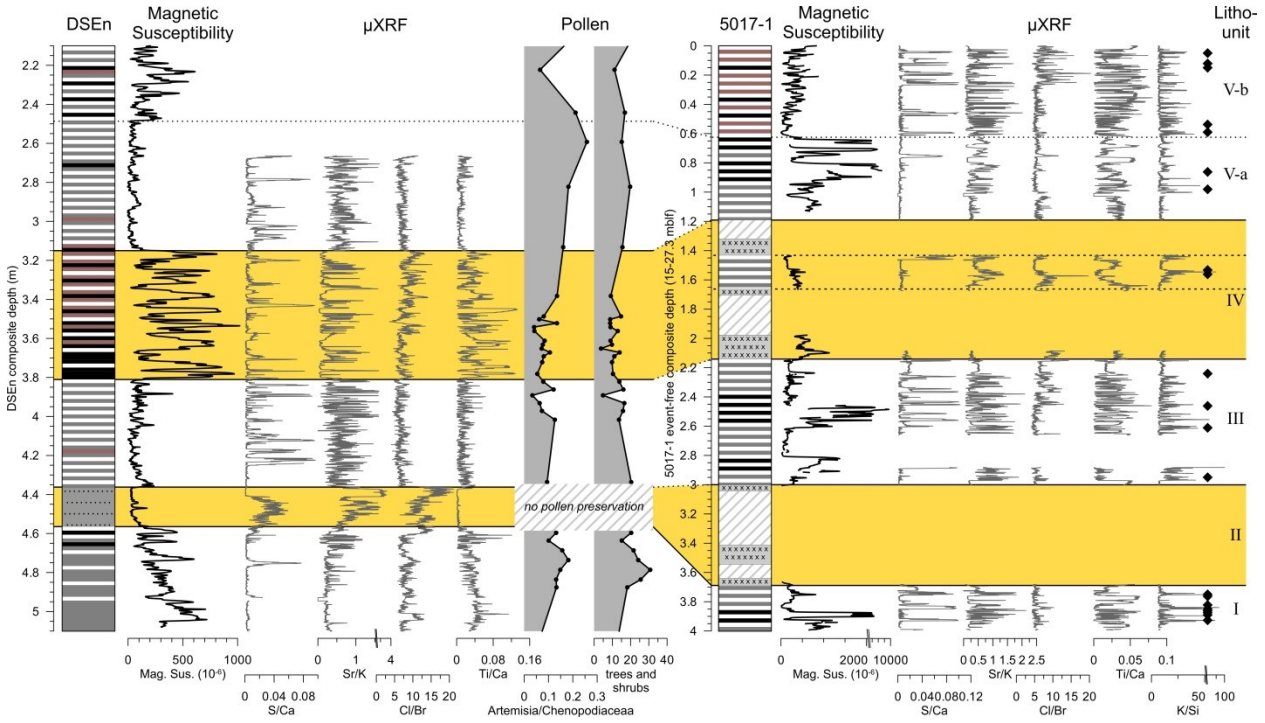

Figure 4-4: Multi-proxy results of the DSEn and 5017-1 analysed core sections: lithology (see Fig. 4-2 for legend), magnetic susceptibility data, µXRF element ratios of S/Ca, Sr/K, Cl/Br, Ti/Ca, selected pollen data (DSEn core only), the µXRF ratio of K/Si and fine detritus occurrences (black diamonds, 5017-1 core only). Lithological units I to V are given for both cores. From core 5017-1 all graded detrital layers thicker than 1 cm (n=55, summed up thickness = 607.4 cm) were excluded so that the lithological log is shown on an event-free depth scale; recovery gaps were reduced to 20% of their original extent to enhance readability of the figure.

Units III and V-a are varved in both cores and appear as regularly alternating aragonite and detrital laminae, frequent gypsum laminae and generally low magnetic susceptibility values. Few peaks in magnetic susceptibility only appear in core 5017-1. In core DSEn, unit III encompasses 398 ± 14 varves (3286 ± 61 to 2874 ± 218 cal yr BP) and in unit V-a 454 ± 2 varves were counted (2548 ± 199 to 2092 ± 63 cal yr BP). In core 5017-1 less varves were counted than in core DSEn (unit III: 314 ± 20 varves, unit V-a: 145 ± 6 varves; Table 4-2). The lower varve counts likely can be explained by erosional processes through frequent thick graded layers. In core DSEn, the average varve thickness in both varved intervals is ~2 mm/yr and coarse grained detrital layers rarely occur, while fine light detritus was frequently detected in thin sections and through peaks in the K/Si ratio (Fig. 4-5). In core 5017-1 varve and sublayer thickness were not determined and fine-grained light detritus was less frequently observed (Fig. 4-4).

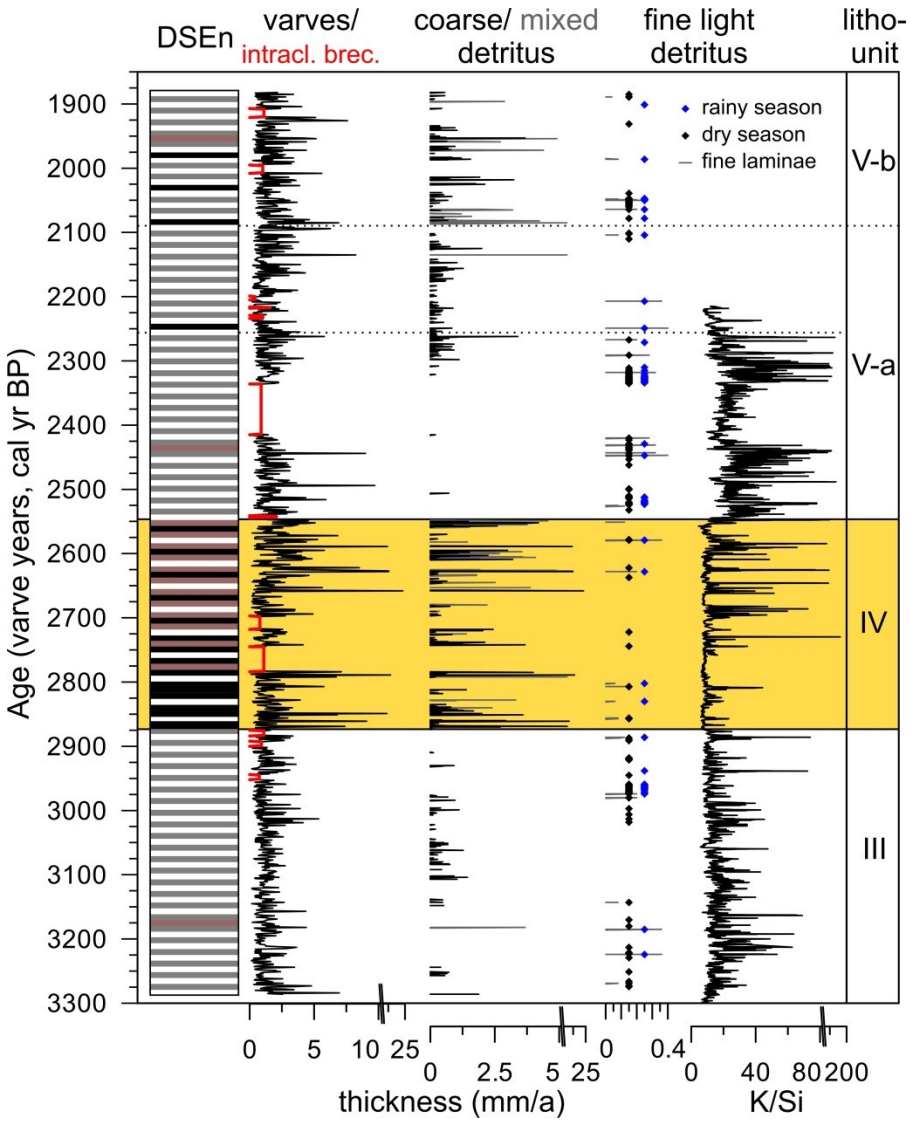

Figure 4-5: Varve counting and thin section analysis results of core DSEn (2.10-4.35 m composite depth): varve thickness including intraclast breccias ('seismites', following Agnon et al., 2006); thickness of coarse and mixed detrital layers; fine light detrital laminae thickness (grey bars) and cloudily distributed occurrences of the same material within aragonite laminae (dry season, black diamonds) and within common detrital layers (rainy season, blue diamonds); K/Si ratio derived from µXRF. Litho-units correspond to those in Fig. 4-4. For a legend of the core lithology see Fig. 4-2.

Unit IV formed between the varved units III and V and is characterised by frequent coarse-grained, commonly graded, dark brown or black detrital laminae as well as significantly increased magnetic susceptibility and Ti/Ca values in core DSEn (3.81-3.15 m). Intercalated aragonite laminae occur only rarely in core DSEn, but still more frequently than in core 5017-1. Compared to 296 ± 30 varves counted in core DSEn (2874 ± 218 to 2548 ± 199 cal yr BP; Fig. 4-5; Table 4-2) only one short varved section containing 37 ± 3 varves appears in core 5017-1. The relatively large counting error of ~22% in DSEn is due to poor varve preservation. Instead of aragonite and clastic detrital laminae, core 5017-1 mainly consists of mixed halite and

detrital marl (2.14-1.19 m; Fig. 4-4). Peaks in the K/Si ratio and fine light detritus occurrences are scarce, but increase to the top of the unit in core DSEn (Fig. 4-5).

Unit V-b (2.48-2.10 m in DSEn, 0.62-0 m in 5017-1; Fig. 4-4; Table 4-2) is a varved section and largely similar to the varved units III and V-a, but some intercalated black and brown coarse detrital layers and higher magnetic susceptibility values are observed in both cores. In this unit 203 ± 7 varves were counted in core DSEn from 2092 ± 63 to 1882 ± 166 cal yr BP (Fig. 4-5; Table 4-2) and in core 5017-1 285 ± 21 varves were counted. The higher count in core 5017-1 likely reflects a different definition of the boundaries between units V-a and V-b since the summed varve count for units V-a and V-b reveals higher varve counts for core DSEn (657 ± 9 varves) than for core 5017-1 (430 ± 27 varves; Table 4-2).

4.4.9 Palynology

Pollen data are only available for core DSEn (Fig. 4-4, Supplement S 4-2) although in unit II pollen grains were not preserved. Varved units I, IV and V-b with a high amount of coarse clastic, black and brown detrital layers are characterised by higher percentages of Chenopodiaceae (up to 45%) and Cichorioideae (up to 22%), which is indicative for a semi-desert environment. *Quercus* and generally trees and shrubs decreased in these units, except for unit I, where the latter achieve a maximum value of ca 30%. The well-varved units III and V-a are characterised by reduced Chenopodiaceae and Cichorioideae values, but moderate tree and shrub percentages (up to 20%) are observed indicating a more prominent Mediterranean vegetation in the catchment (i.e. Judean Mountains). Higher *Olea* values in units I and V indicate settlement phases and more agriculture in the region (Supplement S 4-2). The Artemisia/Chenopodiaceae ratio shows lowest values in units III, IV and V-b and higher values in units I and V-a (Fig. 4-4).

4.5 Discussion

4.5.1 Chronology

4.5.1.1 Core DSEn age model

According to radiocarbon-based age modelling, the analysed sequence of core DSEn (5.10-2.10 m composite depth) comprises the time interval from 3717 ± 155 to 1751 ± 166 cal yr BP. The coarse sand deposit at 4.55-4.35 m depth (lithological unit II) unambiguously correlates to a beach ridge in the nearby Ze'elim outcrop with a well-constrained radiocarbon age of 3500 to 3200 cal yr BP (Bookman (Ken-Tor) et al., 2004; Langgut et al., 2014; Kagan et al., in press). Including these ages in our age model reveals ages of 3442 ± 86 cal yr BP at 4.55 m and 3327 ± 61 cal yr BP at 4.35m for the lower and upper boundaries of the coarse sand deposit in the DSEn profile (Table 4-1). The two ^{14}C dates obtained from organic macro remains in the DSEn sand deposit as well as below, appear about 400 years too old (Table 4-1), most likely due to reworking and, therefore, have been rejected from the age model. Our floating 1351 ± 53 varves

comprising varve chronology established for the interval from 4.35 to 2.10 m depth (litho-units III to V; Fig. 4-5; Table 4-2) has been anchored to the modelled radiocarbon-age range (95.4% confidence interval) of the three ^{14}C dates from this interval. The resulting absolute ages for the varved interval are 3286 ± 61 to 1882 ± 166 cal yr BP. The uncertainty of 7.5% of the varve counts results from a less clear varve definition in intervals lacking annual aragonite laminae and is within the range of the radiocarbon age model. Our varve counting of the uppermost ca 95 cm that overlaps with the counts by Migowski (2001; 583 varves) yields a lower value of the new count (518 varves), mainly due to lower estimations for the intraclast breccias.

Our radiocarbon-based age model reveals ca 300 years older ages than that published by Migowski et al. (2004) despite the fact that both are based on the same radiocarbon dates. The reason for this difference is that Migowski et al. (2004) adjusted the radiocarbon age model to their earthquake chronology based on the interpretation of seismites and matching those with historical earthquake records leading them to reject five radiocarbon ages as too old. In contrast, our age model relies on radiocarbon dating supported by varve counting and correlation to the well constrained age of the Ze'elim beach ridge (Bookman (Ken-Tor) et al., 2004; Langgut et al., 2014; Kagan et al., in press), so that only two ^{14}C dates were rejected as too old (Table 4-1). Since our radiocarbon-derived age model agrees very well with the varve counts, we consider it more accurate than the age model derived from matching to an earthquake calendar because the latter is likely biased by the fact that not all historically reported earthquakes were identified by Migowski et al. (2004).

4.5.1.2 Core 5017-1 age model

The radiocarbon age model of core 5017-1 revealed a time span between 3689 ± 93 and 1760 ± 34 cal yr BP for the study interval (27.3-15 m composite depth). Although most ^{14}C samples were obtained from basal parts of graded layers and thus may suggest re-deposition, we have only found two clearly too old ages which had to be rejected (Table 4-1; Fig. 4-2). One sample (~27.8 m depth) appears to be too old by ca 2350 years while the second (~26.9 m depth) appears only slightly too old by 160 years. One ^{14}C age obtained from a small twig on top of a salt deposit apparently revealed a too young age which can only be explained by displacement of the sample during drilling operation because hard salt deposits were difficult to core (Neugebauer et al., 2014).

4.5.2 Proxy interpretation

The sediments of both cores mainly consist of the laminated detritus facies (*ld* facies; Haliva-Cohen et al., 2012; Neugebauer et al., 2014) with intercalated intervals either of coarse sand (DSEn) or halite (core 5017-1). The main mineral phases formed within the water body at different degrees of evaporation and element concentrations include aragonite, gypsum and halite. The presence of aragonite laminae suggests more humid climatic conditions because aragonite formation requires supply of bicarbonate through freshwater fluxes (Stein et al., 1997). The interpretation of aragonite as proxy for more humid conditions is specific for the Dead Sea

sediments because of the highly saline environment and is not generally valid. In freshwater lakes in the Mediterranean humid conditions are reflected by calcite precipitation, whereas a shift toward aragonite formation reflects drier conditions in such environments (Ariztegui et al., 2010; Koutsodendris et al., 2015). Since aragonite is rich in strontium, the Sr/K ratio is a suitable proxy for aragonite precipitation and thus for more humid periods. Discrete gypsum layers are well reflected in the S/Ca ratio and indicate mixing of the water column during more extreme dry years with higher evaporation (Stein et al., 1997). Gypsum layers are valuable marker layers to correlate sediment profiles not only along the shores of the Dead Sea (e.g. Torfstein et al., 2008), but also cores from the shallow and deep basin (Supplement S 4-1). Halite deposits only occur in the deep basin core and there are reflected in the Cl/Br ratio (Neev and Emery, 1967) and interpreted as proxy for most extreme dry conditions and negative water balance.

Alternating with layers of aragonite and/or gypsum, detrital material from the catchment is transported into the lake by floods during the rainy season in winter (e.g. Garber et al., 1987). Predominant mineral phases in detrital material include carbonates (calcite, dolomite) and siliciclastics (quartz, feldspar). Common winter floods resulted in regular seasonal deposition of detrital sublayers, while thick graded detrital layers indicate extreme and high-amplitude flash-floods as trigger. Therefore, the amount of clastic material deposited is not necessarily related to generally humid climates but might be even higher during drier conditions when the lake level was lower and more erodible material was exposed in the catchment (Migowski et al., 2006). The main proxy for the carbonate component of detrital material is the Ca/(S+Sr) ratio and the siliciclastic component is best represented by the Ti/Ca ratio. With some restrictions, magnetic susceptibility might be used as proxy for the siliciclastic detrital component as well. However, the interpretation of magnetic susceptibility as detrital matter proxy is biased in case of greigite formation (Frank et al., 2007a; 2007b; Ron et al., 2007). Greigite is post-depositionally formed under reducing conditions and exhibits strongly increased susceptibility values (Nowaczyk, 2001).

In the DSEn core mixed layers composed of fine- to coarse-grained chaotically arranged detrital material mostly within an aragonite-matrix often concur with graded layers and likely represent reworking from shallow water favoured by the near-shore position of the DSEn location. In core 5017-1 these mixed layers do not occur. Instead, up to 5 cm thick and commonly fine-grained homogeneous detrital layers often containing significant amounts of organic remains were deposited.

In sediments from both locations, fine-grained and light-coloured detritus is deposited as either cloud-shaped aggregates of calcite and clay minerals within aragonite and detrital laminae or as thin discrete layers and is reflected also in the K/Si ratio (Figs. 4-3 and 4-5). This material is interpreted as traces of reworked dust from the Negev desert. Although these fine traces of dust are not considered as a proxy for total dust flux, since they represent only a minor dust fraction, our high-resolution thin section analyses prove that fine dust is transported into the DSB during times of stronger Mediterranean cyclone activity (Dayan et al., 2008; Haliva-Cohen et al., 2012).

Pollen data is obtained from core DSEn and here we present selected taxa which are interpreted as proxies for changes in humidity, i.e. trees and shrubs, and the Artemisia/Chenopodiaceae (A/C) ratio (Fig. 4-4). Lower tree and shrub as well as A/C values are related to more arid conditions (El-Moslimany, 1990; Herzschuh, 2007; Zhao et al., 2012) and support our sedimentological interpretation. For the lithological units III and IV dated at ~3300-3000 cal yr BP and ~3000-2500 cal yr BP, for which no major lake level changes were reported in previous studies (Bookman (Ken-Tor) et al., 2004; Migowski et al., 2006), we find slightly higher tree and shrub percentages in unit III (on average 14.6%) than in unit IV (on average 10.6%), suggesting more arid conditions during unit IV (Fig. 4-4). Since values of the typical indicator for human settlement *Olea* (Neumann et al., 2007; Litt et al., 2012; Langgut et al., 2014) are low during these two periods (on average 4.1%; Supplement S 4-2), we assume reduced settlement activity during that time. Settlement activity might have been slightly increased during the dry period at ~3000-2500 cal yr BP (lithological unit IV; Supplement S 4-2) as suggested by an increase in pollen of the Cichorioideae family (on average 14% in unit IV) which is regarded as a secondary anthropogenic indicator (Langgut et al., 2014).

4.5.3 Comparison of shallow- and deep-water sediments

The most apparent differences between the shallow-water and the deep-basin cores are (i) the significantly higher sediment thickness in core 5017-1 and (ii) the distinctly different lithology of litho-units II and IV (Fig. 4-4). (i) The thickness of the deep-basin core (ca 12 m) is four times higher compared to core DSEn (ca 3 m) due to the occurrence of up to 80 cm thick turbidites and homogenites as well as distinctly folded sections according to slumping processes in the deep basin (Neugebauer et al., 2014). These mass wasting events likely caused erosion in the deep basin as evidenced by lower varve counts in core 5017-1, like for example by 22% within litho-unit III (Table 4-2). (ii) The coarse sand deposit and predominantly detrital material of litho-units II and IV in core DSEn correspond to two halite-dominated sections in core 5017-1 (Fig. 4-4). Except erosion processes, the varved intervals including aragonite and gypsum laminae (litho-units I, III and V in Fig. 4-4) are rather similar in both cores. However, in core 5017-1 more black and brown detrital layers are intercalated, likely related to the better preservation of organic matter in the deep environment due to reducing conditions (Lazar et al., 2014).

4.5.4 Pronounced dry periods in the Dead Sea region between ~3700 and ~1700 cal yr BP

Based on correlating the shallow- and deep-water sediment facies and multi-proxy analyses, the climatic variability between ca 3700 and 1700 cal yr BP has been reconstructed with a focus on deciphering the most arid phases. Superimposed on the overall drier climate in the eastern Mediterranean compared to the early Holocene (Robinson et al., 2006; Finné et al., 2011 and references therein), two pronounced centennial-scale dry periods occurred (Fig. 4-6).

The dry period between ca 3500 and 3300 cal yr BP had a strong impact on sedimentation and resulted in a massive sand deposit related to a lake level drop at the shallow location (DSEn). At the same time salt was deposited in the deep basin. This dry period caused a lake level decline of ~45 m down to 417 m bmsl (Migowski et al., 2006; Fig. 4‑6) and coincides with a late Bronze age cultural crisis in the entire Levantine region (Kaniewski et al., 2013; Langgut et al., 2014 and references therein; Kagan et al., in press). The only available pollen information in the Dead Sea region from that period is from the Ze'elim beach ridge, based on a single sample that confirms dry conditions through high chenopod and low tree pollen percentages (Langgut et al., 2014). Stable oxygen isotope data from the nearby Soreq Cave indicate stable dry conditions during the entire interval investigated here, with only minor fluctuations of ~0.3‰ (Bar-Matthews et al., 2003; Fig. 4‑6). During this dry phase in the Dead Sea area, the Black Sea region experienced enhanced winter rains (Lamy et al., 2006), which were strongest during the final phase of the Dead Sea dry period at ~3300 cal yr BP (Fig. 4-6), pointing to an enhanced N-S gradient in precipitation during this time. This dry period at the Dead Sea coincides with one of the so-called rapid climate change events (RCC; Mayewski et al., 2004) in the North Atlantic at ~3200 cal yr BP, which has been related to stronger Siberian Highs (Mayewski et al., 1997; Meeker and Mayewski, 2002) and impacted also on the eastern Mediterranean, for example through driving winter SST cooling in the Aegean Sea (Rohling et al., 2002). Stronger Siberian Highs might have changed the nature of cyclogenesis process in the eastern Mediterranean, leading to drier conditions and the abrupt lake level drop at the Dead Sea (Kushnir and Stein, 2010).

The dry period from ca 3000 to 2400 cal yr BP had a less strong impact on the sedimentation regime. The sedimentological evidence in the deep basin again is predominant salt deposition, whereas the shallow location only exhibits an increase in clastic-detrital deposition and reduced aragonite precipitation (litho-unit IV in Figs. 4-4 and 4-5). Sedimentological indications for a significant lake level drop are absent since the presence of varved sediments indicates high lake level and sufficient bicarbonate supply through freshwater inflow. Therefore, this dry period is considered less pronounced than the earlier dry phase at ca 3500-3300 cal yr BP. The occurrence of coarse detrital layers on average every four years (Table 4-2) implies an increase of flooding during that time despite the generally dry conditions. Water supply to the lake through these floods could explain the absence of a major lake level drop at that time. This scenario is in agreement with reports of a rather stable lake level during moderately dry conditions (Bookman (Ken-Tor) et al., 2004; Migowski et al., 2006; Fig. 4‑6).

Dry conditions are supported by a reduction in Mediterranean pollen taxa (mainly *Quercus*; Supplement S 4-2) and very low Artemisia/Chenopodiaceae ratios in this unit (Fig. 4-4), which confirms earlier reports from other pollen records from the Dead Sea margins (Neumann et al., 2007; 2010) and offshore at the base of core DS7-1 (Leroy, 2010). A similar trend can be observed in Ze'elim, where Langgut et al. (2014) interpreted the Iron Age I (ca 1150-950 BCE) as more humid compared to Iron Age II (950-600 BCE). Although settlement activities may have influenced the vegetation during this period (Langgut et al., 2014), the stronger contribution of

the desert and semi-desert vegetation in conjunction with the reduction of all pollen components related to the Mediterranean biome cannot be explained only by human impact, because olive, normally increasing during times of expanded anthropogenic activities, is also affected by this phenomenon. Therefore, it is likely to assume relatively drier conditions in comparison to Iron Age I (see also Langgut et al., 2014).

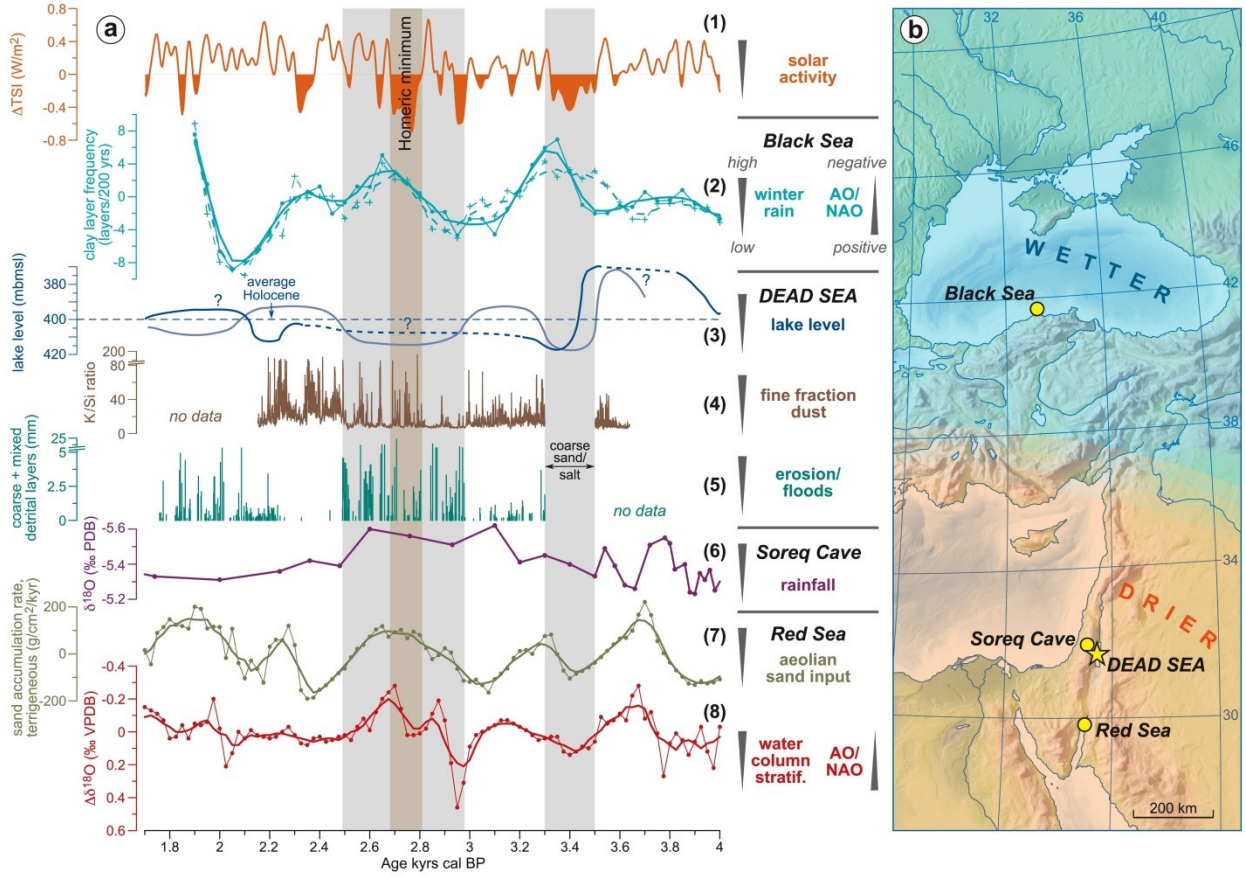

Figure 4-6: (a) Comparison of the Dead Sea data to other records: (1) difference of the total solar irradiance ΔTSI from the year 1986, 1365.57 W/m² (Steinhilber et al., 2009); (2) clay layer frequency record from the Black Sea, cores GeoB7622 (solid lines) and GeoB7625 (dashed lines), thick lines: 3-point moving average (Lamy et al., 2006); (3-5) Dead Sea: (3) lake level reconstruction based on core DSEn (Migowski et al., 2006), light blue line: this study, (4) K/Si ratio from µXRF element scanning (this study), (5) coarse and mixed detrital layer thickness (this study), both (4) and (5) from core DSEn and on radiocarbon-based age-scale; (6) Soreq Cave $\delta^{18}O$ speleothem record (Bar-Matthews et al., 2003) showing only very minor changes over the entire period investigated here; Red Sea: (7) terrigeneous sand accumulation rate and (8) stable oxygen isotope difference $\Delta\delta^{18}O$ between planktic and epibenthic foraminifera, both core GeoB5804-1, thick lines: 5-point moving average (Lamy et al., 2006). Vertical bars indicate the two dry periods detected in this study. AO/NAO: Arctic Oscillation/ North Atlantic Oscillation. (b) Inferred humidity changes in the eastern Mediterranean during the two dry periods at the Dead Sea, discussed here.

The occurrence of extreme flash-floods during generally drier climate might be explained by a reduced intensity (depth) and/or an eastward shift of the Cyprus Low, the dominant weather pattern in this region (Saaroni et al., 2010). Such change in the Cyprus Low would lead to strong

decrease in precipitation in the northern catchment of the Dead Sea, but slightly enhanced rainfall in the western and southern areas (Zangvil et al., 2003) in agreement with the suggested, even if only minor, rainfall increase at Soreq cave (Bar-Matthews et al., 2003; Bar-Matthews and Ayalon, 2004; Fig. 4‑6). One additional argument for a less intense Cyprus Low at around 2800 cal yr BP might be derived from the changes in fine dust components as observed in thin sections (Fig. 4-5). Accepting a positive correlation between dust accumulation in the northern Negev desert and the intensity of the Cyprus Low (Dayan et al., 2008) with less frequent deposition of fine dust during low activity phases of the Cyprus Low and more fine dust during increased Cyprus Low activity is in agreement with our observations. However, we have to be careful with this interpretation since the very fine traces of dust that we observe should not be considered as a classical dust proxy like, for example, sand-sized dust accumulation in the Red Sea (Lamy et al., 2006; Fig. 4‑6), which suggests increased dust deposition during drier periods. Therefore, it remains open if there really was a regional difference in dust deposition between the Red Sea and the Dead Sea (Fig. 4-6), or if this is only due to different proxies applied.

An explanation for contemporaneous drier climate and increased flooding at the Dead Sea is inferred from 20th century reanalysis data of synoptic systems over the EM (Alpert et al., 2004) showing that the frequency of Red Sea Troughs (RST) increased during times of less intense Cyprus Lows in the period 1948-2000, both associated with drier conditions in the EM. The contemporaneous increase of the Active Red Sea Trough (ARST), the stormy and active type of the RST, led to more convective storms and heavy rainfall from the south despite a generally drier climate (Alpert et al., 2004; de Vries et al., 2013). These irregular ARST situations are responsible for major flash-floods in the Negev desert and the southern Dead Sea catchment (Kahana et al., 2002; Dayan and Morin, 2006; Enzel et al., 2008) and may have led to the frequent deposition of coarse detrital layers in our record around 2800 cal yr BP.

Both scenarios of changed atmospheric circulation patterns might account for the co-appearance of drought and strong flood events at the Dead Sea around 2800 cal yr BP. The ultimate trigger for such a shift in atmospheric circulation, however, is unknown. In this respect, the apparent coincidence of the younger dry phase with the Homeric Grand Solar Minimum (GSM) at ca 2800 cal yr BP (Steinhilber et al., 2009; Fig. 4‑6) within dating uncertainties is intriguing. This GSM has been associated with cold and moist climate in the central European and North Atlantic realm (e.g. van Geel et al., 1996; 1999; Magny, 2004; Martin-Puertas et al., 2012), the western Mediterranean (Martin-Puertas et al., 2009) and even in regions further east like the Black Sea (Lamy et al., 2006; Fig. 4‑6), the Caspian Sea (Kroonenberg et al., 2007) and the Eurasian steppe (van Geel et al., 2004). These widespread moist climate conditions have been attributed to a prevalent negative phase of the Arctic/North Atlantic Oscillation likely triggered by the reduced solar irradiation through the so-called ‘top-down’ mechanism (Ineson et al., 2011; Martin-Puertas et al., 2012). In contrast to a predominantly moist Europe, various marine, lake and cave records from the southern part of the eastern Mediterranean including the Dead Sea suggest drier climate at the time of the GSM (Lamy et al., 2006; Fig. 4‑6; Roberts et al., 2011b and references therein).

A major shift of the Arctic/North Atlantic Oscillation in turn might have affected even eastern Mediterranean circulation patterns like the Cyprus Low and the (A)RST. Even if speculative, these complex shifts in atmospheric circulation pattern might have caused a large gradient in precipitation between the Black Sea and Dead Sea areas. However, further investigations including teleconnections to the ITCZ and monsoon systems in the South of the Dead Sea are necessary to better disentangle these atmospheric teleconnections. Therefore, a better regional coverage of high-resolution palaeoclimate records is required to prove our hypothesis.

4.6 Conclusions

Detailed comparison of a shallow-water sediment sequence from the western margin of the Dead Sea with its deep-basin counterpart allowed reconstructing the climatic conditions in the eastern Mediterranean from ~3700 to ~1700 cal yr BP down to annual resolution. Well-laminated sediments with frequent aragonite laminae at both core locations indicate more humid climate conditions. During dry periods and lower lake levels halite deposited in the deep environment, while at the lake's margin enhanced clastic deposition and reduced aragonite precipitation occurred. The abundance of mass wasting deposits in the centre of the lake resulted in fourfold higher sediment thickness of the deep-basin core and even lead to some erosion as inferred from the lower varve counts compared to the shallow core.

The studied time interval is characterised by two pronounced centennial-scale dry periods from ~3500 to ~3300 cal yr BP, coinciding with a cultural crisis in the region during the late Bronze Age, and from ~3000 to ~2400 cal yr BP. The younger dry period coincides with a cool and wet climate in widespread areas of Europe that has been related to a Grand Solar Minimum around 2800 cal yr BP. Despite the overall dry climate during this time in the south-eastern Mediterranean region, the Dead Sea experienced an increase in flooding probably caused by a reduction and eastward migration of the dominant Cyprus Low weather pattern and/or by more frequent intrusions of the Active Red Sea Trough into the Negev desert and the southern Dead Sea catchment. Despite the contrasting climate signature in Europe (wet) and the Dead Sea region (dry) during this period, these changes might be linked through complex teleconnections of atmospheric circulation patterns.

Acknowledgements

We are grateful for constructive comments by two anonymous reviewers and to F. Marret for editing this article. We thank G. Arnold, D. Berger (GFZ Potsdam) and M. Köhler (MK Factory, Potsdam) for their creativity and patience with preparing thin sections, as well as A. Hendrich and M. Dziggel (GFZ Potsdam) for help with the figure design and N. Köller (University of Mainz) for assistance in thin section analysis. Further, we are grateful to E. Kagan (Hebrew University Jerusalem), N. Nowaczyk and S. Lauterbach (GFZ Potsdam) for discussions.

Funding

Funding by the International Continental Scientific Drilling Program (ICDP), the German Science Foundation (DFG Grants FR 1672/2-1 and BR 2208/10-1) and the Helmholtz Centre Potsdam, GFZ (Germany) is gratefully acknowledged. This study is a contribution to the Helmholtz Association (HGF) climate initiative REKLIM Topic 8 ”Rapid climate change derived from proxy data“.

Supplementary material

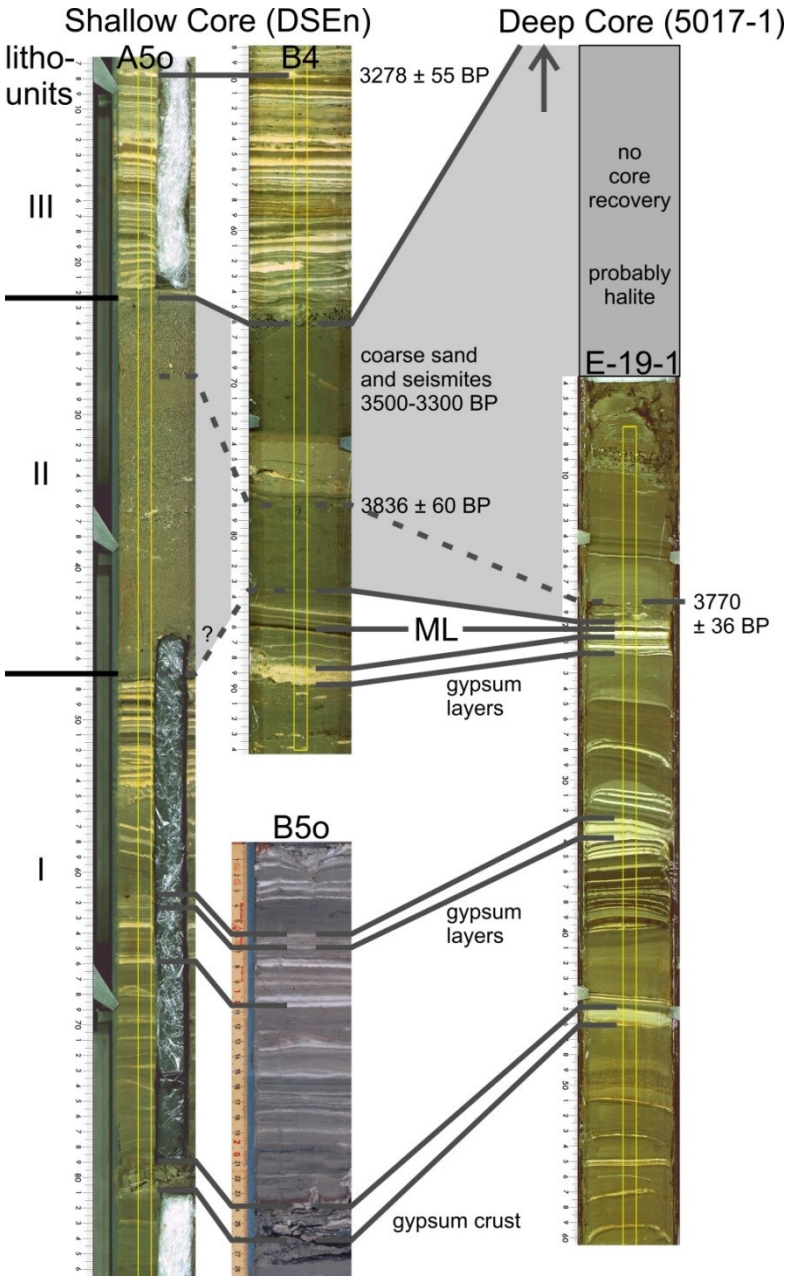

Figure S 4-1: Correlation of cores DSEn and 5017-1 by radiocarbon ages, a marker layer (ML) and a characteristic succession of gypsum deposits.

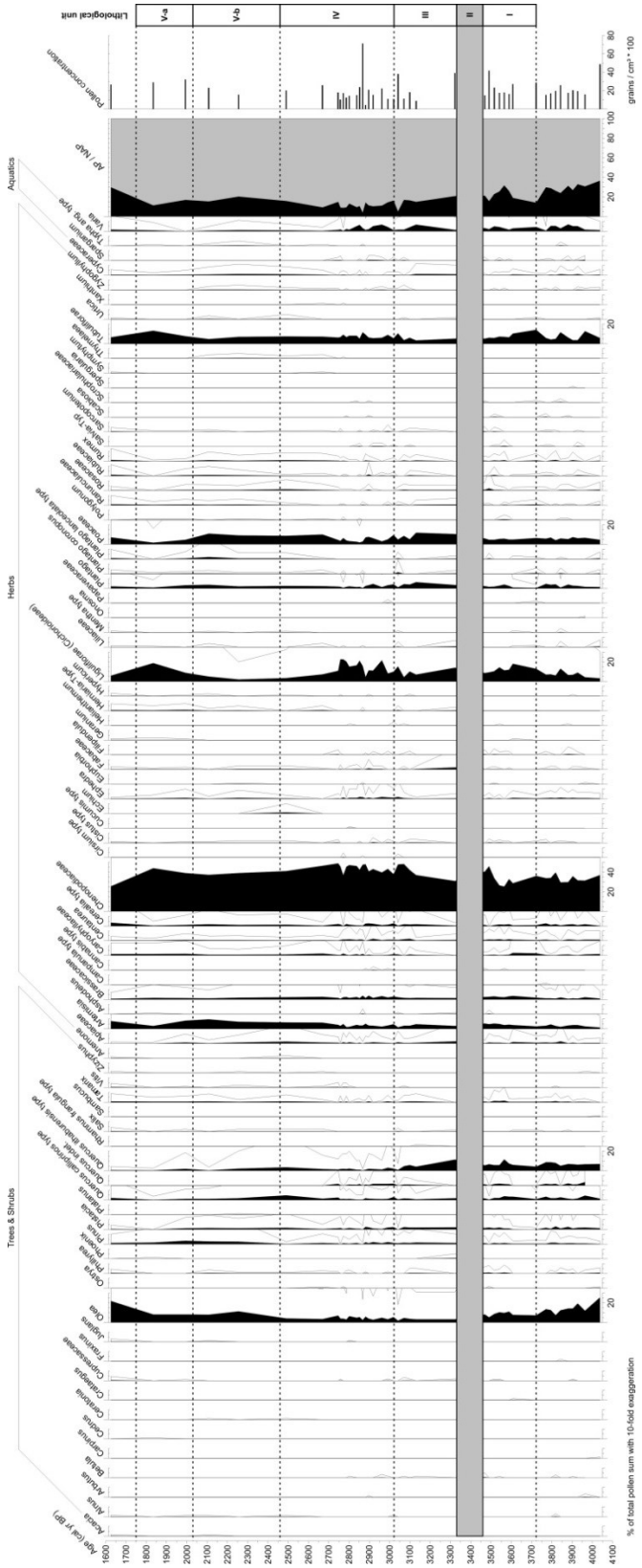

Figure S 4-2: Full pollen diagram of core DSEn for 1600-4050 cal yr BP. Lithological units are given and indicated by dashed lines. No pollen were preserved in LU-II (coarse sand deposit) and this is indicated by a grey bar.

5 Synthesis

5.1 Summary and main conclusions

The main aim of this doctoral project was to reconstruct past climate variability from the Dead Sea sediment record by applying high-resolution micro-facies analyses. For this purpose, sediment cores from the deep Dead Sea basin and the lake's western margin were analysed from multi-millennial down to centennial and annual time-scales. In the following, (a) main results are summarised and conclusions are drawn about how the core objectives of this thesis were met; and (b) the contribution of this work to better understand the climatic variability in the eastern Mediterranean region is discussed in a broader scientific context.

(a) Main results and conclusions

i) Providing the lithostratigraphic framework for the long ICDP deep-basin core including correlation to on-shore sediment formations.

The requirements of this objective were fully met and are presented in Chapter 2. Within this manuscript, the DSDD Project is introduced before focusing on the long deep-basin core 5017-1. The lithological and geochemical characteristics and first radiocarbon and U-Th dating results of the ~455 m long core together with the stratigraphic correlation to exposed sediment formations from the lake's margins reveals that this core comprises the last ca 220 ka. The record covers the upper part of the Amora (parts of or entire penultimate interglacial and glacial), the last interglacial Samra (~135-75 ka), the last glacial Lisan (~75-14 ka) and the Holocene Ze'elim Formations and, therewith, two entire glacial-interglacial cycles. Furthermore, this is the first record from the Dead Sea also covering transitional intervals, i.e. glacial-interglacial or *vice versa* transitions, which are characterised by major reorganisation of the atmospheric circulation and are, hence, of particular interest for palaeoclimate research.

A key aspect of this study as part of this doctoral project is the description and classification of the main lithologies and their geochemical characteristics, as derived from XRF element scanning, which provides the base for high-resolution micro-facies analyses. Three main facies groups are identified: (1) the marl facies, (2) the halite facies and (3) massive, graded and slumped deposits, each of these grouping three different sedimentary facies types (Chapter 2.5.1). A discussion of the hydroclimatic conditions that lead to the deposition of these specific facies is also provided in the manuscript (Chapter 2.6.1). In particular, the finely laminated facies (*aad* – alternating aragonite and detritus, *ld* – laminated detritus, *gd* – gypsum and detritus, and *lh* – layered halite) turned out to be valuable for micro-facies analyses, as these store the past hydroclimatic variability with up to seasonal resolution. In Figure 5-1 the main lithologies and associated lake levels and climate conditions are summarised:

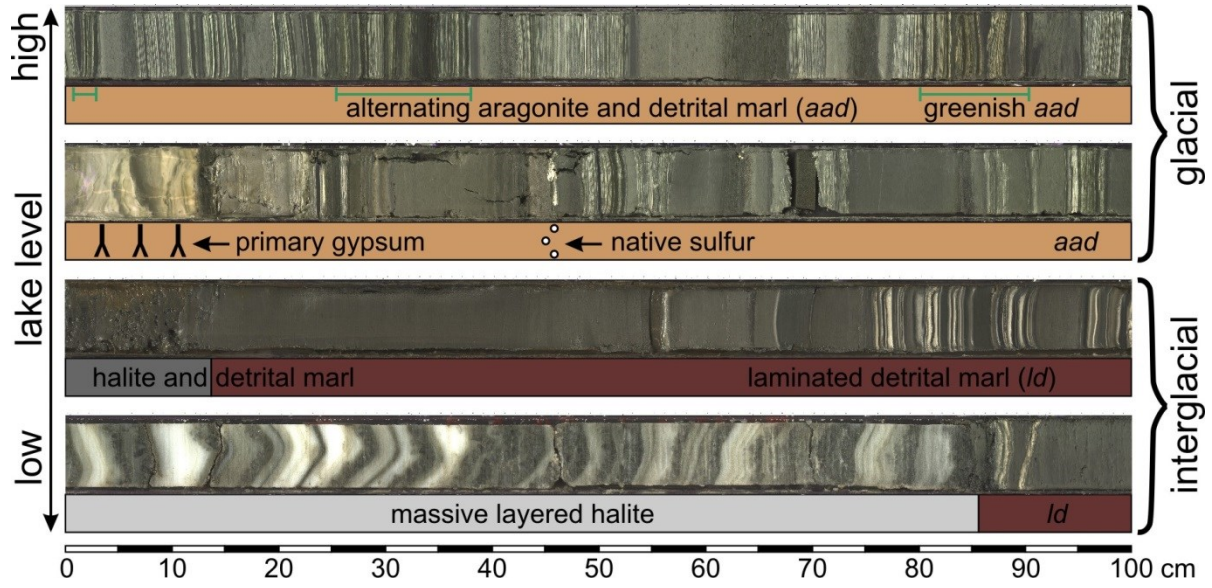

Figure 5-1: Main lithologies occurring in core 5017-1 from the deep Dead Sea basin and associated relative lake levels and glacial/interglacial conditions.

In Chapter 2, it is demonstrated that large parts of the core contain massive, graded and slumped deposits. For example, in the ~112 m encompassing last glacial Lisan Formation only about 40% of the sequence is apparently undisturbed by these mass wasting events. On the one hand, some restrictions arise from the frequent occurrence of these event layers: (1) the total sediment accumulation in the deep basin is substantially higher than expected, so that the initial goal of the ICDP DSDDP to recover the last 500 ka or more of environmental and tectonic history could not be achieved. (2) These mass movement events likely caused erosion of the deep-basin sediments, as is suggested from a comparison of varve-counts to radiocarbon dating results, performed within this thesis (Chapter 4.5.3). This limits the application of independent varve chronologies that were aimed to support the absolute chronology of core 5017-1 for selected intervals. On the other hand, the various manifestations of event deposits itself offer the possibility to establish an event-stratigraphy for the last ~220 ka, which is undertaken within the DSDDP (by E. Kagan, S. Marco, A. Agnon and N.D. Waldmann). Thereby, a challenging task is to decipher the trigger mechanisms for these deposits, which can be earthquakes, hydrometeorological extreme events or lake level fluctuations. Micro-facies analyses potentially allow deciphering these triggers.

ii) Establishing micro-facies analyses of annually laminated sediments by combined thin section microscopy and µXRF measurements as a tool for high-resolution climate reconstruction from the Dead Sea sediments.

This objective was realised within two high-resolution studies presented in Chapters 3 and 4. The combined use of thin section microscopy and µXRF element scanning was utilized for the first time for sediments from the Dead Sea. Micro-facies analyses turned out to be a powerful tool to better understand the depositional processes und underlying hydroclimatic boundary conditions leading to the exceptional heterogeneity of sediments deposited in the Dead Sea basin (DSB).

A particular strength is the more objective characterisation of micro-facies types and of changing sediment compositions through the application of element ratios that are utilized to minimize physical and geometrical sample effects (Weltje and Tjallingii, 2008). Authigenic sediment components include aragonite, gypsum and halite that are best represented by Sr/Ca or Sr/K (for aragonite), S/Ca (for gypsum) and Cl/Br (for halite). The detrital minerogenic components comprise siliciclastics and carbonates. The siliciclastic detrital fraction is characterised through peaks in Si, K, Ti and Fe, which correlate with each other with an R^2 of 0.8 or higher, and is best represented by the Ti/Ca ratio. For the detrital carbonate fraction, the Ca/(Sr+S) ratio turned out to be the best proxy, as therewith the authigenic Ca-containing sediment components, i.e. aragonite and gypsum, are removed from the signal. In Chapter 3, a first attempt is presented to use a combination of these element ratios as proxy for the water balance of the lake. This combination of standardised ratios sums up the three sediment components that are interpreted as indicators for a positive water balance, i.e. aragonite and the two detrital fractions, and subtracts the halite and gypsum sediment components that are related to a negative water balance. This approach worked well for the early last glacial sequence that was analysed in Chapter 3.

However, one has to be careful when interpreting the water balance changes derived from µXRF in terms of changing hydroclimatic conditions because the influence of temperature and evaporation changes can hardly be disentangled. Another problem is the bi-directionality of the detritus proxy for changing humidity in the catchment of the lake: when annual precipitation in the carbonate terrains surrounding the lake is above a certain threshold, the governing process of denudation would be chemical and its rate would increase with higher rainfall (Ryb et al., 2014). This scenario is suggested for periods of *aad* facies deposition, which requires significantly higher supply of freshwater, and applies for the early last glacial sequence (Chapter 3). When annual precipitation drops below the threshold (in an arid to hyperarid environment), the dominant weathering and denudation style would switch from chemical to mechanical (physical) and its rate would increase with increased aridity (Ryb et al., 2014). This is probably valid for the late Holocene as presented in Chapter 4, where the deposition of clastics increases during relatively drier conditions compared to periods when the freshwater supply into the lake is high enough to support aragonite formation. Hence, the above described combination of µXRF element ratios, where increased detritus is used as proxy for a positive water balance, is not applicable for sediments of the *ld* facies, where a higher amount of clastic material indicates drier conditions. Therefore, a thorough understanding of the underlying processes and climate leading to the different micro-facies types requires a multi-proxy approach. This has been performed in Chapter 4 as part of this thesis.

iii) Obtaining high-resolution, multi-proxy time-series of extreme events, like floods and dust storms, and deciphering their relation to changing climate conditions in the Dead Sea region for the Holocene.

A high-resolution, multi-proxy time-series of erosion and dust deposition events has been established for the late Holocene from ca 3700 to 1700 cal yr BP from the shallow-water core

DSEn and its counterpart in the deep-basin core 5017-1 (Chapter 4). This interval was chosen because it contains an almost continuously varved section in core DSEn, it is well dated by radiocarbon dating of terrestrial macro-plant remains and it can be correlated to other on-shore sediment exposures. The multi-proxy approach comprises microscopic thin section analyses, μXRF element scanning, magnetic susceptibility measurements and grain size and palynological analyses. It could be shown that more humid climate conditions lead to the deposition of well-varved sediments of alternating aragonite and/or gypsum and detrital laminae in both the shallow- and the deep-basin sediment cores. Drier climate conditions cause enhanced clastic deposition and reduced aragonite precipitation at the lake's margin, while in the deep basin mainly halite is deposited.

The manuscript especially focused on characterising two pronounced centennial-scale dry periods detected in this late Holocene sequence: (1) a dry period from ~3500 to ~3300 cal yr BP coincides with a late Bronze Age cultural crisis in the Levant and is probably related to one of the so-called rapid climate change events (RCC) in the North Atlantic at ~3200 cal yr BP (Mayewski et al., 2004). The related strengthening of the Siberian High might have influenced the position or strength of eastern Mediterranean cyclones, leading to drought and an abrupt lake level drop at the Dead Sea (Kushnir and Stein, 2010). (2) The most important finding of this study was the identification of a second dry period from ~3000 to 2400 cal yr BP that coincides with the Homeric Grand Solar Minimum at ~2800 cal yr BP and cold and moist climate in widespread areas of Europe and the Eurasian steppes. Because this dry period and lake level decrease at the Dead Sea was less pronounced than the earlier one, the sediments still exhibit lamination, which allowed varve counting and micro-facies analyses. The results indicate an abrupt increase in the frequency of coarse detrital layers that are interpreted as flash-flood events. As pollen data and the rare occurrence of aragonite laminae in core DSEn, as well as halite in core 5017-1 indicate drier conditions, these frequent flash-flood events must have occurred despite a generally drier climate. It was possible to attribute this to a change in synoptic weather patterns, most likely to a less intense Cyprus Low weather pattern, which is responsible for most of the moisture arriving in the watershed of the Dead Sea, and at the same time a more frequent (but sporadic) intrusion of the Active Red Sea Trough situation, which brings moisture from the south and leads to flash-floods in the Negev and in the southern Dead Sea catchment. This scenario was observed during the last decades of the 20th century in concert with increasing aridity in the Mediterranean region. Whereas the two analysed dry periods, however, coincide with colder climate conditions in the North Atlantic region, the recent drought is driven by a man-made increase of global temperature and greenhouse gases.

Another intriguing finding of this study, presented in Chapter 4, is that fine traces of dust can be identified through micro-facies analyses. Thereby, enhanced deposition of this fine fraction dust seems to coincide with more humid climate conditions, which is in agreement with other studies that associate more fine dust deposition in the Negev and Dead Sea with more active phases of Mediterranean cyclones and dust storms (Dayan et al., 2008; Haliva-Cohen et al., 2012). The

coarse fraction dust, which makes up the vast majority of dust deposited in the Dead Sea basin during the Holocene (Haliva-Cohen et al., 2012), can however not be disentangled through micro-facies analyses, as it is considered to be reworked and arrives in the basin together with floods. To detect the total amount and possible sources of dust, other techniques, like for example Sr isotope and εNd measurements, are applied within the DSDDP (D. Palchan, M. Stein).

This study (Chapter 4) is an important step towards a better understanding of climate variability in the Levant and demonstrates the invaluable strength of micro-facies analyses to disentangle small-scale climate shifts and to document hydrometeorological extreme events during the Holocene. Particularly cores DSEn and 5017-1 have great potential to further test how the relationship between atmospheric circulation and climate in the Levant changed during the course of the Holocene and with increasing human influence.

iv) Reconstructing palaeoclimatic changes in the Dead Sea and adjacent areas during the last two interglacials as archived in the ICDP Dead Sea record.

Analysing causes and consequences of past interglacial abrupt climate changes may serve as natural analogue for the recent man-made increase in global temperature, aridification in the Mediterranean region and shrinking of the Dead Sea. In this respect, two centennial-scale dry periods in the eastern Mediterranean region during the late Holocene were analysed within this study (Chapter 4, see (iii) above), which, however, turned out to be related to cooler temperatures in the North Atlantic. The last interglacial, corresponding to MIS 5e between ca 135 and 116 ka (Lisiecki and Raymo, 2005), experienced probably even warmer temperatures than we do today. Interestingly, the deep-basin Dead Sea core 5017-1 exhibits a ca 40 m thick halite sequence that is the thickest halite in the entire core and was deposited during the later part of the last interglacial (see Chapter 2), following a period of more humid climate during the peak of the last interglacial, when moisture may have arrived in the Dead Sea basin from an intensified African monsoon (Torfstein et al., 2015). Overlying this late interglacial halite sequence, a pure gravel layer was deposited that was at first interpreted as beach layer by Stein et al. (2011) and Torfstein et al. (2015), who suggested a nearly desiccation of the lake at the end of the last interglacial. Within this doctoral project (Chapter 3) it is, however, demonstrated that this was likely not the case, as this gravel probably represents a mass wasting event triggered by major lake level fluctuations at the transition from the last interglacial to the early last glacial, equivalent to MIS 5d.

The study presented in Chapter 3 furthermore focused on deciphering the hydroclimatic variability during the early last glacial period (~117-75 ka) reflected in the sediments of the deep Dead Sea basin, as this interval is poorly represented in on-shore deposits and earlier studies of these exposed sediments suggested that climatic conditions at the Dead Sea during that time were similar to the last interglacial climate (Waldmann et al., 2009). In the deep core, however, Lisan-type sediments, i.e. *aad* facies typical for lake high-stands during glacials, were identified (Chapter 3). Based on micro-facies and further sedimentological and geochemical analyses, it

could be shown that (1) two dry intervals, at ~110-108 ± 5 ka and ~93-87 ± 7 ka, coincide with stadial conditions in the North Atlantic and central Mediterranean regions and that (2) two more humid intervals in the Levant, at ~108-93 ± 6 ka and ~87-75 ± 7 ka, correspond to interstadial conditions in Greenland and the central Mediterranean as well as to sapropels S4 and S3 in the Mediterranean Sea. This apparently suggests a close link between climate in the Levant and the Atlantic-Mediterranean system during the time, when northern hemisphere ice sheets built up.

In conclusion, the millennial- and centennial-scale dry periods detected during the early last glacial period and the late Holocene (Chapters 3 and 4) are all related to colder climate conditions in the North Atlantic region. However, other trigger mechanisms, like the major reorganisation of the atmospheric circulation during the last glacial-interglacial transition, can cause salt deposition in the Dead Sea basin as well. Further high-resolution analyses are needed to fully understand the complexity of climate variations leading to drought in the Dead Sea region. Regarding this, the two case studies presented in this thesis are considered to be only a first, important step.

(b) Contribution of this work in a broader scientific context

Micro-facies analyses of varved lake sediments are a powerful tool to better understand past abrupt climate changes and changing frequencies of extreme events down to seasonal resolutions (Brauer et al., 2009). Varved sediment records are, however, relatively scarce in the Mediterranean region or these records are too short in time to establish long time series of climate variability. Some varve chronologies exist exclusively from the northern Mediterranean realm, i.e. from Spain (e.g. Martin-Puertas et al., 2009; Corella et al., 2011), Italy (e.g. Brauer et al., 2008; Martin-Puertas et al., 2014), Albania (Ariztegui et al., 2010), Greece (Koutsodendris et al., 2015) and Turkey (e.g. Landmann et al., 1996; Ojala et al., 2012 and references therein). The Dead Sea is the only record from the Levantine region that is known to comprise long sequences of varved sediments, making it a unique archive that allows deciphering even small-scale climatic changes in this particularly climate-sensitive region. Earlier studies of the varved sequences from the Holocene Dead Sea (Migowski et al., 2004) and the last glacial Lake Lisan (Prasad et al., 2004) did, however, not fully exploit this great potential. This doctoral thesis is the first attempt using a combined approach of microscopic thin section and high-resolution μXRF analyses for the various sediment facies of the Dead Sea. This allowed (1) a comprehensive understanding of depositional processes in the basin and its underlying climatic conditions and (2) the establishment of micro-facies analyses as a standard technique for reconstructing climate from the Dead Sea record.

The Dead Sea basin is a natural laboratory for all kind of geoscientific research, for which the new sediment core 5017-1 from the deep Dead Sea basin obtained within the frame of the ICDP Dead Sea Deep Drilling Project provides the fundament for forthcoming palaeostudies. Therefore, the lithostratigraphic framework for the ~220 ka comprising sediment core, which was developed within this doctoral project, is considered to be an important basis for the entire scientific community dealing with the sediment record of the Dead Sea. Moreover, this work is

one step forward to establish the Dead Sea sediment record as a key archive for climate reconstruction in the eastern Mediterranean region and with supra-regional significance.

5.2 Future perspectives

The Dead Sea sediment record offers various possibilities for further high-resolution studies as well as for testing specific methodological approaches. Ongoing work with the participation of the doctoral candidate is outlined in the following:

Micro-facies of salt

The massive and thick halite sequences of the deep-basin core 5017-1 are characteristic for exceptionally dry periods during the last interglacial and the Holocene and allow, for the first time, studying intervals when the lake level was lower than today and climate was drier. Especially, the layered halite facies (*lh*) is in focus of investigations, as its sedimentation pattern is potentially of annual nature (Chapter 2.6.1). The two-layer *lh* facies-type, which consists of alternating whitish fine-grained halite layers and thin detrital marl laminae (Fig. 2-3), is analysed in more detail. Preliminary results of micro-facies and statistical analyses indicate that this facies-type is likely varved and suggest that annual deposition cyclicity might be controlled by a 7.5-year cycle in the North Atlantic (Palchan, Neugebauer et al., in prep. for *Quaternary Research*).

Calibration of µXRF data

This doctoral study demonstrates that µXRF element scanning is a valuable tool to decipher the chemical characteristics of the Dead Sea sediments (Chapter 2). In particular, element ratios are useful as proxies for the different micro-facies types and, when several ratios are combined, for changes in the water balance of the lake (Chapters 3 and 4). However, µXRF data are expressed as element intensities, which provide at best semi-quantitative information and a conversion to element concentrations is problematic (Weltje and Tjallingii, 2008). To allow for a better quantification of, for example, mass-balance or fluxes, the log-ratio calibration model approach developed by Weltje and Tjallingii (2008) will be applied for the available µXRF data of the Dead Sea sediments (Tjallingii, Neugebauer et al., forthcoming). Calibration will be performed by conventional XRF measurements. This approach might enable calibrating also the continuous, but low-resolution XRF data of core 5017-1 that were measured with a very low measuring time of only 1 second per step. If being successful, a unique geochemical dataset could be provided for the 220 thousand years spanning core 5017-1.

Petrographic analyses of gravels in the deep 5017-1 core

The unexpected occurrence of a pure gravel layer in the deep Dead Sea basin led to the hypothesis that these gravels were likely deposited through a mass waste event because similar

gravels have been identified in the basal parts of slump deposits in core 5017-1 (Chapter 3). These gravels are subject of more detailed petrographic analyses to document their occurrence and to identify possible sources and transport mechanisms (Schwab, Neugebauer et al., in prep. for *Sedimentology*).

Stable oxygen isotopes of aragonite

Stable oxygen isotopes of authigenic aragonite deposited in the Dead Sea have been suggested to be influenced by rainfall and show relatively stable and heavier values of ~4-6‰ for the last glacial Lisan, whereas values of the relatively drier Holocene are lighter, ranging between ~2 and 4‰ (Kolodny et al., 2005). To investigate, whether also small-scale changes in humidity are reflected in $\delta^{18}O$ of aragonite, a total of 245 single aragonite layers were sampled from a ca 2000 years spanning late Holocene interval of core 5017-1, where centennial-scale dry periods were recognised (Chapter 4). In addition to micro-facies analyses, this approach has a great potential to add an independent high-resolution proxy for deciphering small-scale climatic changes. Details about the method and preliminary results are provided in the Appendix A1.

Radiocarbon dating and precise Holocene chronology

The Holocene chronology of core DSEn from the western margin of the Dead Sea has been established by Migowski (2001) based on radiocarbon dating of 20 terrestrial plant remains. Within this doctoral project, the DSEn composite profile has been slightly modified and the age model was improved (Chapter 4; Appendix A2). The composite profile of the deep-basin core 5017-1 has been established as part of this work (Chapter 2.5.2) and provides the base for developing a precise Holocene chronology for this core (Kitagawa, Stein et al., in prep.). Combining the lithological and chronological information of both cores DSEn and 5017-1 will improve existing lake level reconstructions (summarised in Bookman et al., 2006) and allow a better understanding of the Holocene climate variability in the Levant.

Last glacial-interglacial transition

As a response to changed atmospheric circulation patterns during the demise of the last glacial period when continental ice sheets started to decay, Lake Lisan retreated from its maximum level of ~160 m below mean sea level (bmsl) during the last glacial maximum at ~27-24 ka BP to unknown low levels below ~420 m bmsl during the lateglacial at around 13 ka BP and during the early Holocene at ~11-10 ka BP (e.g. Stein et al., 2010). This long-term lake level decrease occurred in several steps of alternating short-term lake level drops and recovering intervals. Thereby, two pronounced lake level drops occurred at ~17-16.5 ka BP and at ~14.5 ka BP, leading to the deposition of thick gypsum layers in the basin and at the margins of the lake (e.g. Torfstein et al., 2008; 2013b). The further expression of lateglacial climate variability in the Dead Sea region from ca 14.5 to 11 ka BP is still a matter of debate because respective sediments are mostly not exposed at the margins. This interval can now be studied in the deep-basin core 5017-1. Within this doctoral work, the uppermost unit (~100-88 m below lake floor) of the deep-core

Lisan Formation was continuously measured for μXRF and 111 thin sections were prepared. This study, which is subject of ongoing work (Neugebauer et al., forthcoming), will enhance our understanding of lateglacial climate variability in the Dead Sea region. Preliminary results are presented in the Appendix A3.

Early Holocene humid period

The early Holocene period is of particular interest for palaeoclimatic studies in the eastern Mediterranean (EM) region. During that time at around 9 ka BP a maximum of northern hemisphere summer insolation forced a northward shift of the ITCZ and a strengthening of the African summer monsoon system, known as the early Holocene African Humid Period (e.g. deMenocal et al., 2000; Renssen et al., 2003). For the same time, several studies of marine, lake and speleothem records suggest more humid climate conditions also in the EM (e.g. Bar-Matthews et al., 2000; Arz et al., 2003; Roberts et al., 2008; Verheyden et al., 2008). To date, it is, however, not clear whether the source for enhanced moisture in the EM during the early Holocene was intensified Mediterranean winter precipitation, the low-latitude Afro-Asian summer monsoons or even a local Mediterranean summer monsoon (see Kutzbach et al., 2014 and references therein). From the Dead Sea sedimentary record there was so far no striking evidence for an outstanding, pronounced humid climate during that time, although Migowski et al. (2006) inferred a major humid phase for the period from ~10 to 8.6 ka BP from their lake level reconstruction. They suggest, however, a similarly major humid phase during the late Holocene, which contradicts with other records from the EM, for which a long-term drying trend was proposed for the last 7 kyr from the middle to late Holocene (e.g. Roberts et al., 2011a). Preliminary results of stable isotope and lipid biomarker analyses of the deep-basin 5017-1 core provide some first hint for humid conditions during the early Holocene, which led to unprecedented increase in microbial activity (Thomas, Levy, Antler, Neugebauer et al., in prep.). Additional and higher resolution analyses are needed to confirm these first results. Another promising approach will be done by regional comparison of the Dead Sea record to the early Holocene palaeolake record of the Tayma Oasis, NW Saudi Arabia (Engel et al., 2012). The latter contains a ca 1000 year sequence of aragonite varves that are subject of seasonal-resolution stable isotope measurements (Plessen et al., in prep.) and micro-facies analyses (Neugebauer, Plessen et al., forthcoming).

The above described perspectives of further high-resolution analyses and approaches to better understand the past climate variability in the Dead Sea region are far from being exhaustive. However, future investigations will benefit from the profound characterisation and climatic interpretation of the various sedimentary facies of the Dead Sea sediments provided within this thesis.

Bibliography

Abu Ghazleh, S., Hartmann, J., Jansen, N. and Kempe, S., 2009. Water input requirements of the rapidly shrinking Dead Sea. Naturwissenschaften 96, 637-643.

Abu Ghazleh, S. and Kempe, S., 2009. Geomorphology of Lake Lisan terraces along the eastern coast of the Dead Sea, Jordan. Geomorphology 108, 246-263.

Agnon, A., Migowski, C. and Marco, S., 2006. Intraclast breccias in laminated sequences reviewed: Recorders of paleo-earthquakes. Geological Society of America Special Papers 401, 195-214.

Allen, J.R.M., Watts, W.A. and Huntley, B., 2000. Weichselian palynostratigraphy, palaeovegetation and palaeoenvironment; the record from Lago Grande di Monticchio, southern Italy. Quaternary International 73–74, 91-110.

Almogi-Labin, A., Bar-Matthews, M., Shriki, D., Kolosovsky, E., Paterne, M., Schilman, B., Ayalon, A., Aizenshtat, Z. and Matthews, A., 2009. Climatic variability during the last ~90 ka of the southern and northern Levantine Basin as evident from marine records and speleothems. Quaternary Science Reviews 28, 2882-2896.

Alpert, P., Osetinsky, I., Ziv, B. and Shafir, H., 2004. Semi-objective classification for daily synoptic systems: Application to the Eastern Mediterranean climate change. International Journal of Climatology 24, 1001-1011.

Ariztegui, D., Asioli, A., Lowe, J.J., Trincardi, F., Vigliotti, L., Tamburini, F., Chondrogianni, C., Accorsi, C.A., Bandini Mazzanti, M., Mercuri, A.M., Van der Kaars, S., McKenzie, J.A. and Oldfield, F., 2000. Palaeoclimate and the formation of sapropel S1: inferences from Late Quaternary lacustrine and marine sequences in the central Mediterranean region. Palaeogeography, Palaeoclimatology, Palaeoecology 158, 215-240.

Ariztegui, D., Anselmetti, F.S., Robbiani, J.M., Bernasconi, S.M., Brati, E., Gilli, A. and Lehmann, M.F., 2010. Natural and human-induced environmental change in southern Albania for the last 300 years — Constraints from the Lake Butrint sedimentary record. Global and Planetary Change 71, 183-192.

Arz, H.W., Lamy, F., Pätzold, J., Müller, P.J. and Prins, M., 2003. Mediterranean Moisture Source for an Early-Holocene Humid Period in the Northern Red Sea. Science 300, 118-121.

Bar-Matthews, M., Ayalon, A. and Kaufman, A., 1997. Late Quaternary Paleoclimate in the Eastern Mediterranean Region from Stable Isotope Analysis of Speleothems at Soreq Cave, Israel. Quaternary Research 47, 155-168.

Bar-Matthews, M., Ayalon, A., Kaufman, A. and Wasserburg, G.J., 1999. The Eastern Mediterranean paleoclimate as a reflection of regional events: Soreq cave, Israel. Earth and Planetary Science Letters 166, 85-95.

Bar-Matthews, M., Ayalon, A. and Kaufman, A., 2000. Timing and hydrological conditions of Sapropel events in the Eastern Mediterranean, as evident from speleothems, Soreq cave, Israel. Chemical Geology 169, 145-156.

Bar-Matthews, M., Ayalon, A., Gilmour, M., Matthews, A. and Hawkesworth, C.J., 2003. Sea–land oxygen isotopic relationships from planktonic foraminifera and speleothems in the Eastern Mediterranean region and their implication for paleorainfall during interglacial intervals. Geochimica et Cosmochimica Acta 67, 3181-3199.

Bar-Matthews, M. and Ayalon, A., 2004. Speleothems as palaeoclimate indicators, a case study from Soreq Cave located in the Eastern Mediterranean Region, Israel, In: Battarbee, R.,

Gasse, F., Stickley, C. (Eds.), Past Climate Variability through Europe and Africa. Springer Netherlands, pp. 363-391.
Bard, E., Hamelin, B., Fairbanks, R.G. and Zindler, A., 1990. Calibration of the ^{14}C timescale over the past 30,000 years using mass spectrometric U-Th ages from Barbados corals. Nature 345, 405-410.
Bard, E., Jouannic, C., Hamelin, B., Pirazzoli, P., Arnold, M., Faure, G., Sumosusastro, P. and Syaefudin, 1996. Pleistocene sea levels and tectonic uplift based on dating of corals from Sumba Island, Indonesia. Geophysical Research Letters 23, 1473-1476.
Bartov, Y., Stein, M., Enzel, Y., Agnon, A. and Reches, Z., 2002. Lake Levels and Sequence Stratigraphy of Lake Lisan, the Late Pleistocene Precursor of the Dead Sea. Quaternary Research 57, 9-21.
Bartov, Y., Goldstein, S.L., Stein, M. and Enzel, Y., 2003. Catastrophic arid episodes in the Eastern Mediterranean linked with the North Atlantic Heinrich events. Geology 31, 439-442.
Bartov, Y., Enzel, Y., Porat, N. and Stein, M., 2007. Evolution of the Late Pleistocene–Holocene Dead Sea Basin from Sequence Statigraphy of Fan Deltas and Lake-Level Reconstruction. Journal of Sedimentary Research 77, 680-692.
Begin, Z.B., Ehrlich, A. and Nathan, Y., 1974. Lake Lisan -The Pleistocene precursor of the Dead Sea. Geological Survey of Israel Bulletin 63.
Belmaker, R., Lazar, B., Stein, M. and Beer, J., 2011. Short residence time and fast transport of fine detritus in the Judean Desert: Clues from ^{7}Be in settled dust. Geophysical Research Letters 38, L16714.
Belmaker, R., Lazar, B., Beer, J., Christl, M., Tepelyakov, N. and Stein, M., 2013. ^{10}Be dating of Neogene halite. Geochimica et Cosmochimica Acta 122, 418-429.
Ben-Avraham, Z., Niemi, T.M., Heim, C., Negendank, J. and Nur, A., 1999. Holocene stratigraphy of the Dead Sea: Correlation of high-resolution seismic reflection profiles to sediment cores. Journal of Geophysical Research: Solid Earth 104, 17617-17625.
Ben Tiba, B. and Reille, M., 1982. Recherches pollenanalytiques dans les montagnes de Kroumirie (Tunisie septentrionale), premiers resultats. Ecologia Mediterranea 7, 75-86.
Bentor, Y.K., 1961. Some geochemical aspects of the Dead Sea and the question of its age. Geochimica et Cosmochimica Acta 25, 239-260.
Bentor, Y.K., 1969. On the evolution of subsurface brines in Israel. Chemical Geology 4, 83-110.
Björck, S., Walker, M.J.C., Cwynar, L.C., Johnsen, S., Knudsen, K.-L., Lowe, J.J. and Wohlfarth, B., 1998. An event stratigraphy for the Last Termination in the North Atlantic region based on the Greenland ice-core record: a proposal by the INTIMATE group. Journal of Quaternary Science 13, 283-292.
Bond, G., Kromer, B., Beer, J., Muscheler, R., Evans, M.N., Showers, W., Hoffmann, S., Lotti-Bond, R., Hajdas, I. and Bonani, G., 2001. Persistent Solar Influence on North Atlantic Climate During the Holocene. Science 294, 2130-2136.
Bookman (Ken-Tor), R., Enzel, Y., Agnon, A. and Stein, M., 2004. Late Holocene lake levels of the Dead Sea. Geological Society of America Bulletin 116, 555-571.
Bookman, R., Bartov, Y., Enzel, Y. and Stein, M., 2006. Quaternary lake levels in the Dead Sea basin: Two centuries of research. Geological Society of America Special Papers 401, 155-170.
Brauer, A., Endres, C., Günter, C., Litt, T., Stebich, M. and Negendank, J.F.W., 1999a. High resolution sediment and vegetation responses to Younger Dryas climate change in varved

lake sediments from Meerfelder Maar, Germany. Quaternary Science Reviews 18, 321-329.

Brauer, A., Endres, C. and Negendank, J.F.W., 1999b. Lateglacial calendar year chronology based on annually laminated sediments from Lake Meerfelder Maar, Germany. Quaternary International 61, 17-25.

Brauer, A. and Casanova, J., 2001. Chronology and depositional processes of the laminated sediment record from Lac d'Annecy, French Alps. Journal of Paleolimnology 25, 163-177.

Brauer, A., Allen, J.R.M., Mingram, J., Dulski, P., Wulf, S. and Huntley, B., 2007. Evidence for last interglacial chronology and environmental change from Southern Europe. Proceedings of the National Academy of Sciences 104, 450-455.

Brauer, A., Mangili, C., Moscariello, A. and Witt, A., 2008. Palaeoclimatic implications from micro-facies data of a 5900 varve time series from the Piànico interglacial sediment record, southern Alps. Palaeogeography, Palaeoclimatology, Palaeoecology 259, 121-135.

Brauer, A., Dulski, P., Mangili, C., Mingram, J. and Liu, J., 2009. The potential of varves in high-resolution paleolimnological studies. PAGES news 17 (3), 96-98.

Briffa, K.R., Osborn, T.J. and Schweingruber, F.H., 2004. Large-scale temperature inferences from tree rings: a review. Global and Planetary Change 40, 11-26.

Bronk Ramsey, C., 2008. Deposition models for chronological records. Quaternary Science Reviews 27, 42-60.

Bronk Ramsey, C., 2009. Bayesian analysis of radiocarbon dates. Radiocarbon 51(1), 337-360.

Brown, S.L., Bierman, P.R., Lini, A. and Southon, J., 2000. 10 000 yr record of extreme hydrologic events. Geology 28, 335-338.

Chapman, M.R. and Shackleton, N.J., 1999. Global ice-volume fluctuations, North Atlantic ice-rafting events, and deep-ocean circulation changes between 130 and 70 ka. Geology 27, 795-798.

Chapman, M.R., Shackleton, N.J. and Duplessy, J.-C., 2000. Sea surface temperature variability during the last glacial–interglacial cycle: assessing the magnitude and pattern of climate change in the North Atlantic. Palaeogeography, Palaeoclimatology, Palaeoecology 157, 1-25.

Cheddadi, R. and Rossignol-Strick, M., 1995. Eastern Mediterranean Quaternary paleoclimates from pollen and isotope records of marine cores in the Nile Cone Area. Paleoceanography 10, 291-300.

Cheddadi, R., Lamb, H.F., Guiot, J. and van der Kaars, S., 1998. Holocene climatic change in Morocco: a quantitative reconstruction from pollen data. Climate Dynamics 14, 883-890.

Coianiz, L., Ben-Avraham, Z. and Lazar, M., 2013. Structural and stratigraphy evolution of the Dead Sea Lake: Insights in an active strike-slip basin, Israel Geological Society Annual Meeting, Akko.

Cook, E.R., D'Arrigo, R.D. and Briffa, K.R., 1998. A reconstruction of the North Atlantic Oscillation using tree-ring chronologies from North America and Europe. The Holocene 8, 9-17.

Corella, J., Moreno, A., Morellón, M., Rull, V., Giralt, S., Rico, M., Pérez-Sanz, A. and Valero-Garcés, B., 2011. Climate and human impact on a meromictic lake during the last 6,000 years (Montcortès Lake, Central Pyrenees, Spain). Journal of Paleolimnology 46, 351-367.

Croudace, I.W., Rindby, A. and Rothwell, R.G., 2006. ITRAX: description and evaluation of a new multi-function X-ray core scanner. Geological Society, London, Special Publications 267, 51-63.

Czymzik, M., Brauer, A., Dulski, P., Plessen, B., Naumann, R., von Grafenstein, U. and Scheffler, R., 2013. Orbital and solar forcing of shifts in Mid- to Late Holocene flood intensity from varved sediments of pre-alpine Lake Ammersee (southern Germany). Quaternary Science Reviews 61, 96-110.

Danin, A., 1988. Flora and vegetation of Israel and adjacent areas, In: Yom Tov, Y., Tchernov, E. (Ed.), The Zoogeography of Israel. Dr. W. Junk Publishers, Dordrecht-Boston-Lancaster, pp. 129-159.

Dayan, U. and Morin, E., 2006. Flash flood-producing rainstorms over the Dead Sea: A review. Geological Society of America Special Paper 401, 53-62.

Dayan, U., Ziv, B., Shoob, T. and Enzel, Y., 2008. Suspended dust over southeastern Mediterranean and its relation to atmospheric circulations. International Journal of Climatology 28, 915-924.

de Vries, A.J., Tyrlis, E., Edry, D., Krichak, S.O., Steil, B. and Lelieveld, J., 2013. Extreme precipitation events in the Middle East: Dynamics of the Active Red Sea Trough. Journal of Geophysical Research: Atmospheres 118, 7087-7108.

deMenocal, P., Ortiz, J., Guilderson, T., Adkins, J., Sarnthein, M., Baker, L. and Yarusinsky, M., 2000. Abrupt onset and termination of the African Humid Period: rapid climate responses to gradual insolation forcing. Quaternary Science Reviews 19, 347-361.

Desprat, S., Combourieu-Nebout, N., Essallami, L., Sicre, M.A., Dormoy, I., Peyron, O., Siani, G., Bout Roumazeilles, V. and Turon, J.L., 2013. Deglacial and Holocene vegetation and climatic changes in the southern Central Mediterranean from a direct land–sea correlation. Clim. Past 9, 767-787.

Develle, A.L., Gasse, F., Vidal, L., Williamson, D., Demory, F., Van Campo, E., Ghaleb, B. and Thouveny, N., 2011. A 250 ka sedimentary record from a small karstic lake in the Northern Levant (Yammoûneh, Lebanon): Paleoclimatic implications. Palaeogeography, Palaeoclimatology, Palaeoecology 305, 10-27.

Dulski, P., Brauer, A. and Mangili, C., in press. Combined μ-XRF and microfacies techniques for lake sediment analyses, In: Rothwell, G., Croudace, I.W. (Eds.), Developments in Paleoenvironmental Research. Springer.

El-Moslimany, A.P., 1990. Ecological significance of common nonarboreal pollen: examples from drylands of the Middle East. Review of Palaeobotany and Palynology 64, 343-350.

Engel, M., Brückner, H., Pint, A., Wellbrock, K., Ginau, A., Voss, P., Grottker, M., Klasen, N. and Frenzel, P., 2012. The early Holocene humid period in NW Saudi Arabia – Sediments, microfossils and palaeo-hydrological modelling. Quaternary International 266, 131-141.

Enzel, Y., Kadan, G. and Eyal, Y., 2000. Holocene Earthquakes Inferred from a Fan-Delta Sequence in the Dead Sea Graben. Quaternary Research 53, 34-48.

Enzel, Y., Bookman, R., Sharon, D., Gvirtzman, H., Dayan, U., Ziv, B. and Stein, M., 2003. Late Holocene climates of the Near East deduced from Dead Sea level variations and modern regional winter rainfall. Quaternary Research 60, 263-273.

Enzel, Y., Agnon, A. and Stein, M., 2006. New Frontiers in Dead Sea Paleoenvironmental Research. Geological Society of America Special Paper 401, p. 253.

Enzel, Y., Amit, R., Dayan, U., Crouvi, O., Kahana, R., Ziv, B. and Sharon, D., 2008. The climatic and physiographic controls of the eastern Mediterranean over the late Pleistocene

climates in the southern Levant and its neighboring deserts. Global and Planetary Change 60, 165-192.

EPICA Community Members, 2004. Eight glacial cycles from an Antarctic ice core. Nature 429, 623-628.

EPICA Community Members, 2006. One-to-one coupling of glacial climate variability in Greenland and Antarctica. Nature 444, 195-198.

Esper, J., Cook, E.R. and Schweingruber, F.H., 2002. Low-Frequency Signals in Long Tree-Ring Chronologies for Reconstructing Past Temperature Variability. Science 295, 2250-2253.

Faegri, K. and Iversen, J., 1989. Textbook of Pollen Analysis, 4th ed. J Wiley, Chichester.

Fairbanks, R.G., 1989. A 17,000-year glacio-eustatic sea level record: influence of glacial melting rates on the Younger Dryas event and deep-ocean circulation. Nature 342, 637-642.

Finné, M., Holmgren, K., Sundqvist, H.S., Weiberg, E. and Lindblom, M., 2011. Climate in the eastern Mediterranean, and adjacent regions, during the past 6000 years – A review. Journal of Archaeological Science 38, 3153-3173.

Fleitmann, D., Burns, S.J., Mudelsee, M., Neff, U., Kramers, J., Mangini, A. and Matter, A., 2003. Holocene Forcing of the Indian Monsoon Recorded in a Stalagmite from Southern Oman. Science 300, 1737-1739.

Frank, U., Nowaczyk, N.R. and Negendank, J.F.W., 2007a. Palaeomagnetism of greigite bearing sediments from the Dead Sea, Israel. Geophysical Journal International 168, 904-920.

Frank, U., Nowaczyk, N.R. and Negendank, J.F.W., 2007b. Rock magnetism of greigite bearing sediments from the Dead Sea, Israel. Geophysical Journal International 168, 921-934.

Fronval, T., Jansen, E., Haflidason, H. and Sejrup, H.P., 1998. Variability in surface and deep water conditions in the nordic seas during the last interglacial period. Quaternary Science Reviews 17, 963-985.

Garber, R., Levy, Y. and Friedman, G., 1987. The sedimentology of the Dead Sea. Carbonates and Evaporites 2, 43-57.

Garfunkel, Z., Zak, I. and Freund, R., 1981. Active faulting in the dead sea rift. Tectonophysics 80, 1-26.

Garfunkel, Z. and Ben-Avraham, Z., 1996. The structure of the Dead Sea basin. Tectonophysics 266, 155-176.

Garfunkel, Z., Ben-Avraham, Z. and Kagan, E., 2014. Dead Sea Transform Fault System: Reviews. Springer, Dordrecht.

Gasse, F., Vidal, L., Van Campo, E., Demory, F., Develle, A.-L., Tachikawa, K., Elias, A., Bard, E., Garcia, M., Sonzogni, C. and Thouveny, N., 2015. Hydroclimatic changes in northern Levant over the past 400,000 years. Quaternary Science Reviews 111, 1-8.

Gertman, I. and Hecht, A., 2002. The Dead Sea hydrography from 1992 to 2000. Journal of Marine Systems 35, 169-181.

Goldstein, S.L., Stein, M., Ben-Avraham, Z., Agnon, A., Ariztegui, D., Brauer, A., Haug, G., Ito, E., Kitagawa, H. and Torfstein, A., 2012. The ICDP Dead Sea deep drill cores: records of climate change and tectonics in the Levant, American Geophysical Union, Fall Meeting, abstract #PP31D-03, San Francisco, Calif.

Greenbaum, N., Ben-Zvi, A., Haviv, I. and Enzel, Y., 2006. The hydrology and paleohydrology of the Dead Sea tributaries. Geological Society of America Special Papers 401, 63-93.

Haase-Schramm, A., Goldstein, S.L. and Stein, M., 2004. U-Th dating of Lake Lisan (late Pleistocene Dead Sea) aragonite and implications for glacial east Mediterranean climate change. Geochimica et Cosmochimica Acta 68, 985-1005.

Hadzhiivanova, E., Waldmann, N., Bookman, R., Neugebauer, I., Brauer, A., Schwab, M.J., Dulski, P., Frank, U. and the DSDDP Scientific Party, 2013. Understanding depositional processes of terrigenous sediments from flash-floods and mass-wasting events in the Dead Sea, Israel Geological Society Annual Meeting, Akko.

Haliva-Cohen, A., Stein, M., Goldstein, S.L., Sandler, A. and Starinsky, A., 2012. Sources and transport routes of fine detritus material to the Late Quaternary Dead Sea basin. Quaternary Science Reviews 50, 55-70.

Hall, J.K., 1997. Topography and bathymetry of the Dead Sea depression, In: Niemi, T.M., Ben-Avraham, Z., Gat, J.R. (Eds.), The Dead Sea: The Lake and Its Setting. Oxford University Press, Oxford, pp. 11-21.

Heim, C., Nowaczyk, N.R., Negendank, J.F.W., Leroy, S.A.G. and Ben-Avraham, Z., 1997. Near East Desertification: Evidence from the Dead Sea. Naturwissenschaften 84, 398-401.

Heimann, A., Steinitz, G., Mor, D. and Shaliv, G., 1996. The Cover Basalt Formation, its age and its regional and tectonic setting: Implications from K–Ar and $^{40}Ar/^{39}Ar$ geochronology. Israel Journal of Earth Sciences 45, 55-71.

Herzschuh, U., 2007. Reliability of pollen ratios for environmental reconstructions on the Tibetan Plateau. Journal of Biogeography 34, 1265-1273.

Höbig, N., Weber, M.E., Kehl, M., Weniger, G.-C., Julià, R., Melles, M., Fülöp, R.-H., Vogel, H. and Reicherter, K., 2012. Lake Banyoles (northeastern Spain): A Last Glacial to Holocene multi-proxy study with regard to environmental variability and human occupation. Quaternary International 274, 205-218.

Hoerling, M., Eischeid, J., Perlwitz, J., Quan, X., Zhang, T. and Pegion, P., 2011. On the Increased Frequency of Mediterranean Drought. Journal of Climate 25, 2146-2161.

Holzhauser, H., Magny, M. and Zumbühl, H.J., 2005. Glacier and lake-level variations in west-central Europe over the last 3500 years. The Holocene 15, 789-801.

Ineson, S., Scaife, A.A., Knight, J.R., Manners, J.C., Dunstone, N.J., Gray, L.J. and Haigh, J.D., 2011. Solar forcing of winter climate variability in the Northern Hemisphere. Nature Geosci 4, 753-757.

IPCC, 2012. Managing the Risks of Extreme Events and Disasters to Advance Climate Change Adaptation, In: Field, C.B., Barros, V., Stocker, T.F., Qin, D., Dokken, D.J., Ebi, K.L., Mastrandrea, M.D., Mach, K.J., Plattner, G.-K., Allen, S.K., Tignor, M., Midgley, P.M. (Eds.), A Special Report of Working Groups I and II of the Intergovernmental Panel on Climate Change. Cambridge University Press, Cambridge, UK, and New York, NY, USA, p. 582.

Johnsen, S.J., Clausen, H.B., Dansgaard, W., Fuhrer, K., Gundestrup, N., Hammer, C.U., Iversen, P., Jouzel, J., Stauffer, B. and steffensen, J.P., 1992. Irregular glacial interstadials recorded in a new Greenland ice core. Nature 359, 311-313.

Kagan, E., Langgut, D., Boaretto, E., Neumann, F.H. and Stein, M., in press. Dead Sea levels during the Bronze and Iron Ages. Radiocarbon Special Issue.

Kagan, E.J. and Marco, S., 2013. Seismically triggered mass movement events from the Dead Sea depocentre, International Workshop "Tectonics of the Levant fault and Northern Red Sea", IPG Paris.

Kahana, R., Ziv, B., Enzel, Y. and Dayan, U., 2002. Synoptic climatology of major floods in the Negev Desert, Israel. International Journal of Climatology 22, 867-882.

Kaniewski, D., Van Campo, E., Guiot, J., Le Burel, S., Otto, T. and Baeteman, C., 2013. Environmental Roots of the Late Bronze Age Crisis. PLoS ONE 8, e71004.

Katz, A., Kolodny, Y. and Nissenbaum, A., 1977. The geochemical evolution of the Pleistocene Lake Lisan-Dead Sea system. Geochimica et Cosmochimica Acta 41, 1609-1626.

Katz, A. and Starinsky, A., 2009. Geochemical History of the Dead Sea. Aquatic Geochemistry 15, 159-194.

Kaufman, A., 1971. U-Series dating of Dead Sea Basin carbonates. Geochimica et Cosmochimica Acta 35, 1269-1281.

Kaufman, A., Yechieli, Y. and Gardosh, M., 1992. Reevaluation of the lake-sediment chronology in the Dead Sea basin, Israel, based on new ^{230}Th/U dates. Quaternary Research 38, 292-304.

Kaufman, A., 1993. An evaluation of several methods for determining ^{230}Th/U ages in impure carbonates. Geochimica et Cosmochimica Acta 57, 2303-2317.

Ken-Tor, R., Agnon, A., Enzel, Y., Stein, M., Marco, S. and Negendank, J.F.W., 2001. High-resolution geological record of historic earthquakes in the Dead Sea basin. Journal of Geophysical Research 106, 2221-2234.

Kiro, Y., Weinstein, Y., Starinsky, A. and Yechieli, Y., 2014. The extent of seawater circulation in the aquifer and its role in elemental mass balances: A lesson from the Dead Sea. Earth and Planetary Science Letters 394, 146-158.

Kolodny, Y., Stein, M. and Machlus, M., 2005. Sea-rain-lake relation in the Last Glacial East Mediterranean revealed by δ^{18}O-δ^{13}C in Lake Lisan aragonites. Geochimica et Cosmochimica Acta 69, 4045-4060.

Koutsodendris, A., Brauer, A., Zacharias, I., Putyrskaya, V., Klemt, E., Sangiorgi, F. and Pross, J., 2015. Ecosystem response to human- and climate-induced environmental stress on an anoxic coastal lagoon (Etoliko, Greece) since 1930 AD. Journal of Paleolimnology, 1-16.

Kroonenberg, S.B., Abdurakhmanov, G.M., Badyukova, E.N., van der Borg, K., Kalashnikov, A., Kasimov, N.S., Rychagov, G.I., Svitoch, A.A., Vonhof, H.B. and Wesselingh, F.P., 2007. Solar-forced 2600 BP and Little Ice Age highstands of the Caspian Sea. Quaternary International 173–174, 137-143.

Krumgalz, B.S., Hecht, A., Starinsky, A. and Katz, A., 2000. Thermodynamic constraints on Dead Sea evaporation: can the Dead Sea dry up? Chemical Geology 165, 1-11.

Kushnir, Y. and Stein, M., 2010. North Atlantic influence on 19th-20th century rainfall in the Dead Sea watershed, teleconnections with the Sahel, and implication for Holocene climate fluctuations. Quaternary Science Reviews 29, 3843-3860.

Kutzbach, J.E., Chen, G., Cheng, H., Edwards, R.L. and Liu, Z., 2014. Potential role of winter rainfall in explaining increased moisture in the Mediterranean and Middle East during periods of maximum orbitally-forced insolation seasonality. Climate Dynamics 42, 1079-1095.

Lamb, H.F. and van der Kaars, S., 1995. Vegetational response to Holocene climatic change: pollen and palaeolimnological data from the Middle Atlas, Morocco. The Holocene 5, 400-408.

Lamy, F., Arz, H.W., Bond, G.C., Bahr, A. and Pätzold, J., 2006. Multicentennial-scale hydrological changes in the Black Sea and northern Red Sea during the Holocene and the Arctic/North Atlantic Oscillation. Paleoceanography 21, PA1008.

Landmann, G., Reimer, A., Lemcke, G. and Kempe, S., 1996. Dating Late Glacial abrupt climate changes in the 14,570 yr long continuous varve record of Lake Van, Turkey. Palaeogeography, Palaeoclimatology, Palaeoecology 122, 107-118.

Landmann, G., Abu Qudaira, G.M., Shawabkeh, K., Wrede, V. and Kempe, S., 2002. Geochemistry of the Lisan and Damya Formations in Jordan, and implications for palaeoclimate. Quaternary International 89, 45-57.

Langgut, D., Almogi-Labin, A., Bar-Matthews, M. and Weinstein-Evron, M., 2011. Vegetation and climate changes in the South Eastern Mediterranean during the Last Glacial-Interglacial cycle (86 ka): new marine pollen record. Quaternary Science Reviews 30, 3960-3972.

Langgut, D., Neumann, F.H., Stein, M., Wagner, A., Kagan, E.J., Boaretto, E. and Finkelstein, I., 2014. Dead Sea pollen record and history of human activity in the Judean Highlands (Israel) from the Intermediate Bronze into the Iron Ages (~2500–500 BCE). Palynology, 1-23.

Laskar, J., Robutel, P., Joutel, F., Gastineau, M., Correia, A.C.M. and Levrard, B., 2004. A long-term numerical solution for the insolation quantities of the Earth. Astronomy & Astrophysics 428, 261-285.

Lazar, B., Sivan, O., Yechieli, Y., Levy, E.J., Antler, G., Gavrieli, I. and Stein, M., 2014. Long-term freshening of the Dead Sea brine revealed by porewater Cl^- and $\delta^{18}O$ in ICDP Dead Sea deep-drill. Earth and Planetary Science Letters 400, 94-101.

Lensky, N.G., Dvorkin, Y., Lyakhovsky, V., Gertman, I. and Gavrieli, I., 2005. Water, salt, and energy balances of the Dead Sea. Water Resources Research 41, W12418.

Leroy, S.A.G., 2010. Pollen analysis of core DS7-1SC (Dead Sea) showing intertwined effects of climatic change and human activities in the Late Holocene. Journal of Archaeological Science 37, 306-316.

Leroy, S.A.G., Marco, S., Bookman, R. and Miller, C.S., 2010. Impact of earthquakes on agriculture during the Roman–Byzantine period from pollen records of the Dead Sea laminated sediment. Quaternary Research 73, 191-200.

Lisiecki, L.E. and Raymo, M.E., 2005. A Pliocene-Pleistocene stack of 57 globally distributed benthic $\delta^{18}O$ records. Paleoceanography 20, PA1003.

Litt, T., Ohlwein, C., Neumann, F.H., Hense, A. and Stein, M., 2012. Holocene climate variability in the Levant from the Dead Sea pollen record. Quaternary Science Reviews 49, 95-105.

Litt, T. and Anselmetti, F.S., 2014. Lake Van deep drilling project PALEOVAN. Quaternary Science Reviews 104, 1-7.

Litt, T., Pickarski, N., Heumann, G., Stockhecke, M. and Tzedakis, P.C., 2014. A 600,000 year long continental pollen record from Lake Van, eastern Anatolia (Turkey). Quaternary Science Reviews 104, 30-41.

Lynch, W.F., 1849. Narrative of the United States' Expedition to the River Jordan and the Dead Sea. Lea and Blanchard, Philadelphia.

Machlus, M., Enzel, Y., Goldstein, S.L., Marco, S. and Stein, M., 2000. Reconstructing low levels of Lake Lisan by correlating fan-delta and lacustrine deposits. Quaternary International 73-74, 137-144.

Magny, M., 2004. Holocene climate variability as reflected by mid-European lake-level fluctuations and its probable impact on prehistoric human settlements. Quaternary International 113, 65-79.

Marco, S. and Agnon, A., 1995. Prehistoric earthquake deformations near Masada, Dead Sea graben. Geology 23, 695-698.

Martin-Puertas, C., Valero-Garcés, B.L., Brauer, A., Mata, M.P., Delgado-Huertas, A. and Dulski, P., 2009. The Iberian–Roman Humid Period (2600–1600 cal yr BP) in the Zoñar Lake varve record (Andalucía, southern Spain). Quaternary Research 71, 108-120.

Martin-Puertas, C., Matthes, K., Brauer, A., Muscheler, R., Hansen, F., Petrick, C., Aldahan, A., Possnert, G. and van Geel, B., 2012. Regional atmospheric circulation shifts induced by a grand solar minimum. Nature Geosci 5, 397-401.

Martin-Puertas, C., Brauer, A., Wulf, S., Ott, F., Lauterbach, S. and Dulski, P., 2014. Annual proxy data from Lago Grande di Monticchio (southern Italy) between 76 and 112 ka: new chronological constraints and insights on abrupt climatic oscillations. Clim. Past 10, 2099-2114.

Mauquoy, D., van Geel, B., Blaauw, M., Speranza, A. and van der Plicht, J., 2004. Changes in solar activity and Holocene climatic shifts derived from ^{14}C wiggle-match dated peat deposits. The Holocene 14, 45-52.

Mayewski, P.A., Meeker, L.D., Twickler, M.S., Whitlow, S., Yang, Q., Lyons, W.B. and Prentice, M., 1997. Major features and forcing of high-latitude northern hemisphere atmospheric circulation using a 110,000-year-long glaciochemical series. Journal of Geophysical Research: Oceans 102, 26345-26366.

Mayewski, P.A., Rohling, E.E., Curt Stager, J., Karlén, W., Maasch, K.A., David Meeker, L., Meyerson, E.A., Gasse, F., van Kreveld, S., Holmgren, K., Lee-Thorp, J., Rosqvist, G., Rack, F., Staubwasser, M., Schneider, R.R. and Steig, E.J., 2004. Holocene climate variability. Quaternary Research 62, 243-255.

Meeker, L.D. and Mayewski, P.A., 2002. A 1400-year high-resolution record of atmospheric circulation over the North Atlantic and Asia. The Holocene 12, 257-266.

Migowski, C., 2001. Untersuchungen laminierter holozäner Sedimente aus dem Toten Meer: Rekonstruktion von Paläoklima und -seismizität, PhD thesis. University of Potsdam, Potsdam, p. 134.

Migowski, C., Agnon, A., Bookman, R., Negendank, J.F.W. and Stein, M., 2004. Recurrence pattern of Holocene earthquakes along the Dead Sea transform revealed by varve-counting and radiocarbon dating of lacustrine sediments. Earth and Planetary Science Letters 222, 301-314.

Migowski, C., Stein, M., Prasad, S., Negendank, J.F.W. and Agnon, A., 2006. Holocene climate variability and cultural evolution in the Near East from the Dead Sea sedimentary record. Quaternary Research 66, 421-431.

Mook, W.G. and Streurman, H.J., 1983. Physical and chemical aspects of radiocarbon dating, Proceedings of the First International Symposium ^{14}C and Archaeology. PACT publications, pp. 31-55.

Nakagawa, T., Gotanda, K., Haraguchi, T., Danhara, T., Yonenobu, H., Brauer, A., Yokoyama, Y., Tada, R., Takemura, K., Staff, R.A., Payne, R., Bronk Ramsey, C., Bryant, C., Brock, F., Schlolaut, G., Marshall, M., Tarasov, P. and Lamb, H., 2012. SG06, a fully continuous and varved sediment core from Lake Suigetsu, Japan: stratigraphy and potential for improving the radiocarbon calibration model and understanding of late Quaternary climate changes. Quaternary Science Reviews 36, 164-176.

Neev, D. and Emery, K.O., 1967. The Dead Sea: Depositional processes and environments of evaporites. Geological Survey of Israel Bulletin, p. 147.

Neev, D. and Hall, J.K., 1979. Geophysical investigations in the Dead Sea. Sedimentary Geology 23, 209-238.

Neev, D. and Emery, K.O., 1995. The destruction of Sodom, Gomorrah, and Jericho: geological, climatological, and archaeological background. Oxford University Press, New York.

Neugebauer, I., Brauer, A., Schwab, M.J., Waldmann, N.D., Enzel, Y., Kitagawa, H., Torfstein, A., Frank, U., Dulski, P., Agnon, A., Ariztegui, D., Ben-Avraham, Z., Goldstein, S.L. and Stein, M., 2014. Lithology of the long sediment record recovered by the ICDP Dead Sea Deep Drilling Project (DSDDP). Quaternary Science Reviews 102, 149-165.

Neugebauer, I., Brauer, A., Schwab, M.J., Dulski, P., Frank, U., Hadzhiivanova, E., Kitagawa, H., Litt, T., Schiebel, V., Taha, N. and Waldmann, N., accepted. Evidences for centennial dry periods at ~3300 and ~2800 cal yr BP from micro-facies analyses of the Dead Sea sediments. The Holocene.

Neumann, F.H., Kagan, E.J., Schwab, M.J. and Stein, M., 2007. Palynology, sedimentology and palaeoecology of the late Holocene Dead Sea. Quaternary Science Reviews 26, 1476-1498.

Neumann, F.H., Kagan, E.J., Leroy, S.A.G. and Baruch, U., 2010. Vegetation history and climate fluctuations on a transect along the Dead Sea west shore and their impact on past societies over the last 3500 years. Journal of Arid Environments 74, 756-764.

NGRIP Members, 2004. High-resolution record of Northern Hemisphere climate extending into the last interglacial period. Nature 431, 147-151.

Niemi, T.M., 1997. Fluctuations of late Pleistocene Lake Lisan in the Dead Sea rift, In: Niemi, T.M., Ben-Avraham, Z., Gat, J.R. (Eds.), The Dead Sea: The Lake and Its Setting. Oxford University Press, Oxford, pp. 226-236.

Niemi, T.M., Ben-Avraham, Z. and Gat, J.R., 1997. The Dead Sea: The Lake and Its Setting, Oxford Monographs on Geology and Geophysics. Oxford University Press, Oxford, p. 286.

Nowaczyk, N.R., 2001. Logging of magnetic susceptibility, In: Last, W.M., Smol, J.P. (Eds.), Tracking Environmental Change Using Lake Sediments Volume 1: Basin Analysis, Coring, and Chronological Techniques. Kluwer Academic Publishers, Dordrecht, Netherlands, pp. 155-170.

Ojala, A.E.K., Francus, P., Zolitschka, B., Besonen, M. and Lamoureux, S.F., 2012. Characteristics of sedimentary varve chronologies – A review. Quaternary Science Reviews 43, 45-60.

Palchan, D., Stein, M., Almogi-Labin, A., Erel, Y. and Goldstein, S.L., 2013. Dust transport and synoptic conditions over the Sahara–Arabia deserts during the MIS6/5 and 2/1 transitions from grain-size, chemical and isotopic properties of Red Sea cores. Earth and Planetary Science Letters 382, 125-139.

Pèrez-Obiol, R. and Julià, R., 1994. Climatic Change on the Iberian Peninsula Recorded in a 30,000-Yr Pollen Record from Lake Banyoles. Quaternary Research 41, 91-98.

Prasad, S., Vos, H., Negendank, J.F.W., Waldmann, N., Goldstein, S.L. and Stein, M., 2004. Evidence from Lake Lisan of solar influence on decadal- to centennial-scale climate variability during marine oxygen isotope stage 2. Geology 32, 581-584.

Prasad, S., Negendank, J.F.W. and Stein, M., 2009. Varve counting reveals high resolution radiocarbon reservoir age variations in palaeolake Lisan. Journal of Quaternary Science 24, 690-696.

Pross, J., Kotthoff, U., Müller, U.C., Peyron, O., Dormoy, I., Schmiedl, G., Kalaitzidis, S. and Smith, A.M., 2009. Massive perturbation in terrestrial ecosystems of the Eastern Mediterranean region associated with the 8.2 kyr B.P. climatic event. Geology 37, 887-890.

Quennel, A.M., 1958. The structural and geomorphic evolution of the Dead Sea rift. Quarterly Journal of the Geological Society 114, 1-24.

Rasmussen, S.O., Bigler, M., Blockley, S.P., Blunier, T., Buchardt, S.L., Clausen, H.B., Cvijanovic, I., Dahl-Jensen, D., Johnsen, S.J., Fischer, H., Gkinis, V., Guillevic, M., Hoek, W.Z., Lowe, J.J., Pedro, J.B., Popp, T., Seierstad, I.K., Steffensen, J.P., Svensson, A.M., Vallelonga, P., Vinther, B.M., Walker, M.J.C., Wheatley, J.J. and Winstrup, M., 2014. A stratigraphic framework for abrupt climatic changes during the Last Glacial period based on three synchronized Greenland ice-core records: refining and extending the INTIMATE event stratigraphy. Quaternary Science Reviews 106, 14-28.

Reimer, P.J., Bard, E., Bayliss, A., Beck, J.W., Blackwell, P.G., Bronk Ramsey, C., Grootes, P.M., Guilderson, T.P., Haflidason, H., Hajdas, I., Hatté, C., Heaton, T.J., Hoffmann, D.L., Hogg, A.G., Hughen, K.A., Kaiser, K.F., Kromer, B., Manning, S.W., Niu, M., Reimer, R.W., Richards, D.A., Scott, E.M., Southon, J.R., Staff, R.A., Turney, C.S.M. and van der Plicht, J., 2013. IntCal13 and Marine13 Radiocarbon Age Calibration Curves 0–50,000 Years cal BP. Radiocarbon 55(4), 1869-1887.

Renssen, H., Brovkin, V., Fichefet, T. and Goosse, H., 2003. Holocene climate instability during the termination of the African Humid Period. Geophysical Research Letters 30, 1184.

Roberts, N., Jones, M.D., Benkaddour, A., Eastwood, W.J., Filippi, M.L., Frogley, M.R., Lamb, H.F., Leng, M.J., Reed, J.M., Stein, M., Stevens, L., Valero-Garcés, B. and Zanchetta, G., 2008. Stable isotope records of Late Quaternary climate and hydrology from Mediterranean lakes: the ISOMED synthesis. Quaternary Science Reviews 27, 2426-2441.

Roberts, N., Brayshaw, D., Kuzucuoğlu, C., Perez, R. and Sadori, L., 2011a. The mid-Holocene climatic transition in the Mediterranean: Causes and consequences. The Holocene 21, 3-13.

Roberts, N., Eastwood, W.J., Kuzucuoğlu, C., Fiorentino, G. and Caracuta, V., 2011b. Climatic, vegetation and cultural change in the eastern Mediterranean during the mid-Holocene environmental transition. The Holocene 21, 147-162.

Robinson, S.A., Black, S., Sellwood, B.W. and Valdes, P.J., 2006. A review of palaeoclimates and palaeoenvironments in the Levant and Eastern Mediterranean from 25,000 to 5000 years BP: setting the environmental background for the evolution of human civilisation. Quaternary Science Reviews 25, 1517-1541.

Rohling, E., Mayewski, P., Abu-Zied, R., Casford, J. and Hayes, A., 2002. Holocene atmosphere-ocean interactions: records from Greenland and the Aegean Sea. Climate Dynamics 18, 587-593.

Rohling, E.J., 2013. Quantitative assessment of glacial fluctuations in the level of Lake Lisan, Dead Sea rift. Quaternary Science Reviews 70, 63-72.

Ron, H., Nowaczyk, N.R., Frank, U., Schwab, M.J., Naumann, R., Striewski, B. and Agnon, A., 2007. Greigite detected as dominating remanence carrier in Late Pleistocene sediments, Lisan formation, from Lake Kinneret (Sea of Galilee), Israel. Geophysical Journal International 170, 117-131.

Rossignol-Strick, M., 1985. Mediterranean Quaternary sapropels, an immediate response of the African monsoon to variation of insolation. Palaeogeography, Palaeoclimatology, Palaeoecology 49, 237-263.

Rubin, S., Ziv, B. and Paldor, N., 2007. Tropical Plumes over Eastern North Africa as a Source of Rain in the Middle East. Monthly Weather Review 135, 4135-4148.

Ryb, U., Matmon, A., Erel, Y., Haviv, I., Benedetti, L. and Hidy, A.J., 2014. Styles and rates of long-term denudation in carbonate terrains under a Mediterranean to hyper-arid climatic gradient. Earth and Planetary Science Letters 406, 142-152.

Saaroni, H., Halfon, N., Ziv, B., Alpert, P. and Kutiel, H., 2010. Links between the rainfall regime in Israel and location and intensity of Cyprus lows. International Journal of Climatology 30, 1014-1025.

Sade, A., Hall, J.K., Sade, H., Amit, G., Tibor, G., Schulze, B., Gur-Arieh, L., ten Brink, U., Ben-Avraham, Z., Keller, C., Gertman, I., Beaudoin, J., Al-Zoubi, A., Akawwi, E., Rimawi, O., Abueladas, A., Mayer, L., Calder, B. and Maratos, A., 2014. Multibeam Bathymetric Map of the Dead Sea, Geological Survey of Israel Report GSI/01.

Sánchez Goñi, M., Cacho, I., Turon, J., Guiot, J., Sierro, F., Peypouquet, J., Grimalt, J. and Shackleton, N., 2002. Synchroneity between marine and terrestrial responses to millennial scale climatic variability during the last glacial period in the Mediterranean region. Climate Dynamics 19, 95-105.

Sánchez Goñi, M.F., Eynaud, F., Turon, J.L. and Shackleton, N.J., 1999. High resolution palynological record off the Iberian margin: direct land-sea correlation for the Last Interglacial complex. Earth and Planetary Science Letters 171, 123-137.

Schlolaut, G., Brauer, A., Marshall, M.H., Nakagawa, T., Staff, R.A., Bronk Ramsey, C., Lamb, H.F., Bryant, C.L., Naumann, R., Dulski, P., Brock, F., Yokoyama, Y., Tada, R. and Haraguchi, T., 2014. Event layers in the Japanese Lake Suigetsu 'SG06' sediment core: description, interpretation and climatic implications. Quaternary Science Reviews 83, 157-170.

Schramm, A., Stein, M. and Goldstein, S.L., 2000. Calibration of the ^{14}C time scale to >40 ka by ^{234}U-^{230}Th dating of Lake Lisan sediments (last glacial Dead Sea). Earth and Planetary Science Letters 175, 27-40.

Seager, R., Liu, H., Henderson, N., Simpson, I., Kelley, C., Shaw, T., Kushnir, Y. and Ting, M., 2014. Causes of Increasing Aridification of the Mediterranean Region in Response to Rising Greenhouse Gases. Journal of Climate 27, 4655-4676.

Shackleton, N.J. and Opdyke, N.D., 1973. Oxygen isotope and palaeomagnetic stratigraphy of Equatorial Pacific core V28-238: Oxygen isotope temperatures and ice volumes on a 10^5 year and 10^6 year scale. Quaternary Research 3, 39-55.

Shackleton, N.J., 1987. Oxygen isotopes, ice volume and sea level. Quaternary Science Reviews 6, 183-190.

Shaliv, G., 1991. Stages in the tectonic and volcanic history of the Neogene basin in the Lower Galilee and the valleys, Geological Survey of Israel, Jerusalem, p. 94.

Siddall, M., Rohling, E.J., Almogi-Labin, A., Hemleben, C., Meischner, D., Schmelzer, I. and Smeed, D.A., 2003. Sea-level fluctuations during the last glacial cycle. Nature 423, 853-858.

Sippel, S. and Otto, F.L., 2014. Beyond climatological extremes - assessing how the odds of hydrometeorological extreme events in South-East Europe change in a warming climate. Climatic Change 125, 381-398.

Sirocko, F., Seelos, K., Schaber, K., Rein, B., Dreher, F., Diehl, M., Lehne, R., Jager, K., Krbetschek, M. and Degering, D., 2005. A late Eemian aridity pulse in central Europe during the last glacial inception. Nature 436, 833-836.

Sneh, A., Bartov, Y., Weissbrod, T., Rosensaft, M., 1998. Geological Map of Israel, 1:200,000. Israel Geological Survey (4 sheets).

Solanki, S.K. and Krivova, N.A., 2007. Solar Variability of Possible Relevance for Planetary Climates, In: Calisesi, Y., Bonnet, R.M., Gray, L., Langen, J., Lockwood, M. (Eds.), Solar Variability and Planetary Climates. Springer New York, pp. 25-37.

Stein, M., Starinsky, A., Katz, A., Goldstein, S.L., Machlus, M. and Schramm, A., 1997. Strontium isotopic, chemical, and sedimentological evidence for the evolution of Lake Lisan and the Dead Sea. Geochimica et Cosmochimica Acta 61, 3975-3992.

Stein, M., Goldstein, S.L. and Schramm, A., 2000. Radiocarbon calibration beyond the dendrochronology range. Radiocarbon 42, 415-422.

Stein, M., 2001. The sedimentary and geochemical record of Neogene-Quaternary water bodies in the Dead Sea Basin - inferences for the regional paleoclimatic history. Journal of Paleolimnology 26, 271-282.

Stein, M. and Goldstein, S.L., 2006. U-Th and radiocarbon chronologies of late Quaternary lacustrine records of the Dead Sea basin: Methods and applications. Geological Society of America Special Papers 401, 141-154.

Stein, M., Torfstein, A., Gavrieli, I. and Yechieli, Y., 2010. Abrupt aridities and salt deposition in the post-glacial Dead Sea and their North Atlantic connection. Quaternary Science Reviews 29, 567-575.

Stein, M., Ben-Avraham, Z. and Goldstein, S.L., 2011. Dead Sea deep cores: A window into past climate and seismicity. Eos, Transactions American Geophysical Union 92, 453-454.

Stein, M., 2014. The Evolution of Neogene-Quaternary Water-Bodies in the Dead Sea Rift Valley, In: Garfunkel, Z., Ben-Avraham, Z., Kagan, E. (Eds.), Dead Sea Transform Fault System: Reviews. Springer Netherlands, pp. 279-316.

Steinhilber, F., Beer, J. and Fröhlich, C., 2009. Total solar irradiance during the Holocene. Geophysical Research Letters 36, L19704.

Stockhecke, M., Sturm, M., Brunner, I., Schmincke, H.-U., Sumita, M., Kipfer, R., Cukur, D., Kwiecien, O. and Anselmetti, F.S., 2014. Sedimentary evolution and environmental history of Lake Van (Turkey) over the past 600 000 years. Sedimentology 61, 1830-1861.

Swierczynski, T., Lauterbach, S., Dulski, P., Delgado, J., Merz, B. and Brauer, A., 2013. Mid- to late Holocene flood frequency changes in the northeastern Alps as recorded in varved sediments of Lake Mondsee (Upper Austria). Quaternary Science Reviews 80, 78-90.

Tjallingii, R., Claussen, M., Stuut, J.-B.W., Fohlmeister, J., Jahn, A., Bickert, T., Lamy, F. and Rohl, U., 2008. Coherent high- and low-latitude control of the northwest African hydrological balance. Nature Geosci 1, 670-675.

Torfstein, A., Gavrieli, I. and Stein, M., 2005. The sources and evolution of sulfur in the hypersaline Lake Lisan (paleo-Dead Sea). Earth and Planetary Science Letters 236, 61-77.

Torfstein, A., Gavrieli, I., Katz, A., Kolodny, Y. and Stein, M., 2008. Gypsum as a monitor of the paleo-limnological-hydrological conditions in Lake Lisan and the Dead Sea. Geochimica et Cosmochimica Acta 72, 2491-2509.

Torfstein, A., Haase-Schramm, A., Waldmann, N., Kolodny, Y. and Stein, M., 2009. U-series and oxygen isotope chronology of the mid-Pleistocene Lake Amora (Dead Sea basin). Geochimica et Cosmochimica Acta 73, 2603-2630.

Torfstein, A., Goldstein, S.L., Kagan, E.J. and Stein, M., 2013a. Integrated multi-site U-Th chronology of the last glacial Lake Lisan. Geochimica et Cosmochimica Acta 104, 210-231.

Torfstein, A., Goldstein, S.L., Stein, M. and Enzel, Y., 2013b. Impacts of abrupt climate changes in the Levant from Last Glacial Dead Sea levels. Quaternary Science Reviews 69, 1-7.

Torfstein, A., Goldstein, S.L., Kushnir, Y., Enzel, Y., Haug, G. and Stein, M., 2015. Dead Sea drawdown and monsoonal impacts in the Levant during the last interglacial. Earth and Planetary Science Letters 412, 235-244.

Tubi, A. and Dayan, U., 2014. Tropical Plumes over the Middle East: Climatology and synoptic conditions. Atmospheric Research 145–146, 168-181.

Tzedakis, P.C., 2005. Towards an understanding of the response of southern European vegetation to orbital and suborbital climate variability. Quaternary Science Reviews 24, 1585-1599.

Tzedakis, P.C., Hooghiemstra, H. and Pälike, H., 2006. The last 1.35 million years at Tenaghi Philippon: revised chronostratigraphy and long-term vegetation trends. Quaternary Science Reviews 25, 3416-3430.

Tzedakis, P.C., 2007. Seven ambiguities in the Mediterranean palaeoenvironmental narrative. Quaternary Science Reviews 26, 2042-2066.

Vaks, A., Bar-Matthews, M., Ayalon, A., Matthews, A., Frumkin, A., Dayan, U., Halicz, L., Almogi-Labin, A. and Schilman, B., 2006. Paleoclimate and location of the border between Mediterranean climate region and the Saharo–Arabian Desert as revealed by speleothems from the northern Negev Desert, Israel. Earth and Planetary Science Letters 249, 384-399.

Vaks, A., Bar-Matthews, M., Ayalon, A., Matthews, A., Halicz, L. and Frumkin, A., 2007. Desert speleothems reveal climatic window for African exodus of early modern humans. Geology 35, 831-834.

Vaks, A., Bar-Matthews, M., Matthews, A., Ayalon, A. and Frumkin, A., 2010. Middle-Late Quaternary paleoclimate of northern margins of the Saharan-Arabian Desert: reconstruction from speleothems of Negev Desert, Israel. Quaternary Science Reviews 29, 2647-2662.

van Geel, B., Buurman, J. and Waterbolk, H.T., 1996. Archaeological and palaeoecological indications of an abrupt climate change in The Netherlands, and evidence for climatological teleconnections around 2650 BP. Journal of Quaternary Science 11, 451-460.

van Geel, B., Raspopov, O.M., Renssen, H., van der Plicht, J., Dergachev, V.A. and Meijer, H.A.J., 1999. The role of solar forcing upon climate change. Quaternary Science Reviews 18, 331-338.

van Geel, B., Bokovenko, N.A., Burova, N.D., Chugunov, K.V., Dergachev, V.A., Dirksen, V.G., Kulkova, M., Nagler, A., Parzinger, H., van der Plicht, J., Vasiliev, S.S. and Zaitseva, G.I., 2004. Climate change and the expansion of the Scythian culture after 850 BC: a hypothesis. Journal of Archaeological Science 31, 1735-1742.

Verheyden, S., Nader, F.H., Cheng, H.J., Edwards, L.R. and Swennen, R., 2008. Paleoclimate reconstruction in the Levant region from the geochemistry of a Holocene stalagmite from the Jeita cave, Lebanon. Quaternary Research 70, 368-381.

Vuillemin, A. and Ariztegui, D., 2013. Geomicrobiological investigations in subsaline maar lake sediments over the last 1500 years. Quaternary Science Reviews 71, 119-130.

Wagner, B., Lotter, A., Nowaczyk, N., Reed, J., Schwalb, A., Sulpizio, R., Valsecchi, V., Wessels, M. and Zanchetta, G., 2009. A 40,000-year record of environmental change from ancient Lake Ohrid (Albania and Macedonia). Journal of Paleolimnology 41, 407-430.

Wagner, B., Wilke, T., Krastel, S., Zanchetta, G., Sulpizio, R., Reicherter, K., Leng, M., Grazhdani, A., Trajanovski, S., Levkov, Z., Reed, J. and Wonik, T., 2014. More Than

One Million Years of History in Lake Ohrid Cores. Eos, Transactions American Geophysical Union 95, 25-26.

Waldmann, N., Starinsky, A. and Stein, M., 2007. Primary carbonates and Ca-chloride brines as monitors of a paleo-hydrological regime in the Dead Sea basin. Quaternary Science Reviews 26, 2219-2228.

Waldmann, N., Stein, M., Ariztegui, D. and Starinsky, A., 2009. Stratigraphy, depositional environments and level reconstruction of the last interglacial Lake Samra in the Dead Sea basin. Quaternary Research 72, 1-15.

Waldmann, N., Torfstein, A. and Stein, M., 2010. Northward intrusions of low- and mid-latitude storms across the Saharo-Arabian belt during past interglacials. Geology 38, 567-570.

Waldmann, N., Hadzhiivanova, E., Neugebauer, I., Brauer, A., Schwab, M.J., Frank, U. and Dulski, P., 2014. Anatomy of mass transport deposits in the Dead Sea; sedimentary processes in an active tectonic hypersaline basin, EGU General Assembly, EGU-2014-11281, Vienna, Austria.

Wang, Y.J., Cheng, H., Edwards, R.L., An, Z.S., Wu, J.Y., Shen, C.-C. and Dorale, J.A., 2001. A High-Resolution Absolute-Dated Late Pleistocene Monsoon Record from Hulu Cave, China. Science 294, 2345-2348.

Weltje, G.J. and Tjallingii, R., 2008. Calibration of XRF core scanners for quantitative geochemical logging of sediment cores: Theory and application. Earth and Planetary Science Letters 274, 423-438.

Woillard, G.M., 1978. Grande Pile peat bog: A continuous pollen record for the last 140,000 years. Quaternary Research 9, 1-21.

Wolff, E.W., Chappellaz, J., Blunier, T., Rasmussen, S.O. and Svensson, A., 2010. Millennial-scale variability during the last glacial: The ice core record. Quaternary Science Reviews 29, 2828-2838.

Wright, J.D., 2000. Global Climate Change in Marine Stable Isotope Records, In: Noller, J.S., Sowers, J.M., Lettis, W.R. (Eds.), Quaternary Geochronology: Methods and Applications. American Geophysical Union, pp. 427-433.

Yechieli, Y., Magaritz, M., Levy, Y., Weber, U., Kafri, U., Woelfli, W. and Bonani, G., 1993. Late Quaternary Geological History of the Dead Sea Area, Israel. Quaternary Research 39, 59-67.

Yechieli, Y., Gavrieli, I., Berkowitz, B. and Ronen, D., 1998. Will the Dead Sea die? Geology 26, 755-758.

Zak, I., 1967. The geology of Mount Sedom. The Hebrew University, Jerusalem, p. 208.

Zangvil, A., Karas, S. and Sasson, A., 2003. Connection between Eastern Mediterranean seasonal mean 500 hPa height and sea-level pressure patterns and the spatial rainfall distribution over Israel. International Journal of Climatology 23, 1567-1576.

Zhao, Y., Liu, H., Li, F., Huang, X., Sun, J., Zhao, W., Herzschuh, U. and Tang, Y., 2012. Application and limitations of the Artemisia/Chenopodiaceae pollen ratio in arid and semi-arid China. The Holocene 22, 1385-1392.

Ziv, B., Dayan, U., Kushnir, Y., Roth, C. and Enzel, Y., 2006. Regional and global atmospheric patterns governing rainfall in the southern Levant. International Journal of Climatology 26, 55-73.

Appendix

A1 Stable oxygen and carbon isotopes of core 5017-1

Method

From a ~17 m long section of the composite core 5017-1 (11-28 m composite depth) as part of the Holocene Ze'elim Formation, a total of 405 samples were collected, of which 304 have been measured for stable oxygen and carbon isotopes (Fig. A1-1). Single aragonite layers (n = 245) were sampled with a thin scalpel from the middle of the layer. Detrital layers were sampled for comparison. Sample pretreatment included (1) drying at 40°C, (2) weighing of 0.8 mg aliquots into glass tubes, (3) rinsing the samples three times with ultra-pure water and (4) drying at 60°C. The samples were treated with 103% H_3PO_4 at 70°C and measurements of $\delta^{18}O$ and $\delta^{13}C$ were carried out with a DELTAplusXL (ThermoFisher Scientific) mass spectrometer that is connected to a Gasbench II tool in the Laboratory for Stable Isotopes (Sediments) of Section 5.2 at the GFZ. Data were calibrated with standards (CO1, C1 and NBS19 relative to VPDB) and analytical precisions are <0.06‰ for $\delta^{13}C$ and <0.08‰ for $\delta^{18}O$.

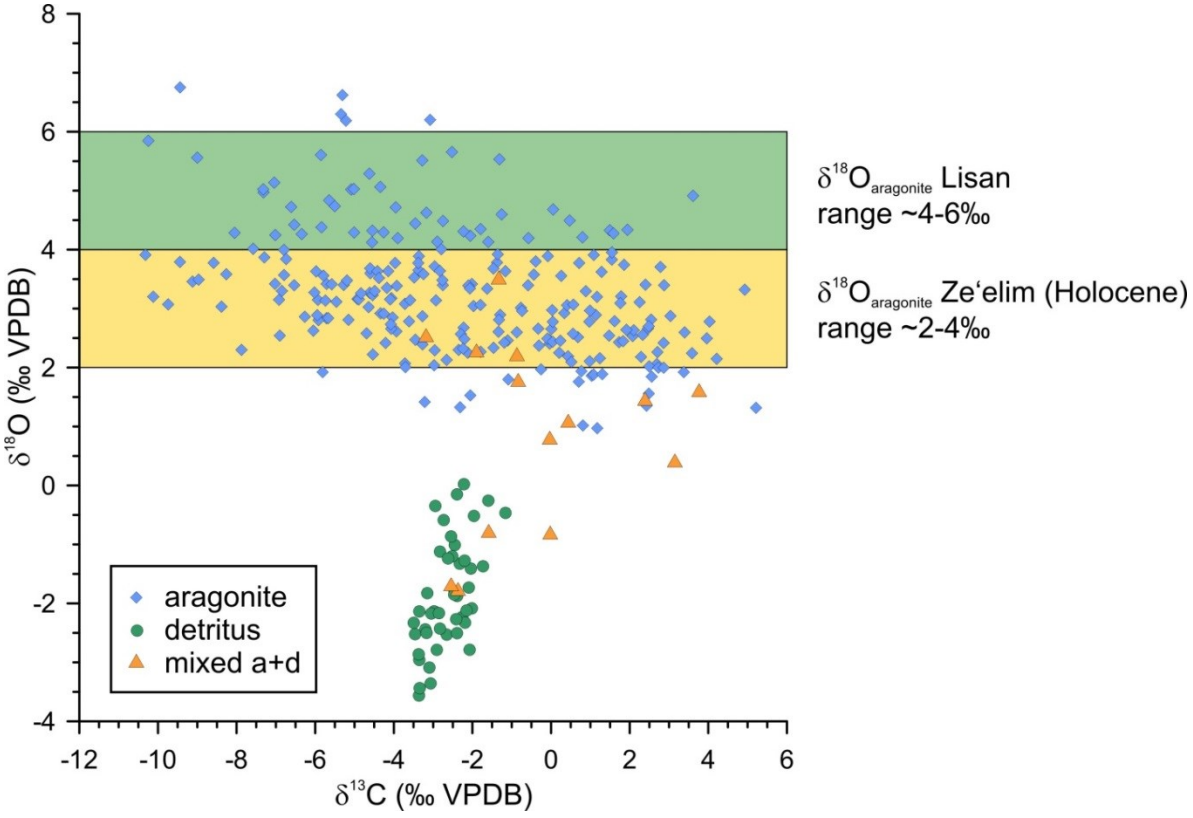

Figure A1- 1: Correlation plot of $\delta^{18}O$ against $\delta^{13}C$ values of all measured samples (n = 304); typical $\delta^{18}O$ ranges of aragonite samples for the last glacial Lisan and the Holocene Ze'elim Formations are given according to Kolodny et al. (2005).

The preliminary results show that the $\delta^{18}O_{aragonite}$ values fall mostly well within a range of ~2-4‰ that are typical Holocene values (Fig. A1-1 above). However, a smaller part of the values fits well into the range of the last glacial Lisan aragonites that formed when climatic conditions were more humid. The $\delta^{13}C_{aragonite}$ values strongly fluctuate as they are influenced by inter-annual and lake-internal effects (Kolodny et al., 2005), but show a weak anti-correlation to $\delta^{18}O_{aragonite}$, consistent in sediment depth (Fig. A1-2 below). In Figure A1-2 a tendency towards lighter $\delta^{18}O_{aragonite}$ and heavier $\delta^{13}C_{aragonite}$ values from ca 17 to 23 m sediment depth and *vice versa* in the lower and upper part of the core sequence can be seen. However, further analysis is ongoing and evaluation is needed to prove these first results.

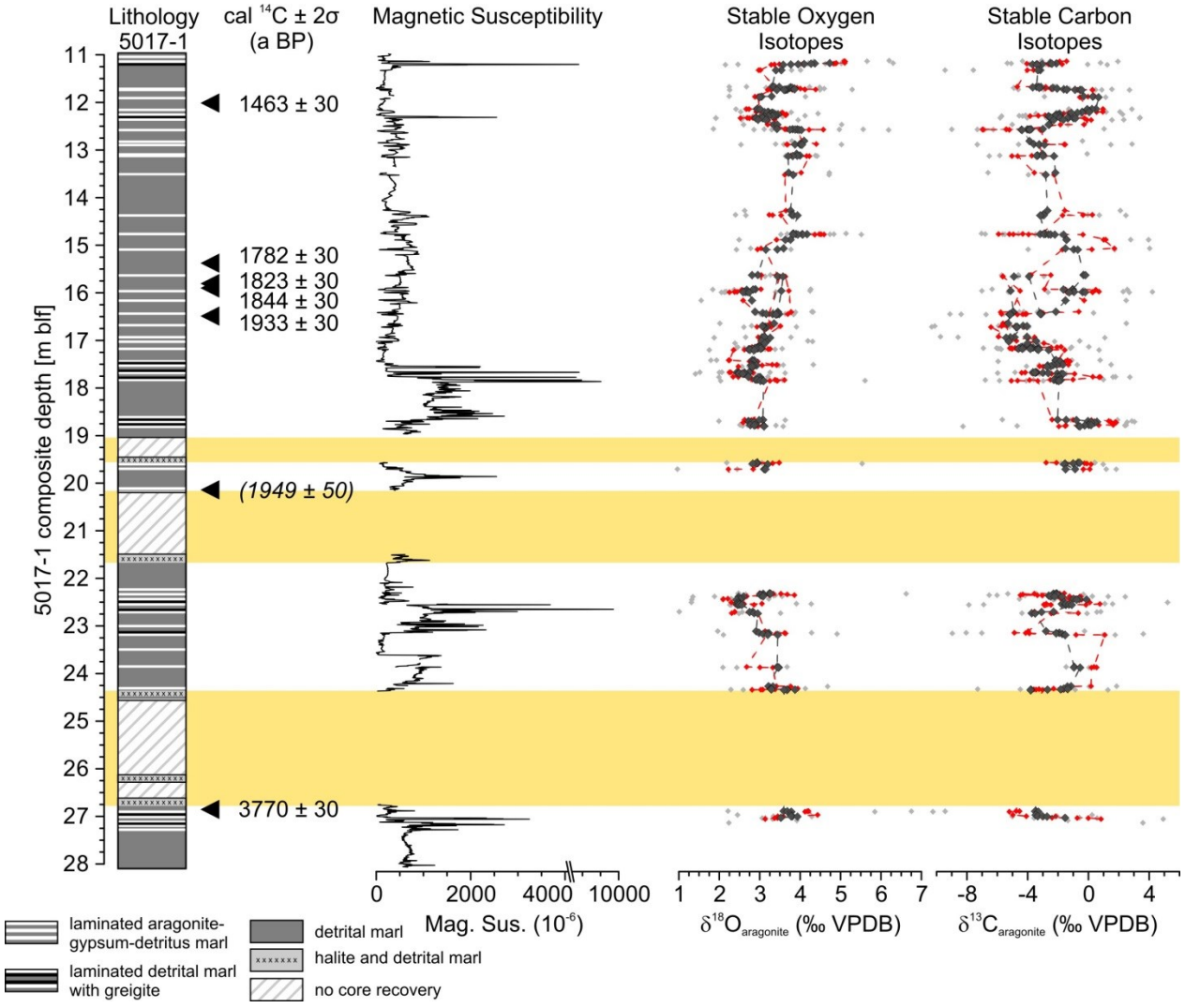

Figure A1- 2: Lithological profile and magnetic susceptibility data of a late Holocene (~1400-3800 cal yr BP) section from core 5017-1 (all data as presented in Chapters 2 and 4); stable oxygen and carbon isotopes of aragonite samples (single values: grey, running means of 5 values: red, running means of 11 values: black).

A2 Improved composite and age model of core DSEn

Table A2- 1: DSEn coring protocol and composite depths; rel – relative, abs - absolute.

					composite (all in cm)						
core	drilled depth (m)	core length (cm, brutto)	core length (cm, net)	corrected core depth (cm)	top (rel)	top (abs)	bottom (rel)	bottom (abs)	length	total (bottom)	remarks
Top1			51.5	-30-21.5	0		10		10	-20	
Top2			51	-20-31	0		33		33	13	
Top3			35.5	13-48.5	0		8		8	21	
C1	0.17-1.17	97	97	17-114	4	21	93	110	89	110	
B1	0.50-1.50	96	96	50-146	48	98	53	103	5	115	
A2	1.00-2.00	96	96	100-196	6	106	94	194	88	203	
B2	1.50-2.50	92	92	150-242	39	189	48	198	9	212	
A3	2.00-3.00	96	96	200-296	1	201	94	294	93	305	
B3	2.50-3.50	98	98	250-348	39	289	91.5	341.5	52.5	357.5	parallel A4: 7-30cm
A4	3.00-4.00	97	97	300-397	43.5	343.5	96	396	52.5	410	
B4	3.50-4.50	96	96	350-446	40.5	390.5	55	405	14.5	424.5	
A5	4.00-6.00	196	196	400-596							
A5-o		96	96	400-496	11	411	96	496	85	509.5	
A5-u		100	100	496-596	0	496	78	574	78	587.5	
B5	4.50-6.50	182	182	450-632							
B5-o		91	91	450-541							
B5-u		91	91	541-632	26.5	567.5	62	603	35.5	623	
A6	4.30-7.00	177	91 (-86)	600-691							
A6-o		98	12 (-86)	514 (600) -612							
A6-u		79	79	612-691	13	625	74	686	61	684	
B6	6.50-8.50	198	198	650-848							
B6-o		98	98	650-748	21.5	671.5	63	713	41.5	725.5	
B6-u		100	100	748-848							
A7	7.00-9.00	196	196	700-896							
A7-o		97	97	700-797	14	714	97	797	83	808.5	
A7-u		99	99	797-896	0	797	61	858	61	869.5	
B7	8.50-10.50	194	194	850-1044							
B7-o		98	98	850-948	18	868	62.5	912.5	44.5	914	
A8	9.00-11.00	200	200	900-1100							
A8-o		98	98	900-998	15.5	915.5	87	987	71.5	985.5	
B7-u		96	96	948-1044	23.5	971.5	48.5	996.5	25	1010.5	A8 o/u parallel
A8-u		102	102	998-1100	17.5	1015.5	97	1095	79.5	1090	
B8	10.50-12.50	195	195	1050-1245							
B8-o		99	99	1050-1149	35	1085	42.5	1092.5	7.5	1097.5	
A9	10.78-12.45	192	145 (-47)	1100-1245							
A9-o		96	49 (-47)	1053 (1100) -1149	48	1101	96	1149	48	1145.5	
A9-u		96	96	1149-1245	0	1149	94	1243	94	1239.5	
B8-u		96	96	1149-1245	88	1237	95	1244	7	1246.5	
A10	12.00-14.00	198	155 (-43)	1245-1400							
A10-o		98	55 (-43)	1202 (1245) -1300	46	1248	98	1300	52	1298.5	
A10-u		100	100	1300-1400	0	1300	87	1387	87	1385.5	
B9	12.31-14.36	195	183	1250-1433							
B9-o		98	86 (-12)	1238 (1250) -1336							
B9-u		97	97	1336-1433	63	1399	94	1430	31	1416.5	
A11	13.51-15.54	199	150	1400-1550							
A11-o		102	53 (-49)	1351 (1400) -1453	65	1416	102	1453	37	1453.5	
A11-u		97	97	1453-1550	0	1453	97	1550	97	1550.5	parallel: B10 oben
B10	14.50-16.50	199	199	1450-1649							
B10-o		99	99	1450-1549							
B10-u		100	100	1549-1649	10	1559	21	1570	11	1561.5	
A12	15.00-17.00	195	146	1554-1698							
A12-o		100	49 (-51)	1503 (1554) -1603	57.5	1560.5	100	1603	42.5	1604	parallel: B10 unten
A12-u		95	95	1603-1698	0	1603	90	1693	90	1694	
B11	16.50-18.50	196	196	1650-1846							
B11-o		98	98	1650-1748	56.5	1706.5	70.5	1720.5	14	1708	
A13	15.64-17.88	182	88	1700-1788							
A13-o		98	4 (-94)	1606 (1700) -1704							
A13-u		84	84	1704-1788	0.5	1704.5	78.5	1782.5	78	1786	
B11-u		98	98	1748-1846	43.5	1791.5	95	1843	51.5	1837.5	
A14	18.00-20.00	196	190	1800-1990							
A14-o		98	92 (-6)	1794 (1800) -1892	44.5	1838.5	55.5	1849.5	11	1848.5	
B12	18.50-19.50	96	96	1850-1946	10.5	1860.5	95	1945	84.5	1933	
A14-u		98	98	1892-1990	59	1951	98	1990	39	1972	
A15	18.29-20.30	176	8	2000-2008							
A15-o		79	0 (-79)	1832 -1911							
A15-u		97	8 (-89)	1911 (2000) -2008	85	1996	97	2008	12	1984	
A16-u		77	55 (-22)	2008 (2030) -2085	22	2030	77	2085	55	2039	

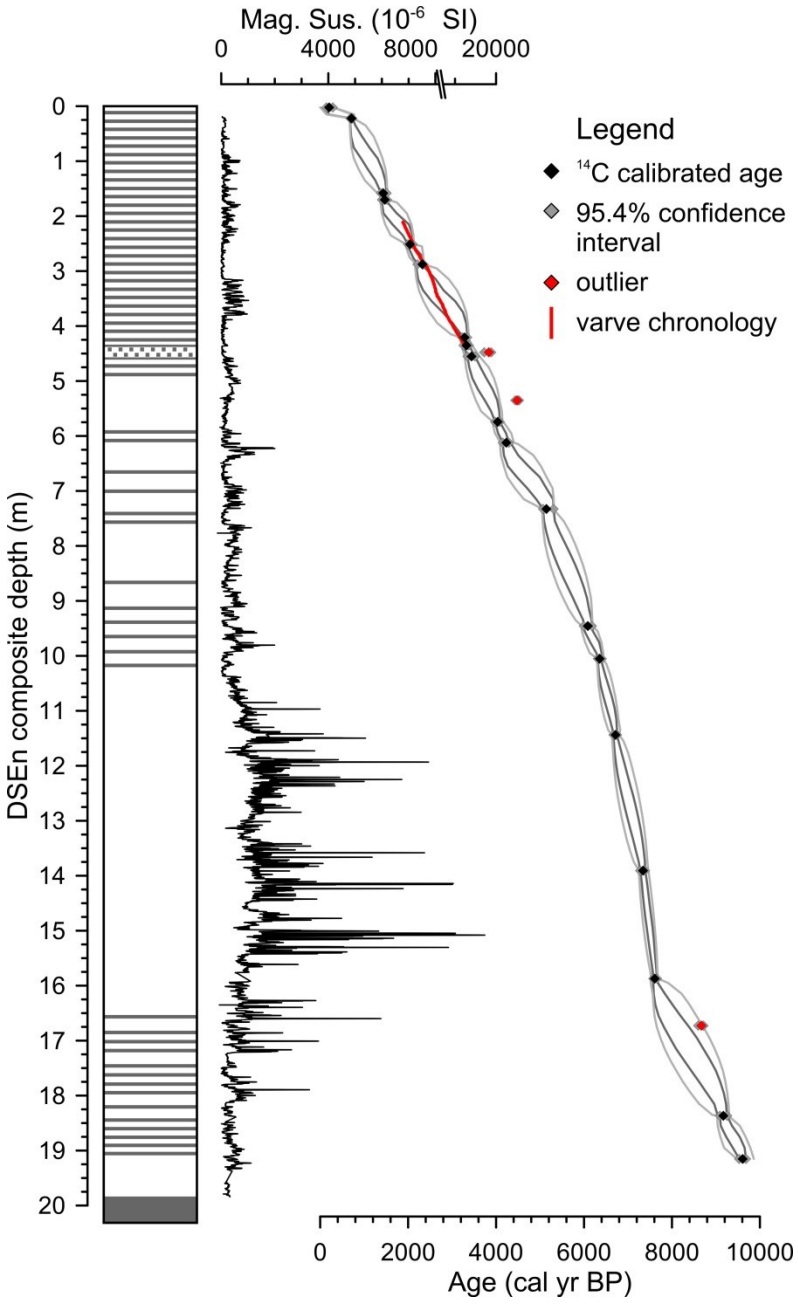

Figure A2- 1: Simplified lithological profile of core DSEn, magnetic susceptibility and improved age model using the P_Sequence(1,0.05,U(-2,2)) deposition model in OxCal 4.2.

A3 Upper Lisan Formation of core 5017-1

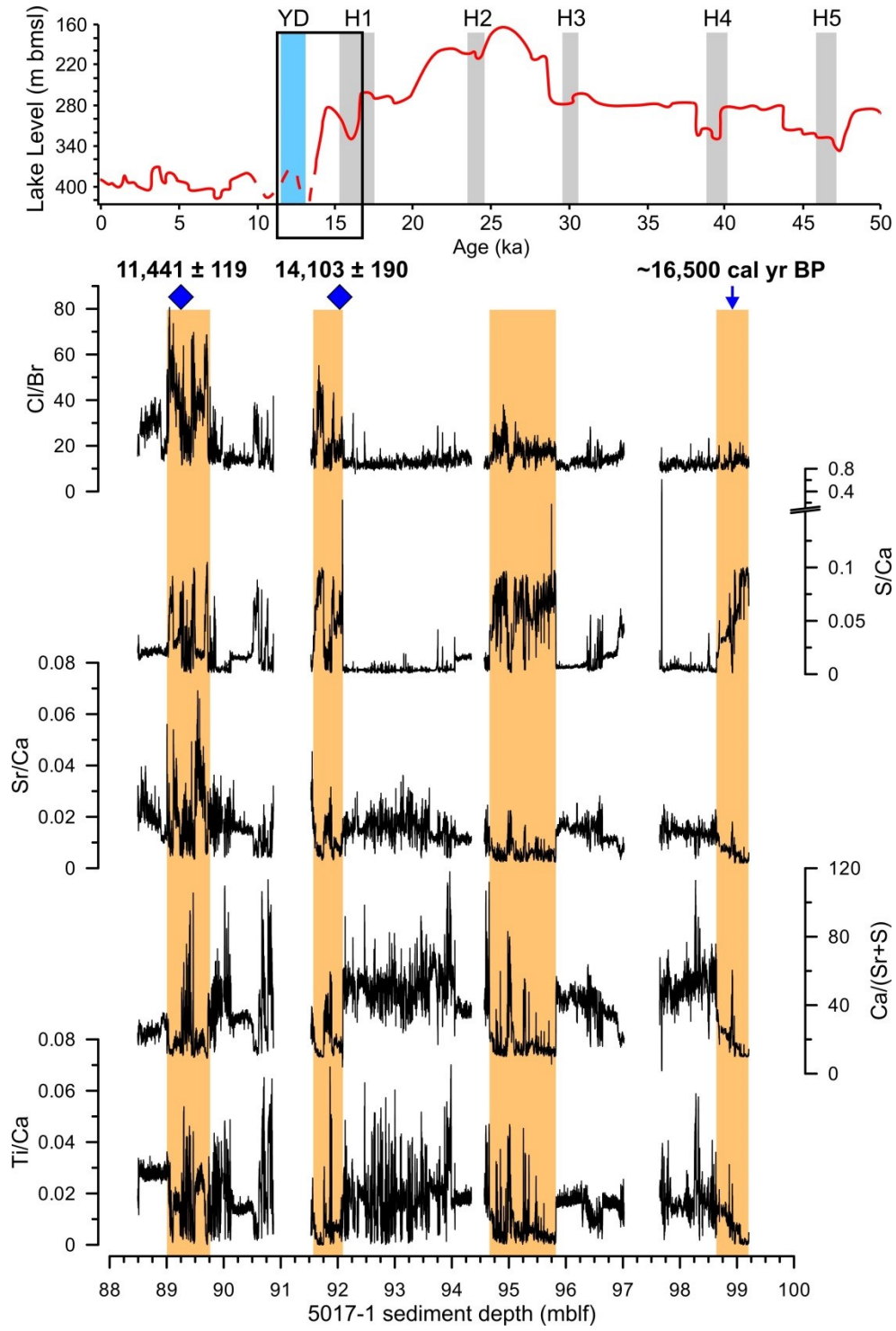

Figure A3- 1: Holocene and last glacial Dead Sea lake level curve (Stein et al., 2010); selected element ratios as derived from µXRF scanning of a ca 11 m long section of core 5017-1 from the deep Dead Sea basin that represents the upper last glacial Lisan Formation from ca 16.5 to 11 ka BP. Orange bars mark prominent gypsum deposits that reflect pronounced lake level drops. Ages are from radiocarbon dating of terrestrial macro plant remains.

A4 Table of content of data-CD

A4-1: Pdf file of the doctoral thesis by Ina Neugebauer

A4-2: Curriculum Vitae and list of publications by Ina Neugebauer

A4-3: Complete list of thin sections and of cores measured for μXRF

A4-4: Data related to Chapter 2

A4-5: Data related to Chapter 3

A4-6: Data related to Chapter 4